UNIVERSITY OF LONDON THESIS

Degree PhD Year 2007 Name of Author RAMOS ALEGRE BRANCO, Tiago

A Study of the Determinants of Release Probability in Hippocampal Synapses

Tiago Ramos Alegre Branco

April, 2007

Thesis presented in partial fulfilment of the degree of Doctor of Philosophy at the University of London

MRC Laboratory for Molecular and Cell Biology, UCL, London

Department of Pharmacology, University College London

ProQuest LLC
789 East Eisenhower Parkway
P.O. Box 1346
Ann Arbor, MI 48106-1346

Acknowledgments

I am most grateful to the Wellcome Trust and the four year Ph.D. Programme in Neuroscience, not only for the generous funding of my studies, but also for providing an outstanding environment in which to learn and develop as a scientist. I am particularly grateful to David Attwell, the head of the programme, for his encouragement, guidance and constant support. I wish to thank my supervisor, Yuki Goda, for giving me the opportunity to work in her lab, providing everything that was needed to pursue every experiment I ever wanted to try, and especially for entrusting me with a much appreciated freedom and independence.

From the beginning of my Ph.D. I had the good fortune of having the perfect partner in crime. Either plating astrocytes at very inconvenient hours while one of us was off on a plane somewhere, running the London marathon or stealing bottles of Port at wedding parties, Kevin D'Arcy and I shared most of the laughs and the moanings. I am most indebted to Kevin Staras, for all his help with the work and the writing, for the very fun and always useful discussions on the intimacy of synaptic vesicles, for the elastic band flicking competitions, and mostly, for all those *cheeky ones for the road.* Thanks also to Christian Dillon, for teaching me that molecular biology is one big shortcut, and that curry is not such a bad thing after all, especially if consumed in Primrose Hill at 5 a.m. after a ridiculous number of pints.

I would like to thank Michael Hausser, my second supervisor, for very fruitful discussions, for his unmatched enthusiasm about neuroscience, and for making me feel at home in his lab, and at all the associated dinners and parties. I am also thankful to Mark Farrant for all his help on the tricky practical sides of electrophysiology, and to Mickey London and Arnd Roth for enlightening discussions and modelling tutorials.

During these four years in London I was fortunate enough to be in the presence of my brother Miguel, whose everyday company and support were so invaluable. Apart from conveniently being a brilliant scientist and academic, and having a remarkable tolerance for my messy behaviour around the flat,

his housekeeping devotion and outstanding cooking skills often saved my life.

I am very grateful to the UCL 8 group, my colleagues in the Ph.D programme, for making my arrival and integration in London so easy and enjoyable. Special thanks to my flatmates Seb Kracun and Isaac Bianco for all the many good times in the flat and in ever so carefully selected pubs, and for continuous education on the fascinating Scottish and English cultures.

Thank you so much to Beverley Clark for her love and support, for her unbelievable patience, everyday troubleshooting of neuroscience, either practical, theoretical or social, and especially for making everything so much more fun.

Finally, I am forever grateful to all my good friends in Portugal for making me feel that I never really left, and to my parents for their love and unconditional support. It has been quite a ride.

To my parents and much missed grandparents,
with love, respect and admiration.

O me! O life!... Of the questions of these recurring;
Of the endless trains of the faithless - of cities fill'd with the foolish;
Of myself forever reproaching myself, (for who more foolish than I,
and who more faithless?)
Of eyes that vainly crave the light - of the objects mean - of the
struggle ever renew'd;
Of the poor results of all - of the plodding and sordid crowds I see around me;
Of the empty and useless years of the rest - with the rest me intertwined,
The question, O me! So sad, recurring - What good amid these, O me, O life?

Answer

That you are here - that life exists and identity,
That the powerful play goes on, and you will contribute a verse.

Walt Whitman (1819-1892)
Leaves of Grass. 1900.

Abstract

The release of neurotransmitter at a synapse is a stochastic process, such that the arrival of an action potential triggers vesicle fusion with a limited probability (p_r). Although p_r is a fundamental parameter in defining synaptic efficacy, it is not uniform across all synapses, and the mechanisms by which a given synapse sets its basal release probability are unknown. This study employed FM-dye imaging, paired whole-cell recordings and serial ultrastructural analysis with 3D reconstruction to address this question. Optical measurements of p_r at single synapses were made in small networks of cultured hippocampal neurons, and suggest a new model of p_r regulation whereby release probability is set locally by the dendrite through a negative feedback mechanism. In synaptically connected pairs of neurons, a high resolution spatial analysis reveals that neighbouring synapses on the same dendritic branch show very similar release probabilities, even though the connection overall has a broad distribution of p_r. Moreover, p_r is negatively correlated with the number of synapses made between the axon and the dendritic branch. Increasing network activity elicits a homeostatic decrease in p_r that is dependent on dendritic depolarization, and imposing a spatially uniform input to the dendrite significantly reduces the variability in p_r. Furthermore, manipulating the activity of a single dendritic branch leads to a spatially selective decrease in p_r. These results indicate that local dendritic activity is the major determinant of basal release probability, and theoretical simulations suggest that this retrograde regulation provides a means to maintain synchronously activated synapses in their operational range.

Contents

List of Figures

Chapter 1

Introduction

Synapses are unique specializations of nerve cells that are found in animals as diverse as the snail, the fly or the human. Like many other cellular features, evolution has perfectly shaped the combination of structure and physiology to ensure that the synapse is successful in its central task - the transmission of information between neurons, where precision, reliability and speed ultimately determines the success of converting sensory input into an appropriate motor output. The study of synaptic physiology is more than 100 years old, but today, more than ever, it is clear from advances in genomics, proteomics and functional imaging techniques that we are still far from fully understanding the transmission of electrical signals from one neuron to another. This chapter starts by briefly outlining our current understanding of synaptic transmission and setting it in its historical context. It then focuses on the topic of this thesis - the probability of releasing neurotransmitter - summarising relevant aspects of this parameter and the experimental techniques available for its study.

1.1 The *inescapable* necessity for specialised contacts between neurons

Like the majority of what is known about synaptic physiology, the junction between motor nerve endings and skeletal muscle - the neuromuscular junction (NMJ) - was the first place where the existence of a special contact for transmission of nerve impulses was suggested. In the early 1860s Wilhem Krause and Willy Kuhne (Cajal, 1923) using basic histological techniques showed that there was a clear separation between nerve endings and the muscle fibers of amphibians, and in 1878 Claude Bernard published a series of experiments using the poison curare to demonstrate that nerve and muscle could be excited independently from each other (Cowan et al., 2001). However, although important and interesting in their own right, the findings of the neuromuscular junction usually seek confirmation in the studies of the spinal cord and brain. In the early second half of the 19th century, knowledge about the constituents of the grey matter was rather limited. Techniques to allow the visualisation of nerve cells had been developed by several histologists and neurologists, such as Meynert, Weigert or Ranvier, but they all lacked the ability to selectively and fully stain the processes of these cells. It was not until 1873 that this problem was solved by the italian Camillo Golgi, who found that processes of nerve cells strongly attract a precipitate of silver chromate (Cowan et al., 2001). This *reazione nera*, now known as the Golgi method, had also the great advantage of only staining about 1% of the cells, which made detailed morphological analysis of the grey matter constitution possible. However, given the formulation of the cellular theory by Schwann and Virchow 40 years before and what had been proposed for the neuromuscular junction, Golgi interpreted his histological preparations in a surprising way. Following the observations of Gerlach in 1872 of a fine network of fibres in sections of the brain and spinal cord, and the suggestion that these resulted from the anastomosis of neuronal processes (Peters et al., 1976), Golgi further expanded and reinforced the view that the grey matter

was a continuous reticulum resulting from the fusion of axonal ramifications - later to be known as the *reticular theory*, which gained support of all the major neurohistologists at the time (Cajal, 1923). Two notable exceptions were Wilhelm His and August Forel, who by studying the embryonic development of neurons and the atrophy of injured neurons respectively, suggested that nerve cells had *free endings*, which implied that they were individual entities (Cowan et al., 2001). But it was not until the methodical, perfectionist, highly detailed and labour intensive work of Santiago Ramon y Cajal that the so called *neuron doctrine* gained a full experimental foundation. Improving Golgi's technique to study all parts of the brain and spinal cord (Figure 1.1), Cajal ironically reached a diametrically opposite conclusion. In his own words (Cajal, 1923):

> The laws governing the morphology and connections of the nerve cells in the grey matter, which became patent first in my studies of the cerebellum, were confirmed in all the organs which I successively explored. I may be permitted to formulate them at once: 1. The collateral and terminal ramifications of every axis cylinder end in the grey matter, not in a diffuse network as maintained by Gerlach and Golgi, and most other neurologists, but by free arborizations arranged in a variety of ways (...). 2. These ramifications are applied very closely to the bodies and dendrites of the nerve cells, a contact or articulation being established between the receptive protoplasm and the ultimate anoxic branchlets. From the anatomical laws stated spring two physiological corollaries: 3. Since the final rootlets of the axis cylinders are applied closely to the bodies and dendrites of the neurons, it must be admitted that the cell bodies and their protoplasmic processes enter into the chain of conduction, that is to say, that they receive and propagate the nervous impulse, contrary to the opinion of Golgi, according to whom these parts of the cell perform a merely nutritive role. 4. The continuity of the substance between cell and cell

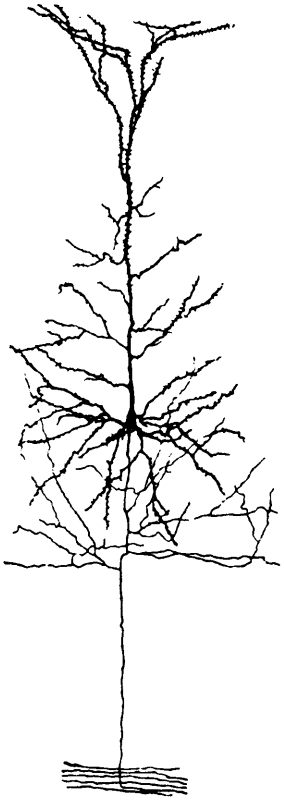

Figure 1.1: Cajal's drawing of a neuron stained with the Golgi method. Image shows a single pyramidal cell from the rabbit cerebral cortex. Adapted from Cajal (1995).

> being excluded, the view that the nerve impulse is transmitted by contact, as in the junctions of electric conductors, or by an induction effect, as in induction coils, becomes inescapable.

Although it was necessary to wait almost 50 years for electron microscopy to be applied to the nervous system, and unequivocally show the separation of cellular membranes to finally convince all neuroanatomists of the *neuron theory* (in 1906 in his Nobel lecture, Golgi referred to the neuron doctrine as *generally recognised to be going out of favour*), the idea that the grey matter is composed of structurally and functionally independent units gained wide

acceptance. It was thus *inescapable*, as Cajal put it, that some kind of contact was established between neurons. Despite the very limited information about these contacts, and while still arguing for their existence, in 1897 Charles Sherrington, whose lifetime work on spinal reflexes and inhibition not only further supported the neuron theory but also elucidated some fundamental features of synaptic transmission, wrote in the seventh edition of Michael Foster's *Textbook of Physiology* (Foster and Sherrington, 1897):

> So far as our present knowledge goes we are led to think that the tip of a twig of the [axonal] arborescence is not continuous with but merely in contact with the substance of the dendrite or cell body on which it impinges. Such a special connection of one nerve cell with another might be called 'synapsis'.

It is interesting to note that while nowadays the term *synapse* usually refers to the static structural connection between an axon and a dendrite or cell body, Sherrington was very keen that the term adopted did not imply a passive union, as the term *junction* originally proposed to him by Sharpey Schafer did, but that it rather suggested an essentially active process between neurons (Sherrington, 1897):

> As to *junction* I feel we are less easily reconcilable. (...) The mere fact that junction implies *passive* union is alone enough to ruin the term (...). Synapse, which *implies* a catching on, e.g., by one wrestler of another - is really much closer to the mark. But I am not a bit wedded to the word: if you could suggest an English word containing the notion which is not already overburdened with applications. I have been trying to find one but cannot. *Conjunction* is even worse than *junction.*

1.2 The structure of synapses

Since the first electron microscopy (EM) studies of the nervous system in 1955 (De Robertis and Bennett, 1955; Palay and Palade, 1955), our knowledge of synaptic anatomy has evolved greatly, moved not only by advances in electron microscopy techniques, but also by the constant necessity for having a *palpable* support to hypotheses of synaptic physiology. There are two very distinct classes of synapses: electrical synapses, that propagate the electrical impulse directly, and chemical synapses, in which the propagation of the signal occurs via a chemical intermediate. Electrical synapses are standard gap junctions between neurons, and apart from having been the delight of the 19th century *Reticularists* had they been known at the time, they are traditionally thought to be involved in the synchronisation of neuronal circuits (Cowan et al., 2001) and will not be discussed here. As for chemical synapses (henceforth referred to as synapses) in the central nervous system (CNS), their morphological diversity is immense, presumably an evolutionary sub-specialisation to the specific neural circuit they belong to. This section will briefly describe the general features of excitatory synapses in the brain, which also apply to the hippocampal synapses studied in this thesis.

In the most typical case, synapses are formed between expansions of axonal branches or their endings - the presynaptic compartment, and a dendrite or the cell body of the neuron - the postsynaptic compartment. They are defined by specializations of the plasma membrane at either site of contact and the extremely close apposition of the pre and postsynaptic membranes. The presynaptic site is populated by neurotrasmitter-filled vesicles, while the postsynaptic membrane is thickened by neurotransmitter receptors and numerous scaffolding proteins (Figure 1.2A).

1.2.1 The presynaptic compartment

The main task of the presynaptic compartment is to release neurotransmitter upon electrical stimulation. Not surprisingly, the morphological hallmark of

this compartment is the presence of 20-50 nm electron-lucent spherical vesicles, roughly uniform in size and diameter, filled with glutamate (Harris and Sultan, 1995; Schikorski and Stevens, 1997). Description of synaptic vesicles was first presented almost simultaneously in April 1954 by George Palade (on the rat CNS, communication to the America Association of Anatomists, Palay and Palade 1955), and by Eduardo de Robertis and Stanley Bennet (on the frog sympathetic ganglia and neuropile of the earth worm nerve cord, communication to the American Physiological Society) who in their fist paper on the subject curiously noted (De Robertis and Bennett, 1955):

> A vesicular or granular component of the synapse is described, and is deemed to be of interest and worthy of further study in view of the special permeability and pharmacological properties attributed to synaptic membranes.

There are on average 270 vesicles in each hippocampal synaptic terminal (Schikorski and Stevens, 1997), although this number can vary from a couple of tens to many hundreds from terminal to terminal. Serial sectioning and 3D reconstruction shows that this compartment has roughly a volume of 0.1 μm^3 and that synaptic vesicles are usually grouped in a cluster of variable degrees of compactness (Harris and Sultan, 1995; Schikorski and Stevens, 1997). Although, as described below, it is possible to functionally identify several different pools of vesicles, there appear to be no clear spatial or morphological correlates of these pools within the main cluster. One exception is a group of 2-30 vesicles (Harris and Sultan, 1995; Schikorski and Stevens, 1997) that are in direct contact with the region of the plasma membrane where vesicle fusion occurs - morphologically docked vesicles - which include a pool of vesicles with a high probability of undergoing full fusion and which will be discussed later in more detail. Synaptic vesicles have been extensively characterized biochemically, and it is clear that their membrane is heavily populated by an ever growing list of proteins that either participate in ion or neurotransmitter transport, or in one of the several steps of vesicle trafficking (Takamori et al., 2006).

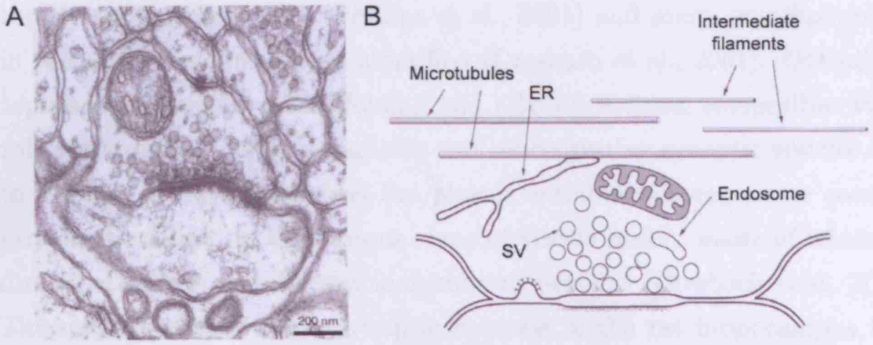

Figure 1.2: Ultrastructure of the synapse. (A) Electron micrograph of a synapse where several synaptic vesicles can be recognised in the presynaptic compartment. The active zone is identified by a dense matrix, where some vesicles appear to be docked at the presynaptic plasma membrane. A thick membrane undercoat is present postsynaptically, the postsynaptic density, in precise register with the specialised portion of the presynaptic plasma membrane. (B) Schematic illustration of the major cellular organelles present in the presynaptic compartment. SV, synaptic vesicle; ER, endoplasmic reticulum. Adapted from Cowan et al. (2001).

The other very characteristic ultrastructural component of the presynaptic compartment is the region over which vesicles interact with the presynaptic membrane in the process of neurotransmitter release - termed the active zone (Couteaux and Pecot-Deschavassine, 1970; Landis et al., 1988). In most EM preparations this portion of the membrane appears to be thicker or denser than others, which is mainly due to a submembranous coat of electron dense fibrillar material that sends short, ill defined filaments back to the vesicle cluster area (Landis et al., 1988). Freeze-fracture EM studies of this area, when the fracture plane separates the lipid bilayer and exposes the hydrophobic interiors of the membranes *en face* views, have revealed that these dense fibrillar projections form a hexagonally organized *presynaptic vesicular grid*, whose intervals or pits are thought to be specialised membrane areas for vesicle docking (Pfenninger et al., 1972; Ceccarelli and Hurlbut, 1980). This presynaptic grid has recently been isolated and characterized ultrastruc-

turally and biochemically (Phillips et al., 2001) and many proteins present in the active zone have been identified (Dresbach et al., 2001). Overall, cytoplasmic proteins have scaffolding and adaptor actions, compatible with a role of the active zone in organising and concentrating synaptic vesicles close to the site of fusion, whereas the plasma membrane components contains protein specialised in the various steps of vesicle fusion, many of which are direct partners of specific vesicle membrane proteins (Dresbach et al., 2001). The majority (90%) of presynaptic boutons in the rat hippocampus have only one clearly distinguishable active zone, with a mean area of 0.039 μm^2 and a high coefficient of variation (0.56), while their shape varies greatly without any particular arrangement being preferred (Schikorski and Stevens, 1997). A strong positive correlation has been reported between the presynaptic compartment volume, active zone area, number of docked vesicles and total number of vesicles, indicating that these parameters scale together with the size of the bouton (Schikorski and Stevens, 1997; Murthy et al., 2001).

This basic description and the specific values relate to EM studies of fixed rat brain. Schikorski and Stevens in their 1997 work also studied hippocampal synapses from neurons in culture, similar to the ones used in this thesis. They found no major differences between the two groups, but a clear tendency for smaller active zones and vesicle clusters, fewer docked vesicles and a higher percentage of boutons containing more than one active zone. These variations, from the intact brain, are unlikely to be representative of cultured hippocampal synapses in general given the reduced sample size of this study and the variability of culture conditions between different laboratories. Rather, they highlight the point that synapses in culture retain all the identifiable ultrastructural specialisations that are observed in the brain.

Apart from these specialisations, EM shows that the presynaptic compartment also contains many other cellular organelles common to other parts of the neuron (Figure 1.2B). However, they notably lack the machinery for bulk protein synthesis and therefore rely on cytoskeletal elements such as intermediate filaments, for the transport of necessary components from and

back to the cell body. The high energy required by the synaptic vesicle cycle is provided by mitochondria which are frequently observed close to the vesicle cluster, as are elements of the smooth endoplasmic reticulum whose main function is to act as a store of intracellular calcium. Endocytotic organelles can be identified, and probably result not only from vesicle retrieval but also from regular housekeeping functions (Cowan et al., 2001). Interestingly, the active zone area and its close surroundings is exclusively populated with vesicles and no other organelles (Landis et al., 1988).

1.2.2 The postsynaptic compartment

The plasma membrane of the postsynaptic compartment that directly opposes the presynaptic site is filled with an array of mostly transmembrane proteins that act as different kinds of neurotransmitter receptors, probably arranged heterogeneously and responsible for converting the chemical signal back into an electrical one. Underneath it lies a dense matrix known as the *postsynaptic density* (PSD), originally defined ultrastructurally as an electron-dense thickening, 40-50 nm wide and up to a few hundred nanometers long. Numerous molecules have been found to be present and specially enriched in the postsynaptic density, including cytoskeletal elements, signal transduction proteins, adhesion molecules and enzymes. Together, they not only act as an anchor for neurotransmitter receptors but constitute an organelle in their own right, capable of profoundly shaping synaptic transmission (Cowan et al., 2001).

1.2.3 The synaptic cleft

The synaptic cleft is the space between the pre and postsynaptic cellular membranes where neurotransmitter is released. This space is on average 20 nm wide with a variable length (Schikorski and Stevens, 1997; Savtchenko and Rusakov, 2007), and has an extremely small volume ($\sim 2\text{x}10^{-3}\mu\text{m}^3$, Harris and Sultan 1995) which presumably is essential to generate a high con-

centration of glutamate after the release of a limited number of molecules. Instead of being a void space, the cleft is filled not only with proteins of the extracelullar matrix but also with interacting extracellular domains of many pre and postynaptic membrane proteins. Besides their obvious function in maintaining both sides of the synapse closely apposed and aligned, the molecules in the synaptic cleft are necessary for the development of the synaptic specializations themselves, and are prime candidates for mediating retrograde signals, which allow the postsynaptic site to modulate the presynaptic function.

1.3 Chemical synaptic transmission

At the end of the eighteen century Luigi Galvani elicited contractions in the frog limb muscles by passing current through its medulla, and posited that electricity is propagated from nerves to muscle. One hundred years later, Bois-Reymond discovered that nerves were electrically polarised at rest - *resting potential*, and that stimulation elicited the active propagation of an electrical potential along the nerve - *action potential* (AP). At this time, he proposed that the transmission of electrical signals from the nerve to the muscle was either chemical, via *a stimulatory secretion in the form of a thin layer of ammonia, lactic acid, or some other powerful stimulatory substance*, or purely electrical (in Cowan et al., 2001). The first experimental evidence for a chemical type of transmission came from J. Newport Langley in the early 1900s, when he performed a series of experiments on the peripheral autonomic ganglia using nicotine and curare, which led him to the suggestion that *the nervous impulse should not pass from nerve to muscle by an electric discharge, but by the secretion of a special substance at the end of the nerve* (Langley, 1906). More definitive experiments were made in 1921 by Otto Loewi, who after having famously dreamt of the experimental design, demonstrated that the vagal inhibition of the frog's heart was mediated by a chemical substance - at the time termed *Vagusstoff* and later found to be

acetylcholine (ACh, see Cowan et al., 2001). In the next few years, Henry Dale and Wilhelm Feldberg provided evidence that the same was true for the smooth muscle innervation of other organs (Dale and Feldberg, 1934a,b; Feldmeyer and Sakmann, 2000). However, at the same time, inspired by the presence of an initial fast component in the response of smooth muscle synapses, and by the speed of transmission to skeletal muscle, John Eccles was a forceful advocate of the view that although prolonged and slow actions were chemically-mediated, fast transmission was strictly electrical (Eccles, 1982). His opinion started to change in 1936 following the publication of two papers by Dale, Feldberg, Marthe Vogt and G.L. Brown, which showed unequivocally that the motor nerve impulse released ACh at the neuromuscular junction, and that close intraarterial ACh application elicited a brief muscle twitch, thereby leaving little doubt about the role of ACh in neurotransmission (Brown et al., 1936; Dale et al., 1936). Two years later, the discovery of the synaptic potential by Gopfert and Schaefer and its initial studies by Stephen Kuffler, made Eccles change to be in *complete support of ACh transmission* (Eccles, 1982) for the NMJ. However, the nature of transmission in CNS synapses was still unknown, and the *soup versus spark controversy* was far from finished. Driven by the lack of evidence of ACh action in the CNS and by the fact that all experiments to date could still be interpreted by an electrical model of transmission, Eccles continued to pursue this hypothesis and eventually extended it to synaptic inhibition in the spinal cord. But it was Eccles himself who in 1951, after having formulated an ingenious and very rigourous and testable Popperian hypothesis of inhibition, proved his theory wrong. As he describes it (Eccles, 1982):

> A microelectrode had been inserted into a biceps-semitendinosus motorneuron (...) we had recognised that on the electrical model for inhibitory action the microelectrode would be in a brief positively going electrical field, whereas on the chemical hypothesis ... it would record a brief negative potential. Thus it was a clear test. If the quadriceps volley cause the trace to go up it was

electrical, if down it was chemical. It went down!

Many years and experiments later, it is now clear that chemical transmission is the major mode of signal transmission in the peripheral and central nervous system, and Eccles again, provides an enlightening statement on its *raison d'être* (Eccles, 1982):

> We are left with the impression that chemical transmission was an essential evolutionary advance which made possible the design of brains with all the infinite complexity required for higher nervous functions. Chemical transmission is much more effective and selective, and it gives a specificity of action from neuron to neuron, together with a large amplification factor in the transmission process. But, even more important, chemical transmission provides the opportunity for inhibition that plays such a key role in the elegant patterns of activity that we now are beginning to understand in the mammalian brain. Electrical inhibition requires complex neuronal design; it is much less effective, although quicker in action.

1.3.1 The quantal nature of transmitter release

By the early 1950s there was a clear sense that synaptic transmission was chemical in nature, and that at the neuromuscular junction it was mediated by ACh. During this time, Bernard Katz and his colleagues, working at University College London made a series of fundamental observations on the *secretory function of the motor nerve ending* (Katz, 1969) that would irreversibly change the field of synaptic transmission. When making intracellular recordings from the motor end-plate, Katz and Paul Fatt noticed that if they watched the oscilloscope at high amplification they would constantly find randomly occurring brief depolarisations, of about 0.5 mV with a rapid rise and a slower decay, the shape closely resembling a full blown end plate potential (EPP), albeit spontaneous and smaller in amplitude (Figure

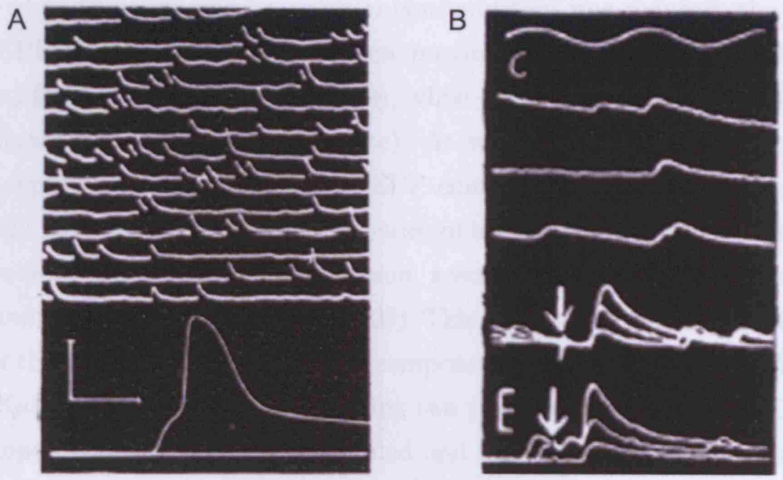

Figure 1.3: Intracellular recordings from the motor end-plate. (A) High amplification traces showing spontaneous activity at the end plate, where several miniature end-plate potentials can be identified. Lower trace shows the response to a nerve stimulus at lower amplification for comparison. Scale bars: 50 mV and 2 ms for the lower part, and 3.6 mV and 47 ms for the upper part. (B) Recording in low extracellular calcium concentration. The upper three traces show spontaneous potentials and the lower records show EPP responses to stimulation (stimulus marked by arrow). Step-wise fluctuations of the EPP can be observed, and the amplitude of the smallest response is similar to an mEPP. From Fatt and Katz (1952).

1.3A). Although this was initially attributed to a local injury discharge at the nerve endings, Fatt and Katz pursued its investigation in *nerve-muscle preparations which seemed to be above any such suspicion* and provided a full description of what they termed *miniature end-plate potentials* (mEPPs).

They showed that mEPPs were due to release of ACh from the nerve terminal, and suggested that this release occurred from *discrete ACh-release patches within them [nerve terminals]* given the constancy of their amplitude (Fatt and Katz, 1952, 1950b). Furthermore, they observed the *curious effect*

that when the extracellular calcium concentration was reduced, the size of the EPP diminished as it had been previously reported (Fatt and Katz, 1950a; Del Castillo and Stark, 1952), while the size of the mEPP remained unaffected (mEPPs were *all-or-none*). At very low calcium concentrations, they reported that the size of the EPP could sometimes be *no larger than a single miniature e.p.p.* and that series of nerve impulses evoked responses whose sizes varied *in a step-like fashion, seemingly corresponding to multiples of a miniature discharge* (Figure 1.3B). This led them to the initial idea that under these conditions the EPP was composed of definite *quanta* of ACh (Fatt and Katz, 1952). During the following two years, Katz and Jose del Castillo developed this idea in a more detailed and quantitative way, and proposed what has since been known as the *quantal theory* of synaptic transmission (Del Castillo and Katz, 1954). By adjusting the calcium concentration to a point where the nerve stimulus failed to elicit an EPP 50% of the times, they restated that the EPP is built up of multiple mEPPs or *quanta*. They suggested that there is a population of N units capable of responding to a nerve impulse, and that each one has an average probability p_r, of actually responding. The mean number of units responding to a nerve impulse, m, is therefore:

$$m = Np_r \tag{1.1}$$

termed the *quantal content*. Katz and del Castillo then argued that under their recording conditions, p_r should be very small and n rather large, such that the number of units that make up the EPP in a large series should follow a Poisson distribution. They succeeded in proving this hypothesis experimentally, and demonstrated that the amplitude histogram of EPP responses has predictable and individualised peaks at fixed intervals, revealing the underlying quantal unit they are composed of. This was taken as very good evidence for the quantal nature of synaptic transmission at the motor-end plate, and numerous subsequent studies confirmed this theory.

At that point, the mechanism of ACh release was unknown, and it was initially proposed that it could result from either the spontaneous or evoked

electrical excitation of *release spots* in the membrane terminal (Fatt and Katz, 1952). However, as already mentioned, synaptic vesicles were described only one year after the quantal hypothesis had been put forward, and it did not take long for them to be the prime candidates for the quantal storage and release of ACh (Del Castillo and Katz, 1955). In a review in 1956, del Castillo and Katz wrote (Del Castillo and Katz, 1956):

> Recent electron microscope studies have shown ...granules or vesicles ... which may well be the intracellular corpuscles to which ACh is attached. (...) One might suppose that when a critical collision occurs between an intra-cellular ACh-carrier and the membrane of the nerve terminal the two barriers opened simultaneously and the ACh-contents of the carrier particle are suddenly discharged.

This idea became known as the *vesicle hypothesis* and rapidly established itself as the leading hypothesis in the field. Plausible as it was, it proved remarkably hard to provide convincing experimental evidence to support it. It took nearly 15 years until ACh was found to be present in synaptic vesicles by the biochemical studies of Paul Whittaker (Whittaker, 1968), and to show ultrastructurally that vesicles interact and fuse with the plasma membrane upon nerve stimulation. This was initially hinted by Couteaux who suggested that that plasmalemmal pockets in EM preparations could correspond to vesicles caught in the act of exocytosis (Couteaux and Pecot-Deschavassine, 1970), and confirmed by the experiments of John Heuser and Tom Reese who first showed that synaptic vesicles were depleted from the terminal after intense stimulation (Heuser and Reese, 1973) and that by precisely timing stimulation with freeze-fracture EM, it was possible to reliably find vesicles in several states of fusion with the membrane and correlate their number to the quantal content estimated by electrophysiological recordings (Heuser et al., 1979). Although the vesicle hypothesis continues to be challenged (Vautrin and Barker, 2003), more recent high resolution amperometric

measurements in the leech (Bruns and Jahn, 1995; Bruns et al., 2000), capacitance measurements in the Calyx of Held (Sun and Wu, 2001), and live imaging of single vesicle dynamics in rat hippocampal synapses (Gandhi and Stevens, 2003; Aravanis et al., 2003) or in the retina bipolar cells using Total Internal Reflection Fluorescence microscopy (Zenisek et al., 2000), to quote a few examples, make the quantal release of neurotransmitter by vesicles the most likely scenario.

While elegant and direct electrophysiological evidence for the quantal theory is abundant for the NMJ, its demonstration for synaptic transmission in the CNS has been much harder. The reasons behind it are varied, and they mainly revolve around the fact that one neuron receives many synapses from different inputs, which makes it impossible to relate the miniature events recorded to the evoked response of the input under study, and that even one axon can make multiple synapses in different dendritic locations, thereby generating variable quantal amplitudes due to different degrees of electrotonic attenuation. Other factors that contribute to the difficulty in testing the quantal hypothesis in the CNS synapses are the small size of individual quanta, an apparently high amplitude variability of single quanta, and the instability of most preparations which typically only allows the collection of small samples. These difficulties are clearly reflected in the great variety of methods and techniques developed to date for the analysis of synaptic potentials in the CNS, some of which will be discussed later. Even so, there are several seemingly successful quantal descriptions of CNS synaptic transmission. These come from studies using sharp microelectrode recordings, including 1) the work by M. Kuno (Kuno, 1964) in group 1 synapses on motorneurons using the method of failures; 2) the use of amplitude histograms deconvolution in the same neurons (Edwards et al., 1976; Jack et al., 1981), and in the large excitatory postsynaptic potentials (EPSPs) of the dorsospinocerebellar tract synapses (Walmsley et al., 1987); 3) the finding of very clear histogram peaks in the inhibitory synapses to Mauthner cells (Korn et al., 1981, 1982); 4) the analysis of EPSPs in CA1 pyramidal cells of the hippocampus (Sayer et al.,

1989; Larkman et al., 1991); as well as the application of the patch-clamp technique to 1) the inhibitory synapses of the dentate gyrus (Edwards et al., 1990), 2) hippocampal CA3 and CA1 pyramidal cells (Malinow, 1991; Kullmann and Nicoll, 1992; Jonas et al., 1993) and 3) hippocampal cell cultures (Bekkers and Stevens, 1995), to quote a few examples (reviewed in (Redman, 1990; Korn and Faber, 1991; Stevens, 1993; Bekkers, 1994; Walmsley, 1995)). However, while all of these studies provide indirect support for the quantal composition of synaptic potentials, direct evidence that Bernard Katz theory is valid in the CNS came from Jeffrey Isaacson and Bruce Walsmley, when in 1995 they were able to count the number of evoked quanta directly in the auditory brainstem and show that their release was Poisson in nature, in the same way Katz and his colleagues did so in the frog NMJ (Isaacson and Walmsley, 1995).

1.3.2 The synaptic vesicle cycle

Since the work of Heuser and Reese in 1973 (Heuser and Reese, 1973), we know that not only synaptic vesicles fuse with the presynaptic plasma membrane and release their contents, but also that they are somehow locally formed and reused. This process is known as the vesicle cycle and is the fastest and most tightly regulated of all cellular transport pathways (Sudhof, 1995), with the prime function of coupling the action potential to the release of neurotransmitter (Figure 1.4A).

The first step of this process may be considered to be the uptake of neurotransmitter molecules into synaptic vesicles, a process that relies on specialised transporter proteins and on the energy provided by a vacuolar proton pump that generates an electrochemical gradient across the vesicle membrane (Cowan et al., 2001). Neurotransmitter-filed vesicles then diffuse towards the active zone, and most likely guided by the highly organized ultrastructural apparatus mentioned above they reach and attach to the presynaptic plasma membrane - a process known as *docking*. Docked vesicles are then thought to undergo a rate-limiting *priming* step, which probably constitutes a par-

tial fusion reaction. Priming involves an ordered sequence of protein-protein interactions, which in a basic view results in the formation of a core trimeric complex between two plasma membrane proteins - syntaxin and SNAP-25 - and one vesicle membrane protein - synaptobrevin/VAMP, that forces the vesicle and plasma membrane close together. Although it is not clear if this step ends in a hemi-fusion of membranes resulting intermediate state, or a full one with a fusion pore in some kind of blocked state, primed vesicles only require a rise in the calcium concentration of the presynaptic compartment to complete exocytosis (Sudhof, 1995). Docked and primed vesicles have the same ultrastructural appearance and are thought to correspond to the morphologically docked vesicles already described.

The calcium requirement for neurotransmission has long been known (Del Castillo and Stark, 1952). After the action potential arrives at the presynaptic terminal, a well described co-operative action of calcium (Dodge and Rahamimoff, 1967) is necessary for the release process itself (and not for the spread of depolarization, (see Katz and Miledi 1965a)). The details of this *calcium hypothesis* have been extremely difficult to elucidate, and most of our knowledge to date comes from studies on the squid giant presynaptic terminal and on the calyx of Held. The link between the AP-induced depolarization of the terminal and the entry of calcium depends on the presence of a high density of multiple types of voltage-gated calcium channels in the presynaptic membrane. Once the channels are open, computer simulations and diffusion models predict that calcium enters the terminal and generates a very big and highly localized rise in concentration. Experiments using calcium chelators with different binding rates, calcium indicator proteins or calcium uncaging, amongst others, tentatively support the view that signalling occurs within microdomains, composed either by a single channel or by overlap of several channels (Meinrenken et al., 2003; Augustine et al., 2003; Schneggenburger and Neher, 2005). This implies a very tight geometry between the calcium channels and the Ca^{2+}-binding effector proteins - *calcium sensors* -that trigger the final stages of vesicle fusion. Since

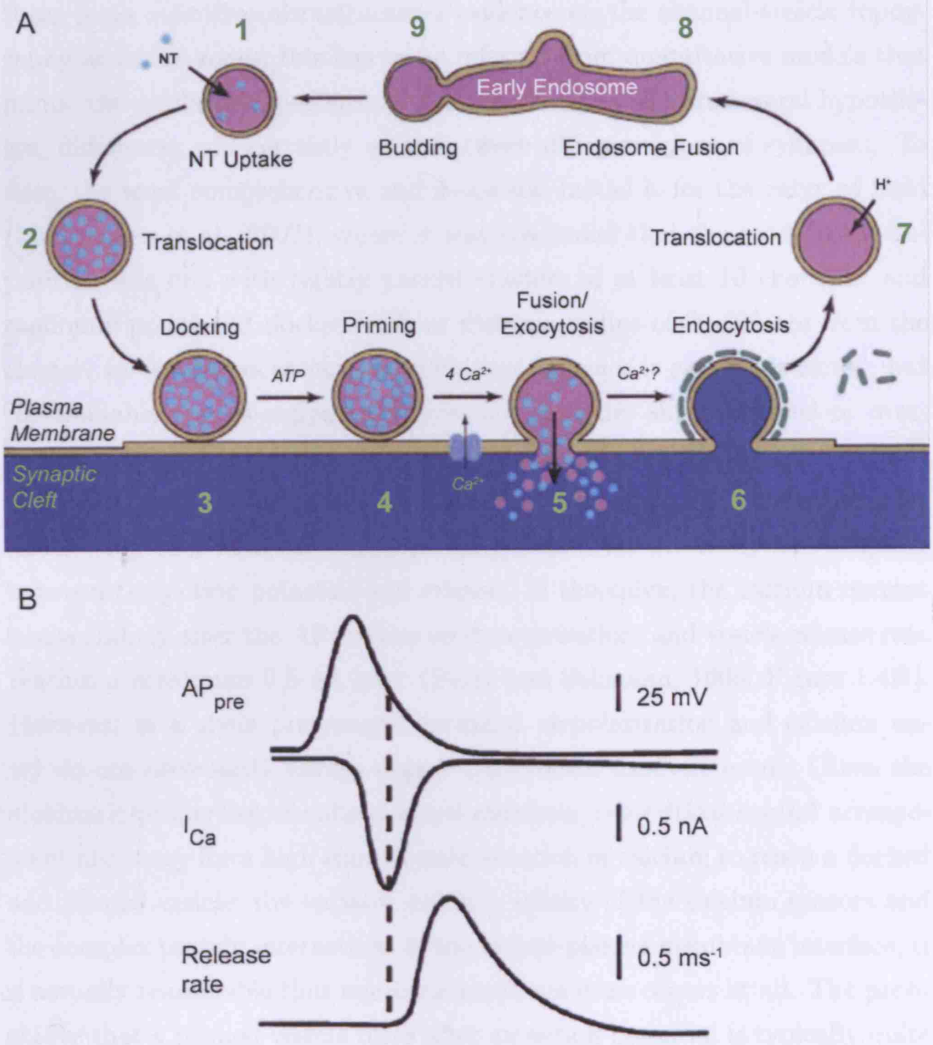

Figure 1.4: The process of neurotransmitter release. (A) Cartoon illustrating several general steps in the synaptic vesicle cycle, as described in detail the text. Adapted from Sudhof (1995). (B) Reaction sequence and time course of neurotransmitter release in the Calyx of Held. Time-locked traces show the presynaptic action potential waveform (top), the resulting calcium current in the presynaptic terminal (middle), and the inferred rate of neurotransmitter release that results from it (bottom). Adapted from Meinrenken et al. (2002).

there is no definitive ultrastructural evidence on the channel-vesicle topography at active zones, this has to be inferred from quantitative models that mimic the available experimental data. Although there are several hypotheses, differences will certainly exist between different types of synapses. To date, the most comprehensive and successful model is for the calyx of Held (Meinrenken et al., 2002), where it was concluded that the most likely disposition was one with tightly packed clusters of at least 10 channels, and randomly positioned docked vesicles within a radius of 30-300 nm from the cluster. In the hippocampus, experimental evidence is rather restricted, but the available results support the presence of either single channel or overlapping domains of calcium signaling (Augustine et al., 2003). The result of these very localized calcium dynamics in the triggering of neurotransmitter release, together with the vesicle priming step, is an extremely fast coupling between the action potential and release. In the calyx, the calcium current peaks shortly after the AP maximum depolarization, and vesicle release rate reaches a maximum 0.5 ms later (Borst and Sakmann, 1996, Figure 1.4B). However, in a given presynaptic terminal, depolarization and calcium entry do not necessarily always trigger a successful exocytic event. Given the stochastic properties of voltage-gated channels, the critical spatial arrangement necessary for a high enough concentration of calcium to reach a docked and primed vesicle, the variable calcium affinity of the calcium sensors and the complex protein interactions at the vesicle-plasma membrane interface, it is actually remarkable that neurotransmitter release occurs at all. The probability that a primed vesicle fuses after an action potential is typically quite low, and different docked vesicles can have different probabilities, presumably a reflection of their topography or some unknown intrinsic differences (Meinrenken et al., 2002; Trommershauser et al., 2003). Interestingly, the exact amplitude and time course of the calcium current are directly reflected in the magnitude and time course of release, emphasising the view that the entry of calcium in the presynaptic terminal proportionally and temporarily raises the probability of vesicle fusion, which is minimal in the resting state (Katz

and Miled, 1965; Barrett and Stevens, 1972; Borst and Sakmann, 1999). As for the molecular identity of the calcium sensor, despite a lack of clear consensus and definitive evidence, synaptotagmins have been the most popular candidates for the job. They are integral vesicle membrane proteins with two calcium binding domains, and a variety of genetic approaches indicate that the interaction of calcium with synaptotagmins is crucial for exocytosis. One proposed mechanism of action is that the calcium binding to synaptotagmin causes one of its domains to partially insert in the presynaptic plasma membrane, resulting in the destabilisation of the fusion intermediate and opening of the fusion pore (Sudhof, 2004).

After vesicle exocytosis and release of neurotransmitter, the elegant use of extracellular endocytic tracers in the EM studies of Heuser and Reese showed that synaptic vesicles are locally recycled. Exactly how the presynaptic terminal accomplishes this is still a matter of debate. The most widely accepted model and the one with direct experimental evidence is that after exocytosis and full collapse of the vesicle into the plasma membrane, a standard clathrin-mediated endocytosis selectively retrieves the membrane and the vesicular components. This is supported not only by the ultrastructural identification of clathrin-coated pits at sites close to the active zone (particularly after stimulation, Heuser and Reese, 1973; Gad et al., 1998), but by numerous genetically induced disruptions of the clathrin pathway in a variety of organisms (Cowan et al., 2001). After endocytosis, retrieved vesicles are either immediately refilled with neurotransmitter and return to the release site (Murthy and Stevens, 1998), or they are transported to and sorted in endossomal intermediates from which new vesicles are formed, the whole process requiring 30-60 s for a vesicle to be available again for exocytosis in rat hippocampal neurons (Ryan and Smith, 1995). One fascinating aspect of synaptic vesicle recycling is the strict coupling between exo and endocytic events, a fundamental balance necessary to prevent changes in the presynaptic membrane size (Cowan et al., 2001; Gad et al., 1998). Apart from clathrin-mediated endocytosis, two other mechanisms have been proposed to

operate. The first one was suggested by Ceccarelli exactly at the same time as Heuser and Reese published their work (Ceccarelli et al., 1973) and has been a matter of intense debate in the field, with a consensus far from being reached. Moved by the extremely fast rate of vesicle recycling apparent in some studies (~1.6 s, Klingauf et al., 1998; Pyle et al., 2000), this model proposes that neurotransmitter is released through the fusion pore without full membrane collapse, and that vesicles are retrieved by a direct and rapid reversal of this process - commonly referred to a *kiss-and-run* (Fesce et al., 1994). In hippocampal neurons, although work from several groups using different imaging techniques supports this hypothesis (Klingauf et al., 1998; Aravanis et al., 2003; Harata et al., 2006; Gandhi and Stevens, 2003; Pyle et al., 2000), a recent study has called these results into question and proposed that the dominant mechanism of vesicle retrieval is clathrin-mediated endocytosis (Granseth et al., 2006). A third mode of endocytosis involves the formation of deep membrane infoldings away from the site of fusion, from which new vesicles are formed via a clathrin-mediated pathway(Royle and Lagnado, 2003; Takei et al., 1996).

1.3.3 Short-term plasticity and vesicle pools

The sequence of events outlined above is a summary of what happens after the arrival of a *single* action potential (i.e. isolated in time). Realistic inputs to neurons however, often generate a variable number of action potentials in close succession of one another, and the effects of this on neurotransmitter release are varied, depending on the type of synapse, number and frequency of the action potentials. In the simplest case, when a pair of closely spaced stimuli arrive at the presynaptic terminal - usually referred to as *paired pulse* stimulation - one of two outcomes is generally observed: the postsynaptic response increases - *facilitation*, or it decreases - *depression*, an effect termed *short-term plasticity* (STP) that typically does not last more than hundreds of milliseconds (Figure 1.5A). In all synapses studied, facilitation is entirely presynaptic in origin and it results from either an increase in the probability

of vesicle fusion and/or an increase in the number of release-ready vesicles. Since the experiments of Katz and Miledi it is clear that calcium ions are required for facilitation, and that this depends on the calcium that after the local rise diffuses and equilibrates throughout the terminal after the first stimulus - known as the *residual calcium hypothesis* (Katz and Miledi, 1968). This has been confirmed by several experiments in which the kinetics of facilitation are changed by manipulating calcium, and this type of data combined with theoretical modelling suggest that facilitation results from calcium interactions with a site (or more than one) different from the one that triggers fast transmitter release (Zucker and Regehr, 2002). In the case of depression, first described more that 60 years ago (Eccles et al., 1941), both pre and postsynaptic factors may be involved in the reduction of the synaptic response. The most common mechanism appears to be a presynaptic decrease in the release of neurotransmitter. In the simplest model, this reflects a temporary decline in the number of release-ready vesicles after a release event, which reduces the likelihood that any vesicles are released again upon stimulation. Interestingly, experimental evidence in some systems as well as modeling studies have suggested that the accumulation of residual calcium accelerates the recovery from this temporary depression, possibly by speeding up the replenishment of vesicles (Zucker and Regehr, 2002; Stevens and Wesseling, 1998) or alternatively by facilitating the release of vesicles in the cluster that under normal circumstances would not participate in the release process (Wu and Borst, 1999). Other mechanisms that have been linked to short-term depression are the desensitisation of postsynaptic ligand-gated receptors and the action of modulatory substances from the activated terminals, postsynaptic cells or even neighbouring cells (Zucker and Regehr, 2002). As it can be easily predicted from the basic mechanisms proposed for facilitation and depression, at most synapses both forms of short-term plasticity operate concurrently, and theoretical models that account for this are able to reproduce the experimental data with a satisfactory degree of success (Dittman et al., 2000; Sun et al., 2005). By adjusting the extracellular

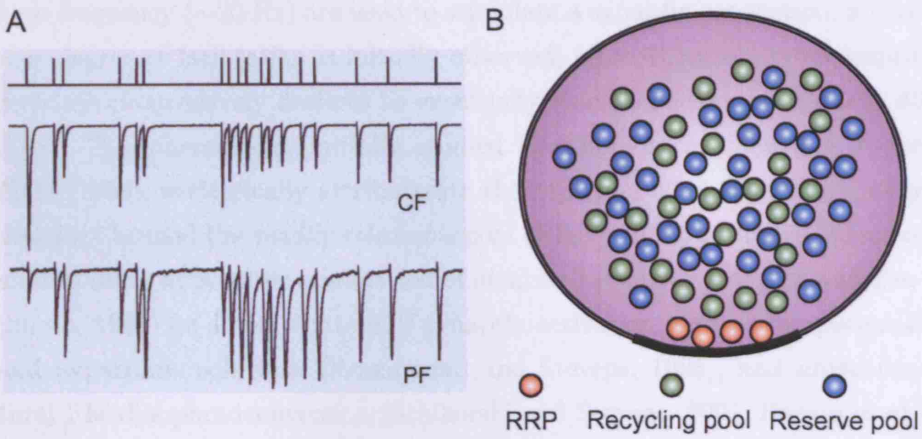

Figure 1.5: Short-term plasticity of synaptic responses and the different vesicle pools. (A) Response of a Purkinje cell to an irregular stimulation pattern (top, vertical bars indicate time of AP delivery) of the climbing fibre input (CF, middle) or of the parallel fiber input (PF, bottom). When two or more stimuli are close together, climbing fiber responses show depression while parallel fiber synapses facilitate. Adapted from Cowan et al. (2001). (B) Cartoon illustrating three different pools of vesicles in a presynaptic terminal. While the readily releasable pool (RRP) typically corresponds to vesicles apposed to the active zone, there is no apparent positional distinction between the recycling and reserve pools.

concentration of calcium and magnesium, facilitation and depression can be isolated to some extent and their time course inferred. Although there are marked heterogeneities between individual synapses (Dobrunz and Stevens, 1997), facilitation in CA1 hippocampal excitatory synapses starts as early as 5 ms, reaches a peak at around 15 ms and then decays exponentially over 500 ms (Dobrunz et al., 1997), with a time constant of 400 ms for neurons in culture (Mennerick and Zorumski, 1995). Paired-pulse depression starts immediately after vesicle release, and hippocampal synapses in culture recover exponentially with a time constant of 5 s (Mennerick and Zorumski, 1995).

In the hippocampus, when more than two action potentials at relatively

high frequency (~20 Hz) are used to stimulate a synaptic connection, a variable degree of facilitation is initially observed, after which the postsynaptic response progressively declines to eventually reach a plateau after about 40 APs. This phenomena, initially studied by Elmqvist and Quastel in the NMJ (1965), is classically attributed to the depletion of all the release-ready vesicles - termed the *readily releasable pool* (RRP). In hippocampal cultures, studies using hypertonic stimulation of identified synapses (Stevens and Tsujimoto, 1995) or a combination of synaptic activation with action potential and hypertonic solutions (Rosenmund and Stevens, 1996), and ultrastructural FM-dye photoconversion (Schikorski and Stevens, 2001; Harata et al., 2001b), have concluded that at the level of an individual synapse the RRP corresponds to the 2-30 vesicles that are morphologically docked at the active zone (reviewed in Rizzoli and Betz, 2005, see Figure 1.5B). If stimulation continues after the RRP has been depleted, the steady-state response observed reflects the balance between exocytosis and the refilling of release sites. The vesicle source for this refilling is a pool of vesicles that recycles continuously and is refilled by newly recycled vesicles - the *recycling pool* - constituting about ~40 percent of the total cluster (Darcy et al., 2006a). The remainder of vesicles make up a pool that does not directly participate in the vesicle cycle under any conditions - the *reserve pool* - and it has been proposed that this may potentially act as a reservoir for the recycling pool, which when accessed could rapidly increase its size without a need for a change in the overall size of the vesicle population (Harata et al., 2001a).

1.4 The quantal parameters q, N and p_r

The Katz quantal theory of synaptic transmission was originally derived under low extracellular calcium conditions where the probability of releasing one quanta is very low. As the NMJ has a very high number of release sites, the mean quantal content was shown to closely follow Poisson statistics. After the same results were obtained by a number of other labs, the question

shifted to whether this theory would hold true under more physiological conditions. If the number of release sites recorded is smaller, as it is usually the case for synapses in the CNS or focal extracellular recordings in the NMJ, and if higher concentrations of calcium are used, thereby increasing the probability of release, the probability that k quanta are released, *P(k)*, will follow a binomial distribution (Bennett and Kearns, 2000):

$$P(k) = \frac{N!}{(N-k)!\,k!}\, p_r^k (1-p_r)^{n-k} \tag{1.2}$$

where N is the number of release sites and p_r the average probability of each site releasing one quanta. The overall postsynaptic response size is obtained from the mean number of units active (equation 1.1) times the average response of each one of them to an individual quanta - q, the *quantal size*:

$$A = Np_rq \tag{1.3}$$

The applicability of the simple binomial model of release was first confirmed by Johnson and Wernig (1971), and Zucker (1973) in the NMJ and later by many reports in a variety of CNS synapses, where amplitude histograms were successfully fitted with binomial distributions (reviewed in Redman, 1990) and stationary (Silver et al., 1998; Reid and Clements, 1999) and non-stationary (Meyer et al., 2001; Scheuss and Neher, 2001) excitatory postynaptic currents (EPSCs) fluctuations followed the binomial prediction. Although these three quantal parameters are conceptually simple, their identity and properties are still a matter of ongoing debate.

1.4.1 The quantal size - *q*

The quantal size is the amplitude of the postsynaptic response elicited by release of the neurotransmitter contained in a single quanta. It thus depends essentially on two main factors: the number and quality of the postsynaptic receptors and the number of neurotransmitter molecules released. Which of these two factors is the most relevant is not clear, and one particularly controversial issue is whether the limited number of postsynaptic

receptors at CNS synapses are saturated by the release of a single quanta. If so, then receptor number will define the quantal size. If not, then the quantity of neurotransmitter released will be the determining factor. In the last two decades, numerous studies where quantal analysis was performed by fitting multiple Gaussian curves to amplitude distributions, estimated a very small single-site variance with a coefficient of variation (CV) sometimes under 0.10 (Walmsley, 1991; Redman, 1990). As this variability can be fully accounted for by the recording noise and the stochastic properties of postsynaptic receptors, it was concluded that there was not much room for other sources of variation and therefore it was likely that the receptors were saturated. However, other CV estimates based on the use of putative single site recordings, on experiments with competitive antagonists (Auger and Marty, 2000) and on single site glutamate iontophoresis (Liu et al., 1999; McAllister and Stevens, 2000) have suggested that in the hippocampus both α-amino-3-hydroxy-5-methylisoxazole-4-propionic acid (AMPA) and N-methyl-D-aspartic acid (NMDA) type receptors are unlikely to be saturated by one quantum. One recent modelling study proposes that postsynaptic receptor activation occurs in a limited ($\sim$250 nm) hotspot which is smaller than many synapses, implying that the quantal size is highly dependent on the density of the channels (Raghavachari and Lisman, 2004). Traditionally, the quantal size is estimated by recording miniature events. In the NMJ, mEPPs amplitude histograms have a gaussian distribution with a CV of 0.30. The observed variability amongst individual events was originally attributed to the recording noise, individual variation between sites and short-term plasticity interactions between closely released quanta (Fatt and Katz, 1952). In the CNS however, the mEPSC amplitude distribution is typically highly skewed to larger values (CV up to 0.60), and two basic explanations for this have been put forward: either it is due to an intrinsic variability of quantal sizes at each release site, or it primarily reflects the participation of many release sites with diverse characteristics (Bekkers and Clements, 1999; Auger and Marty, 2000). Attempts to resolve this issue by recording quantal sizes from

individual release sites have reached conflicting conclusions. In hippocampal synapses, single bouton stimulation with local perfusion of hyperosmotic or hyperkaelemic solutions (Bekkers et al., 1990; Tang et al., 1994; Liu and Tsien, 1995) or loose patch-clamp recordings from single boutons (Forti et al., 1997) showed either the same highly skewed distribution supporting the intrasite variability model, or a gaussian one suggesting that quantal sizes at individual sites have a low CV. Alternatively, quantal sizes can be estimated from evoked release at putative single release sites, and for hippocampal neurons both skewed and gaussian distributions were obtained (Chen et al., 2004; Auger and Marty, 2000). Taken together, the available data seems to suggest that for glutamatergic hippocampal synapses the quantal size is subject to both intra and intersite variations. For hippocampal slices the average quantal conductance is 0.2 nS and for cultured cell 0.8 nS (Bekkers et al., 1990).

1.4.2 The number of release sites - N

In any statistical model of synaptic transmission, N is defined as the number of sites that can release a quantum of neurotransmitter. The search for a physical or morphological correlate of N is as old as the first applications of binomial models to CNS synapses. While general speculations about it date back to the late 1960s (discussed in Zucker, 1973), the first work to address this was made on the inhibitory synapses onto the Mauthner cell, where Korn et al reported a striking correlation between the binomial N obtained from statistical analysis of inhibitory postsynaptic potential (IPSP) amplitudes in paired recordings and the number of synapses and active zones between the recorded cells (Korn et al., 1981, 1982). Subsequent studies using combinations of electrophysiology, morphological analysis and/or electron microscopy reached similar conclusions in cultured spinal neurons (Pun et al., 1986), hippocampal and cortical pyramidal cells (Gulyas et al., 1993; Buhl et al., 1997), hippocampal cultures (Bekkers and Stevens, 1995) and in excitatory synapses in the barrel cortex (Silver et al., 2003). Therefore, the number of functional

active zones directly corresponded to the binomial N, and because by definition N is the number of sites that can release the contents of one vesicle, single active zones became synonyms of single release sites. Given that more than one release-ready vesicle exists at each active zone, it was proposed that after one fusion event has occurred, some unknown mechanism prevents the fusion of the remaining vesicles until the next action potential arrives (Korn et al., 1982; Dobrunz et al., 1997). However, to date no cellular or molecular mechanism has been found capable of restricting fusion events to one per active zone, and given the many different sizes and geometric shapes of single active zones that span considerable distances (Harris and Sultan, 1995), it is not immediately clear how such a mechanism could be biologically implemented. More likely, the exocytosis of a single vesicle per active zone simply reflects the very low fusion probability of each vesicle that makes it. In recent years, several groups using a variety of preparations, including the hippocampus, have reported the simultaneous fusion of more than one vesicle at individual active zones (Tong and Jahr, 1994; Auger et al., 1998; Prange and Murphy, 1999; Wadiche and Jahr, 2001; Oertner et al., 2002). The functional significance of this multivesicular release will depend on the saturation state of the postsynaptic receptors, and it is not clear if this is a general property of all synapses. However, the occurrence of multivesicular release implies that probably the most correct physical interpretation of binomial N is the total number of available vesicles that are ready for release, across all active zones that mediate a given synaptic connection - i.e. the total number of releasable quanta.

1.4.3 The probability of release - p_r

In a simple binomial model of synaptic transmission, the probability of release is the average probability that each release site will release one quantum of neurotransmitter upon stimulation. Given the above interpretation of the binomial N, release probability will be the probability that a fusion event occurs at each site occupied with a release-ready vesicle when an action

potential arrives. As mentioned in the previous section, this probability is a time dependent function, that is minimal in the resting state and increases with a time course that follows closely the entry of calcium in the terminal. The average release probability of each vesicle during this period of raised calcium concentration is typically very low, and for hippocampal cultures a recent estimation is ~0.06 (Murthy et al., 2001). Given that hippocampal synapses have 2-30 morphologically docked vesicles, a subset of which will be primed and ready to release, the probability that a given synapse will release one quantum of neurotransmitter is the sum of the fusion probability of all individual release-ready vesicles. Indeed, there is a very good correlation between the fraction of primed vesicles (Hanse and Gustafsson, 2001), RRP size, number of morphologically docked vesicles, active zone size and the synapse release probability (Murthy et al., 1997, 2001; Dobrunz, 2002). In this thesis, the term *release probability* p_r, refers to the probability that one synapse with a single active zone releases a quantum of neurotransmitter after one action potential. For hippocampal excitatory synapses the reported average is ~0.2-0.3 (Hessler et al., 1993; Rosenmund et al., 1993; Allen and Stevens, 1994; Dobrunz and Stevens, 1997; Dobrunz et al., 1997; Murthy et al., 1997, 2001).

1.5 Methods for estimating release probability

Release probability can be estimated in many different ways, each method having different advantages and disadvantages and being more suitable to a particular preparation or question. In general, most of them rely on electrophysiological recordings, optical imaging or a combination of both. Although as described above the concept of release probability dates back to the original formulation of the quantal theory, in Poisson models of release N and p_r by definition cannot be estimated independently, and only the mean quantal content can be measured. Estimations of release probability therefore rely

on the assumption that synaptic transmission follows either simple or more complex binomial statistics under the conditions being studied. Most of the available methods have been successfully applied to hippocampal preparations, either in slice or in culture, and the most relevant ones will now be briefly described. While some allow a full estimation of all quantal parameters, others are directed to release probability only.

1.5.1 Quantal analysis

Quantal analysis is the term usually used to describe any method that allows estimation of the three classic quantal parameters of a synaptic connection, and therefore constitutes a means of measuring release probability. Although the original method employed by Katz to describe quantal transmission, and other approaches directly derived from it, have been successful in NMJ preparations, as explained above, their application to CNS synapses is rather problematic. Because of this, over the last 30 years several alternative methods have been developed. Of these, the one probably closest to the original scheme of del Castillo and Katz has been popularised by John Bekkers (Bekkers, 2003). When calcium in the extracellular recording solution is substituted by strontium, evoked release becomes markedly asynchronous and individual miniature events, presumably originating from the activated synapses, can be identified. An amplitude distribution of these events is then convoluted with a binomial model for transmission, and p_r and N are adjusted to achieve the best fit to the amplitude distribution of the synchronous evoked responses. An attraction of this method is that it is straightforward and easy to implement, but the downside is that it relies on the assumption that asynchronous miniature events are an adequate description of the true quantal size, and it only has been used with simple binomial statistics. The most widely applied method of quantal analysis is the direct fitting of amplitude distributions with specific release models. Traditionally, this involves the analysis of so-called peaky histograms, where amplitudes fluctuate between modes occurring at integral multiples of a unit

- the quantal size for the connection under study. A major problem with this approach is the requirement for the presence of clear histogram peaks that, for many reasons, can be obscured or distorted. A further complication is to ensure that the peaks are truly quantal in nature, and not simply artifacts of finite sampling or non uniformities of the quantal parameters (Clements, 1991; Walmsley, 1995). This can be done using a variety of statistical techniques that test for multimodality and extract the distribution that underlies the data (Redman, 1990; Stricker and Redman, 2003; Kullmann, 1992; Larkman et al., 1997a; Stratford et al., 1997). The combinatorial rule that best describes the relative probability of each peak is then searched for by testing the distribution against different models of release and choosing the best fit. Theoretically, this quantal analysis method yields most information about the underlying quantal parameters, although its application is often precluded by the absence of histogram peaks. One method used with great success in the NMJ (Katz and Miledi, 1965b; Johnson and Wernig, 1971; Zucker, 1973) and reproduced in calyx synapses (Isaacson and Walmsley, 1995) is to reduce the extracellular calcium concentration to the point where evoked responses are composed of very few quanta and fail many times. Due to the natural asynchrony of the release process, if the quantal events are fast and easily resolved above noise, it is possible to directly count them and estimate not only the quantal size, but also the remainder of the parameters if a particular model of release is assumed. Unfortunately, no information can be obtained about the statistics of release under more physiological conditions, and although simple binomial models were successfully used in the NMJ (Zucker, 1973), in the CNS, Isaacson and Walmsley describe their data with the Poisson law, thereby lacking estimates for N and p_r. More recently, a quantal analysis procedure termed variance-mean (V-M) or multi-probability fluctuation analysis (MPFA) has been adapted from the non-stationary fluctuation noise analysis originally applied to ion channel recordings (Clements and Silver, 2000; Clements, 2003; Silver, 2003; Silver et al., 1998). The underlying premise of this approach is that if the release

process is binomial, then changing release probability theoretically produces a parabolic relationship between mean amplitude and variance of the evoked response. This can be tested experimentally by recording synaptic responses in different release probability conditions (achieved by changing the calcium concentration for example) and fitting a binomial model to the variance-mean plot. If sufficient number of conditions are used (5 or more) and long epochs are obtained for each one, either simple or compound binomial models can be reliably fitted to the data and the quantal parameters extracted. Apart from assuming that N and q do not change with the experimental manipulation of release probability, very long and stable recordings are usually required for this technique to yield robust results. All of these methods can be combined with morphological reconstructions of the recorded cells to achieve a more detailed description of the connection under study. Although a powerful approach when applied correctly, quantal analysis yields estimations of release probability always by statistical inference, and is therefore inferior to more direct methods if only this parameter is of interest.

1.5.2 Paired-pulse ratio

The paired-pulse ratio (PPR) is a measure defined as the amplitude ratio of the second to the first synaptic response after stimulating the connection with two action potentials at high frequency, and it reflects the degree of facilitation/depression observed. Values above one indicate facilitation, whereas depression leads to a PPR less than one. As detailed above, both facilitation and depression compete in the same terminal. Although the final outcome certainly depends on many factors, a particularly important one is the release probability. Given that a major determinant of short-term depression is vesicle depletion, synapses with higher release probabilities will have a more pronounced depression and hence a lower PPR. This implied relation has been explored extensively and PPR analysis is certainly the most widely used method for probing release probability. One major caveat is that in most cases the direct relationship between p_r and PPR is not known, and

therefore only relative inferences can be made. Also, one general assumption is that this relation is linear. However, there is no reason to believe that this is necessarily the case, and at single synapse level a highly sublinear relation has been reported (Dobrunz and Stevens, 1997; Murthy et al., 1997). This implies that whereas a change in PPR is probably consistent with a change in p_r, the inverse is not necessarily true.

1.5.3 Failure rate

When a synaptic connection is stimulated, if its release probability is sufficiently low and the total number of release sites is not very high, then sometimes none of the available sites will release neurotransmitter and no response will be elicited in the postsynaptic cell. This situation is termed a *failure* of synaptic transmission, and the frequency at which it occurs is usually taken as an indication of the underlying release probability (Feldmeyer and Sakmann, 2000). Although this is a very simple method, a major problem is that the failure rate depends not only on pr, but equally on the number of release sites. Furthermore, it requires that p_r and N are low enough for synaptic transmission to fail at all. Nevertheless, when failures can be reliably observed and identified, their rate of occurrence can provide a very useful relative estimation of release probability in situations where the number of release sites is known to be very similar.

1.5.4 Progressive block of NMDA synaptic current

The first direct measures of release probability in glutamatergic hippocampal synapses were obtained almost simultaneously by Rosenmund et al (1993) in autaptic cell cultures, where one cell forms synapses with itself, and by Hessler et al (1993) in CA1 pyramidal cells in slice. The method described makes use of the irreversible NMDA open channel blocker MK-801. If NMDA synaptic currents are isolated and recorded in the presence of MK-801, the response amplitude is progressively reduced due to the increasing amount of

receptors that became irreversibly blocked after use. The rate of this progressive block is exponential and will reflect in part the release probability. If p_r is high then more terminals will release transmitter, more postsynaptic NMDA channels will open and the progressive block will be faster. To convert this relative measure of p_r into a quantitative one, a kinetic model incorporating the time course of glutamate in the cleft, the NMDA channel open probability and the MK-801 binding rate is used to predict the progressive block, assuming p_r was 1.0 in all terminals, and this is then compared to the actual measured block rate. Unfortunately this technique can only be used for synapses with large NMDA currents which is not always the case, and therefore may bias the measurement to a synapse population with a particular release probability.

1.5.5 Single synapse stimulation

The four methods above provide estimates of release probability for the whole population of stimulated synapses. If information about the properties of individual synapses is required then alternative techniques have to be employed. One approach used in hippocampal slice preparations is the so-called minimal stimulation. In this method, whole-cell currents are usually recorded from CA1 pyramidal cells while stimulating the Schaffer collateral, and the stimulus intensity is reduced to the point where only one axon is being activated, as judged by a high failure rate, the stability of the average current amplitude over a range of intensities close to the response threshold and the invariance in the response latency and shape (Raastad et al., 1992; Stevens and Wang, 1995). Given that action potential threshold fluctuations and conduction failures do not make significant contributions for the response unreliability (Allen and Stevens, 1994), synaptic release probability can be directly obtained from the response success rate. The disadvantages of this method are that it underrepresents synapses with very low or very high release probability and that it is impossible to know if really only one axon is stimulated or that it only makes one synapse with the recorded cell. One

related technique that has been applied to hippocampal cell cultures is the local stimulation of visually identified synaptic boutons (Chen et al., 2004). Synapses are initially labelled with FM-dyes (see below) and a whole-cell recording is established in the cell of interest. A fine-tipped theta pipette is then positioned a few micrometers away from a dye-stained synapse that appears to contact the chosen neuron, and the terminal is depolarised by application of brief current pulses between the pipette barrels. Putative quantal responses can in this way be recorded and the release probability measured directly. One problem with this approach is the difficulty in distinguishing single synapses from, for example, a pair of synapses close together, which can appear as a single FM-dye stained punctum due to the diffraction limits of light microscopy resolution. Alternatively, a single FM-dye labelled synapse may contain multiple release sites. In this case, only post-hoc ultrastructural analysis can unequivocally establish the true synaptic constitution of the FM-dye positive puncta. Another problem is that the AP-independent depolarization of the terminal might yield calcium currents with unrealistic kinetics that are translated into a non-physiological release process.

1.5.6 Optical methods

If a connection between two neurons is mediated by more than one synapse, as is the case for some intact hippocampal circuits and certainly for hippocampal cultures, then single synapse stimulation clearly provides an incomplete picture of synaptic release probability. Optical methods for estimating pr have the great advantage of combined single synapse resolution for more than one contact and identification of their spatial location. Of the available techniques, the FM family of dyes have proved to be a particularly powerful and successful approach for the study of the vesicle cycle, and increasingly, of release probability. They were originally developed by Fei Mao at Molecular Probes (Betz et al., 1992) and constitute a group of fluorescent styryl dyes that have a lipophilic hydrocarbon tail that has a high affinity with the membrane, and a positively charged head group that prevents FM-dye molecules

from crossing the plasma membrane. By modifying the tail length and head-tail links, a whole family of FM-dye variants has been generated, with different membrane affinities and fluorescence properties (Cochilla et al., 1999). The most commonly used ones are the green emitting FM1-43 (excitation peak 479 nm, emission peak 598 nm) and the red-shifted FM4-64 (excitation peak 506 nm, emission peak 750 nm). Because they only emit strong fluorescence when inserted in the membrane and the dye-membrane association is fully reversible, FM-dyes have ideal properties for analysing vesicle exocytosis and endocytosis. When the dye is in contact with synapses and inserted in the plasma membrane, stimulation of the presynaptic terminal and vesicle exocytosis will cause the collapsed vesicle membrane to become stained given the dye's fast partitioning rate. After endocytosis, FM-dye becomes trapped inside the vesicle, and if several vesicles per terminal are stained, washing away excess surface dye will reveal the fluorescence of the active individual terminals, which can be taken as a measure of endocytosis (Betz et al., 1992; Ryan et al., 1993, see Figure 1.6A). Stimulating the terminal again will result in fusion of dye-labelled vesicles and fluorescence loss due to FM-dye departitioning from the membrane, therefore allowing exocytosis to be monitored (Betz et al., 1992; Ryan et al., 1993, see Figure 1.6B).

FM-dyes can also be photoconverted to an electron-dense product which allows ultrastructural identification of recycled vesicles in electron micrographs (Henkel et al., 1996; Harata et al., 2001b; Darcy et al., 2006a). To measure release probability with FM-dyes, one possible approach used by Murthy et al in hippocampal autapses (1997) is to label vesicles using a small number of action potentials (20-30) delivered at low frequency (0.5-1 Hz). By assuming that there is a one to one relation between exo and endocytosis, and that labelled vesicles are not re-released (the total stimulation time is similar to the full recycling time), the integrated fluorescence intensity of each terminal is proportional to p_r. The conversion of fluorescence to an absolute value of release probability is more problematic and depends on the correct estimation of the fluorescence intensity of single vesicles. This can be

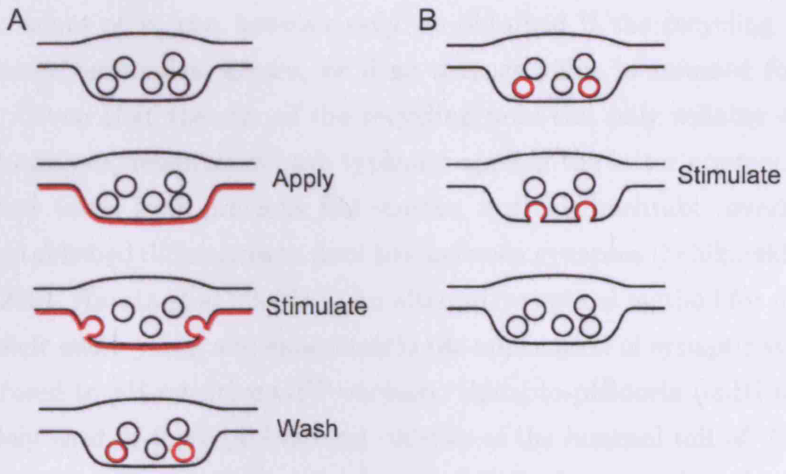

Figure 1.6: Probing synaptic function with FM-dyes. (A) Cartoon illustrating the loading of FM-dye into synapses. Following application of the dye to the outer leaflet of the plasma membrane, the synaptic vesicle cycle is activated and the membrane of vesicles that undergo exocytosis becomes labelled. After vesicle retrieval, the non-endocytosed dye is washed to reveal discrete fluorescent puncta representing synaptic vesicle clusters. (B) When an FM-dye loaded synapse is stimulated, labelled vesicles that are exocytosed loose the FM-dye molecules from their membrane.

done by stimulating the terminals with very few APs (1-5) and looking for evenly spaced peaks in a histogram of intensities that presumably correspond to fluorescence from integral numbers of stained vesicles (Ryan et al., 1997; Murthy et al., 1997; Slutsky et al., 2004). Unfortunately this procedure is extremely prone to sampling artifacts, and as it is usually done independently of the main experiments, it relies on an unlikely stability of the imaging system. One other approach to measure p_r with FM-dye is to directly monitor vesicle exocytosis by live imaging the fluorescence loss of a terminal under low frequency stimulation. Synapses with high p_r will destain at higher rates than synapses with low p_r, and the fluorescence loss rate can therefore be taken as a relative measure of release probability (Zakharenko et al., 2001).

Absolute values of p_r can however only be obtained if the recycling pool size for every terminal is known, or if an average value is assumed for all of them. Given that the size of the recycling pool can only reliably come from EM analysis, researchers have typically applied the latter approach by using values taken from previous EM studies, but this inevitably overlooks the well-established differences in pool size between synapses (Schikorski and Stevens, 2001; Harata et al., 2001b). An alternative optical method for monitoring vesicle endocytosis and exocytosis is the application of synaptic vesicle proteins fused to pH-sensitive GFP variants. Synapto-pHluorin (spH) is the most widely used of these probes, and consists of the lumenal tail of VAMP fused to ecliptic pHluorin (Miesenbock et al., 1998). Because of the lumenal localisation of VAMP and the intrinsically low pH values inside vesicles, the pHluorin molecules are quenched in resting state, so that do not fluoresce strongly. Upon stimulation and exocytosis, pHluorins become exposed to the extracellular medium and their fluorescence transiently increases, making them a useful marker of vesicle fusion (Sankaranarayanan et al., 2000). Estimates of release probability can either be obtained by direct imaging of single fusion events if the signal-to-noise resolution is good enough (Gandhi and Stevens, 2003), or more commonly by measuring the fraction of the recycling pool released by single APs (Granseth et al., 2006). While the former heavily depends on the assumption that the minimal fluorescence rise is due to a single vesicle and is always detectable, and the latter requires the pool size to be known for a p_r value to be obtained, the main problem with this technique is that it relies on the overexpression of a non-native protein. A different type of optical approach to measure p_r is to image postsynaptic NMDA receptor-mediated calcium accumulation in single contacts or spines as a measure of glutamate release (Oertner et al., 2002; Yuste et al., 1999; Koester and Johnston, 2005; Emptage et al., 2003). However, there are some limitations with this method, namely that it is restricted to synapses with NMDA receptors, and ultimately relies on a less direct measure than the use of vesicular markers. Moreover, other problems are contaminations from cal-

cium arising from voltage-gated calcium channels (VGCC) or internal stores, glutamate spillover from neighbouring synapses and the fact that apparent failures can arise from unsuccessful opening of the transmitter bound channels due to stochastic gating.

1.6 The variability of release probability

In most studies of synaptic function, release probability is assumed to be the same for all terminals that mediate a connection. However, when del Castillo and Katz formulated their theory of synaptic transmission they insightfully noted that *the chances p may differ greatly for the individual constituents* and therefore the measured pr for the overall connection should be regarded as an average of p_r at individual synapses. The question arises then whether release probability is uniform at all synapses or if indeed there is considerable variability between terminals.

The first evidence that the latter could be the case came, as it is often the case, from studies in the NMJ. Direct focal recordings from different regions of the endplate belonging to one motoraxon, and sometimes combined with morphological and ultrastructural reconstructions, showed that in the crayfish opener muscle, boutons at different locations have different release probabilities (Bittner, 1968; Atwood and Bittner, 1971; Frank, 1973; Cooper et al., 1996) and that one axon innervating two different types of muscles can exhibit facilitation for one and depression for the other (Parnas, 1972). Similar findings were reported from focal recordings in the frog NMJ (Bennett et al., 1986; Robitaille and Tremblay, 1987, 1991) and double muscle recordings in the lobster stomatogastric system (Katz et al., 1993). This type of experiment, where the output of one axon is evaluated in two or more postsynaptic targets and the short-term plasticity properties analysed, proved very useful in depicting pr variability in the CNS. In the leech nociceptive system, two different motor cells innervated by the same sensory cell display opposite forms of STP (Muller and Nicholls, 1974), the same

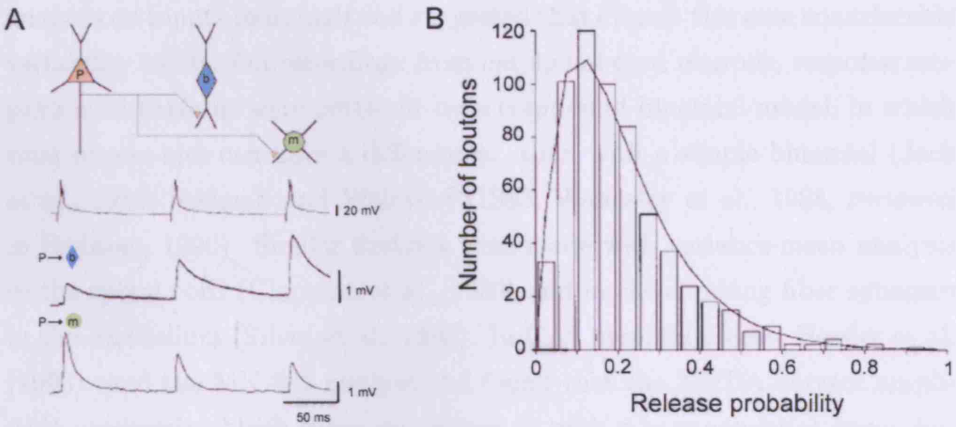

Figure 1.7: Synapses from a single axon can have heterogeneous release probabilities. (A) Triple whole-cell recording from layer 2/3 in the neocortex, where one pyramidal cell (P) is connected to a bipolar cell (b) and to a mitral cell (m). Synapses onto the bipolar cell facilitate, indicating a low p_r, whereas synapses to the mitral cell show depression, revealing a higher release probability. Adapted from Reyes et al. (1998). (B) Distribution of release probabilities obtained with FM-dye imaging in hippocampal autapses. From Murthy et al. (1997).

being observed in the cat spinal cord (Koerber and Mendell, 1991), in the giant reticulospinal axon synapses onto spinal neuron in the lamprey (Brodin et al., 1994), in hippocampal cultures (Mennerick and Zorumski, 1995), and in whole-cell recordings of cortical layer 2/3 and 5 circuits (Reyes et al., 1998; Markram et al., 1998, see Figure 1.7A). For some multiple target recordings in the cricket (Davis and Murphey, 1993) and locust interneurons (Laurent and Sivaramakrishnan, 1992), successful quantal analysis was possible, which confirmed that different release probabilities underlie the differences in short-term plasticity (reviewed in Davis, 1995). More recently, Koester et al (2005) performed optical quantal analysis using single synapse calcium imaging in layer 2/3 pyramidal cells, and showed that release probability is normalised to the postsynaptic cell. All these studies in the CNS report release probability variability as a function of different targets. However, a classic quantal

analysis on inputs to a single cell suggested that even in this case considerable variability exists. On recordings from cat spinal cord neurons, response amplitude histograms were better fit by a compound binomial model, in which each release site can have a different p_r, than with a simple binomial (Jack et al., 1981; Redman and Walmsley, 1983; Walmsley et al., 1988, reviewed in Redman, 1990). Similar findings were made with variance-mean analysis in the spinal cord (Clamann et al., 1989) and in the climbing fiber synapses in the cerebellum (Silver et al., 1998). In CA1 pyramidal cells, Hessler et al. (1993) used the MK-801 method and found that the NMDA current amplitude progressive block curve was better fit with a bi-exponential curve, implying at least two groups with very different p_r. In another study, Stevens and colleagues reported a wide pr range with the minimal stimulation technique (Dobrunz and Stevens, 1997; Huang and Stevens, 1997). Even in the limiting case of autaptic cell cultures, release probability can be extremely non-uniform, as demonstrated by the MK-801 approach (Rosenmund et al., 1993) and also by measuring p_r at all synapses with FM-dyes (Murthy et al., 1997). In the latter work, Murphy et al reported a wide and continuous distribution of release probabilities, skewed to larger values and with a coefficient of variation above 0.5 (Figure 1.7B), a finding recently confirmed by other groups (Slutsky et al., 2004; Granseth et al., 2006). In support of this observation, the distribution of active zone sizes and the number of morphologically docked vesicles is very similar (Schikorski and Stevens, 1997). It is thus clear that, at least in some systems, synapses from a single axon can have different release probabilities, even when making contacts in the same postsynaptic cell. Because the rate and type of information transfer within a network depends on the p_r and STP properties of connections, a great advantage of non-uniform release probabilities is that one axon is capable of converting the same input into a variety of outputs depending on the target cell, greatly increasing its computational functions. How different combinations of release properties and postsynaptic targets arise is not clear, but a variety of retrograde messengers either during synapse development

or in more mature stages could be responsible (Davis and Murphey, 1994). Release probability variability for synapses in the same cell is however not at all understood, both in the function it might serve or the mechanisms that implement it.

1.7 Modifications of release probability

The dynamic nature of release probability is well evident in the process of short-term plasticity, where both facilitation and depression can be explained by changes in p_r. Beyond these short lived changes, 'basal' release probability is also not static and can be subject to numerous and more durable modifications that have an immediate impact on the strength of a synapse. By far the best studied of these type of changes are long-term potentiation (LTP) and long-term depression (LTD), two forms of plasticity which are candidate mechanisms underlying associative memory. That a change in the properties of release can account for LTP/LTD, has been heavily debated, but it now seems clear that at least in some circuits this can be the case. Of the many possibilities, presynaptic expression of LTP/LTD have been linked with increased concentrations of cleft glutamate, changes in the mode of exocytosis, enhanced vesicle turnover or structural changes in the presynapse (reviewed in Lisman and Raghavachari, 2006 and Krueger and Fitzsimonds, 2006).

Another class of long-term changes in release probability with particular relevance to this thesis is homeostatic plasticity. Homeostasis, a term coined by Cannon to describe the apparent *fixité du milieu intérieur* introduced by Claude Bernard (Berne and Levy, 1998), is a central concept in the physiology of all systems that describes their ability to remain stable despite fluctuations in the external environment. Evidence for the operation of such a mechanism in the nervous system came from the observation that when skeletal muscle is denervated its excitability and spontaneous contractions increase, a phenomenon that became known as denervation supersensitivity

(Sharpless, 1964). Later, a notable theoretical study predicted that neuronal excitability should be controlled by a compensatory feedback that maintains the neuron target activity (LeMasson et al., 1993). This was elegantly demonstrated in the lobster stomatogastric ganglion cells, which when cultivated in isolation without any synaptic input, were seen to re-balance their intrinsic conductances and regenerate their rhythmic bursting behavior (reviewed in Marder and Goaillard, 2006). In the mammalian CNS, activity block of cortical cultures leads to a rebound hyperactivity in the network when activity is allowed to resume (Ramakers et al., 1990), and this can be explained by homeostasis of synaptic transmission. The first quantal parameter shown to be directly regulated was the quantal size, when Turrigiano et al found a compensative change in mEPSC size after 48 hrs of AP block (Turrigiano et al., 1998). Although initially controversial, it has now been shown that release probability can also be modified to achieve synaptic homeostasis. This was first convincingly demonstrated in the Drosophila NMJ by elegant experiments carried out by Davis and colleagues. When a motorneuron is biased to differentially innervate one of two adjacent targets by overexpression of a cell adhesion molecule in one muscle only, both muscle targets develop normal levels of depolarization due in part to changes in presynaptic neurotransmitter release and active zone density (Davis and Goodman, 1998b; Stewart et al., 1996). In other mutants where postsynaptic excitability is decreased by partially eliminating glutamate receptors (Petersen et al., 1997), overexpressing PKA (Davis et al., 1998), reducing the number of ACh receptor clusters (Sandrock et al., 1997) or overexpressing Kir 2.1 (an inward rectifying potassium channel, Paradis et al., 2001), release probability is increased to restore normal levels of activity (reviewed in Davis and Goodman, 1998a). In hippocampal cell cultures, changes in release probability also mediate homeostatic plasticity. Blocking glutamate receptors or AP generation leads to an increased mEPSC frequency and synaptic vesicle recycling (Bacci et al., 2001; Thiagarajan et al., 2005, 2002), increased active zone size, number of docked vesicles and overall release probability (Murthy et al., 2001),

and overexpression of Kir 2.1 in a single neuron results in increased mEPSC frequency and synapse size (Burrone et al., 2002). A similar phenotype is also seen in hippocampal organotypic slice cultures (Galante et al., 2001) and cortical cultures (Wierenga et al., 2006). All these mechanisms together are thought to serve the important function of stabilising positive feedback mechanisms like LTP/LTD, preventing synapse silencing or saturation and maintaining a constant output range (Burrone and Murthy, 2003; Turrigiano and Nelson, 2004). It is thus clear that, at any given time point, the release probability of a synapse will be a result of many different influences working in combination.

1.8 Concluding remarks

Release probability is a fundamental parameter of synaptic transmission that determines both its strength and dynamic adaptation to input. Although we understand some of the mechanistical factors that determine p_r, we do not know what orchestrates these mechanisms and ultimately determines what release probability a given synapse has. A vexing illustration of our lack of understanding and perhaps one of the most intriguing aspects of release probability, is that even synapses from one axon onto one target can adopt a very different p_r - and we have no idea why this is the case and what functional role this may serve. In this thesis these two questions will be addressed, and a model by which individual synapses set their release probability will be proposed.

Chapter 2

Materials and Methods

All experiments presented in this thesis have been performed in primary cultures of hippocampal neurons. Primary neuronal cultures have been used over the past 15 years in the study of neuronal physiology, and have proven extremely valuable, in particular in studies of synaptic function. When neurons in early developmental stages are plated on a suitable substrate, they develop and acquire a phenotype that closely matches what is found in a more physiological environment. Synaptic connections are established as early as 5-6 days in vitro (DIV), and synapses are generally considered to have matured after 10-12 DIV (Renger et al., 2001). Simple networks of neurons with high connectivity grow as flat monolayers in a controlled environment. Thus, this system is ideally suited for combinations of electrophysiological recordings, imaging and pharmacological manipulations. Cultures from the hippocampus were chosen for this thesis mainly because they have been extensively characterised in the literature and validated as a reliable and consistent experimental paradigm.

Release probability was studied using three different methods: 1) FM-dye imaging combined with analysis of cell morphology, 2) electron microscopy, and 3) standard electrophysiology techniques, namely paired whole-cell recordings of synaptically connected cells.

All chemicals/reagents used that are not listed below were obtained from

Sigma-Aldrich or BDH/Merck. In the Buffers and Solutions tables, *RT* indicates room temperature and *Filter* indicates sterilisation with a 0.2 μm filter.

2.1 Dissociated hippocampal cell culture

2.1.1 Materials

Table 2.1: Chemicals / Reagents / Products, used for cell culture

Product	*Company*	*Address*
12 mm glass coverslips	Assistent	Sondheim, Germany
Collagen from rat tail	extracted in the lab	UCL, UK
DNase I	Calbiochem	California, US
Eagle's Basal Medium (BME)	Invitrogen	Paisley, UK
Fetal Calf Serum	Sigma-Aldrich	Dorset, UK
Glutamax	Gibco/Invitrogen	Paisley, UK
Hank's Balanced Salt Solution (HBSS)	Invitrogen	Paisley, UK
HPLC gradient water	Sigma-Aldrich	Dorset, UK
Neurobasal	Invitrogen	Paisley, UK
Papain	Worthington	Lakewood, US
Poly-D-lysine (PDL)	Beckton Dickinson	California, US
Tissue culture plastics	Beckton Dickinson or Corning	California,US New York, US
Trypsin	LMCB	UCL, UK
Trypan Blue	Gibco/Invitrogen	Paisley, UK

Table 2.2: Buffers and Solutions, used for cell culture

Buffer/Solution	*Ingredients*	*Storage*	*Sterilisation*
Astrocyte Growth Medium	BME, 20 mM glucose, 10 mM HEPES, 1 mM sodium pyruvate, 2 mM glutamax, 10 % fetal calf serum	4 °C	Filter
Dissection Solution	HBSS with 10 mM HEPES	On ice	Filter
Neuronal Growth Medium	Neurobasal, 2 mM Glutamax, 0.15 % glucose, 10% fetal calf serum	4 °C	Filter
Neuronal Growth Medium	Neurobasal, 2 mM Glutamax, 0.15 % glucose, 5% fetal calf serum, 1% Penicillin/Streptomycin, 10 mM KCl	4 °C	Filter
Papain Solution	Dissection solution containing 1.5 μM calcium chloride, 2 mg/mL L-cysteine, 0.1 μg/mL DNase I, 0.5 mM EDTA, 30 units of papain	RT	Filter
PDL-collagen mix	Acetic acid (0.025%), 1:8 dilution rat tail collagen, 5 μg/mL PDL in HPLC water	RT	-

2.1.2 Methods

Cultures were grown on 12 mm glass coverslips that were washed overnight in 100% nitric acid, then rinsed with deonised water for 2-3 hrs and stored in 100% ethanol. As required, coverslips were placed in 24-well plates, sprayed lightly with a PDL-collagen mix and sterilised by UV radiation for 15 mins in a fume hood. They were then stored in sealed plastic bags and used within two months.

To provide support for neuronal growth, neurons were plated on top of an astrocyte feeder layer. To prepare it, residual cells from a dissection were grown in T-25 flasks in astrocyte growth medium. When astrocytes were close to confluency they were detached by trypsinization and plated onto PDL-collagen coated coverslips at 3,000 cells per well in 500 μL of astrocyte growth medium. Only the central 8 wells of a 24-well plate were used and the outer ones were filled with 500 μL of water to minimise evaporation. After 2-3 days, small, discrete islands composed of 4-5 astrocytes had developed.

For hippocampal dissection, newborn Sprague Dawley rats (P0-P1) obtained from UCL Central Biological Unit were used. All procedures were done according to the Animals (Scientific Procedures) Act 1986. Animals were euthanised, the skin and skull opened with a pair of scissors and the brain removed with a spatula. The two brain hemispheres were separated with a no.10 blade and immersed in ice cold dissection solution. The tissue was then placed under a dissection microscope and the midbrain and the meninges were removed using two fine forceps to expose the hippocampus. Using a no.10 blade and a spatula the whole hippocampus (CA1-3 and dentate gyrus) was then dissected out, cut into 1 mm x 1 mm pieces and placed in papain solution at 37 ^{o}C. After 35 mins the papain solution was then replaced by pre-warmed neuronal plating medium and the tissue triturated with a flame polished glass Pasteur pipette. To estimate the number of viable cells, 45 μL of the cell solution was mixed with 5 μL of 0.4% trypan blue and neurons in this volume counted with an haemocytometer placed under a stereo-microscope. Neurons were plated at 30,000 cells per well in

500 μL of neuronal plating medium on top of the previously grown astrocyte islands. After 4-24 hrs all the media was replaced by 500 μL of neuronal growth media and typically after another 2 days 4 μM (final concentration) of cytosine arabinoside was added in 100 μL of media to prevent astrocytic overgrowth. Cells were used for experiments between 10-15 DIV.

2.2 Electrophysiology

2.2.1 Materials

Table 2.3: Chemicals / Reagents / Products, used for electrophysisology

Product	*Company*	*Address*
150F-7.5 glass capillaries	Harvard Apparatus	Edenbridge, UK
Acquisition system	Axon Instruments/ Molecular Devices	Berkshire, UK
Bicuculline methochloride	Tocris Bioscience	Bristol, UK
CNQX	Tocris Bioscience	Bristol, UK
Creatine Phosphate	Calbiochem/Merk	Nottingham, UK
DB2 micropipette holders	G23 Instruments	UCL, UK
DL-AP5	Tocris Bioscience	Bristol, UK
LN junior 22 micromanipulators	Luis & Neumann	Ratingen, Germany
MgATP	Sigma-Aldrich	Dorset UK
Na2ATP	Sigma-Aldrich	Dorset UK
Na3GTP	Sigma-Aldrich	Dorset UK
TC-324B Temperature controller	Warner Instruments Inc	Endinbridge, UK
Tetrodotoxin (TTX)	Tocris Bioscience	Bristol, UK

Table 2.4: Buffers and Solutions, used for electrophysisology

Buffer/Solution	*Ingredients*	*Storage*	*Sterilisation*
External solution	125 mM NaCl, 5 mM KCl, 10 mM D-glucose, 10 mM HEPES, 2 mM $CaCl_2$, 1 mM $MgCl_2$ (pH 7.30)	4 °C	Filter
Internal solution	115 mM $KMeSO_4$, 5 mM KCl, 4 mm NaCl, 10 mM HEPES, 0.5 $CaCl_2$, 10 mM creatine phosphate, 2 mM MgATP, 2 mM Na_2ATP, 0.3 mM Na_3GTP, 10 mM glutamic acid, 100 μM Alexa 488 or 500 μM Alexa 350 hydrazide (pH 7.20)	-20 °C	Filter
Gramicidin internal solution	Internal solution modified to 40 mM KCl, 90 $KMeSO_4$, 10 mM EGTA and 10 μg/mL Gramicidin A	Made fresh	-

2.2.2 Methods

Electrophysiological recordings were performed as originally implemented by Sakman and Neher (Hamill et al., 1981). Paired recordings from visualised cells in the whole-cell configuration were obtained in both voltage-clamp and voltage recording modes.

A coverslip was placed in a custom made perspex material chamber and cells were visualised using an Olympus IX-71 inverted microscope. Pipettes were pulled from borosilicate glass on a horizontal Sutter Instruments puller using a one step program (3-5 MΩ), filled with internal solution using a non-metallic syringe needle (Microfil, World Precision Instruments) attached to

a 1 mL syringe through a 4 mm syringe filter (Nalgene, Hereforf, UK) and placed in DB2 holders. The amplifier was a Multiclamp 700B connected to a Pentium 4 running at 3.06 GHz via a Digidata 1322A and Clampex 9.2 was used as the acquisition software. Two CV-7B headstages were placed in Junior LN manipulators mounted on the stage of the microscope. The coverslip was continually perfused with an external solution at 1-2 ml/min via a gravity flow perfusion system and heated to 34±1 °C with an in-line heater. Suction was driven by a vacuum pump.

To obtain a recording neurons of interest were selected using a phase contrast 10x objective(n.a. 0.30) and were patched under 40x (n.a. 0.85) magnification with differential interference contrast (DIC) optics. Positive pressure was applied using mouth control and pipettes were lowered onto the surface of the cell until a clear dimple was observed, at which point the positive pressure was withdrawn and very gentle suction was applied. Seal formation was monitored in voltage-clamp mode using a 5 mV pulse, and holding current (voltage command -60 mV) was applied to help the seal formation. Gigaohm seals between 1 and 10 GΩ were generally obtained more-or-less instantaneously. Pipette capacitance was cancelled semi-automatically using the in-built Multiclamp circuit. To obtain the whole-cell configuration, ramping suction was applied until the membrane patch was ruptured. Whole-cell capacitance and series resistance were estimated using the amplifier compensation controls. Series resistance was not routinely compensated. Data were acquired at 50 kHz and low-pass filtered online at 10 kHz with a 4-pole Bessel filter. To establish the presence of a synaptic connection, one cell was voltage-clamped at -70 mV (corrected online for a junction potential of 10 mV) and APs were elicited in the other cell in voltage-recording mode by injecting 0.5-1 nA current pulses of 1-2 ms duration. If a synaptic connection was found, the presynaptic cell was maintained in voltage-recording mode and the postsynaptic cell in voltage-clamp. To briefly characterise the connection as excitatory or inhibitory, the presynaptic neuron was stimulated at low frequency while the holding potential of the postsynaptic cell

stepped from -80 mV to +20 mV. For paired pulse experiments the inter-pulse interval was 50 ms and a minimum of 30 sweeps were acquired at 0.1 Hz. For recordings in low calcium, the stimulation frequency was 1 Hz and 100-300 traces were obtained. When it was necessary to further manipulate the patched cells, pipettes were gently removed in voltage-clamp mode and the membrane allowed to reseal. Perforated-patch recordings with gramicidin were obtained by filling the tip of the pipette with normal internal solution, and backfilling it with gramicidin internal solution. After a Gigaohm seal was obtained, access resistance was monitored in voltage-clamp mode by a 5 mV pulse. After around 30-40 mins, the access resistance was below 30 MΩ and recordings were initiated.

2.3 Fluorescence Imaging

2.3.1 Materials

Table 2.5: Chemicals / Reagents / Products, used for fluorescence imaging

Product	*Company*	*Address*
Advasep-7	Sigma-Aldrich	Dorset, UK
Alexa 488/350 hydrazide	Molecular Probes	Paisley, UK
FM4-64	Molecular Probes/Invitrogen	Paisley, UK
Mouse GluR2 antibody, extracellular, clone 6C4, Cat. No. MAB397	Chemicon	Hampshire, UK
Metamorph Software	Molecular Devices LTD	Berkshire, UK
Mouse Cy-2 antibody	Jackson Immunoresearch/Stratech	Cambridgeshire, UK

2.3.2 Methods

Fluorescence imaging was performed using standard epifluorescence microscopy. The same inverted Olympus IX-71 microscope used for electrophysiological recordings was equipped with a mercury burner lamp and a Princeton Instruments 1392 x 1040 cooled-CCD camera. Three different filter set were used: 475/40 nm excitation, 505LP dichroic and 535/45 nm emission filters for Alexa-488, FM1-43fx and Cy-2; 535/30 nm excitation, 595LP dichroic and 645/75 nm emission for FM6-64; and 365/50 nm excitation, 400 LP dichroic and 450/65 nm emission for Alexa-350. Images were acquired at 12-bit using Metamorph (7.0) software running in a Pentium 4 computer, connected to the camera via a 5 MHz PCI card. The fluorescence shutter was controlled by a Uniblitz VMM-D1 mechanical shutter driver.

Visualisation of cell morphology

To identify all the processes of two connected cells, patch pipettes were filled with fluorescently conjugated hydrazides. Alexa 488 and 350 were used interchangeably as fluorochromes. Due to the reduced brightness of Alexa 350, the working concentration had to be increased to 5x from the manufacter's suggestion of 100 μM to allow unequivocal identification of the smaller processes. Once a paired whole-cell recording was established, neurons were left to fill for at least five mins and cellular processes imaged sequentially.

FM-dye imaging

Individual synapses were visualised and studied using FM-dyes as introduced above. FM 4-64 or FM 1-43FX, the fixable analogue of FM 1-43, were incorporated into synapses by inducing vesicle recycling with a high potassium solution or field stimulation. For high potassium induced labelling, coverslips were incubated with a 10 μM FM-dye solution in 40-90 mM KCl for 1 min at room temperature. Even though this protocol produces an abnormal depolarization of the presynaptic terminals, Harata et al. (2001a) have shown

that it labels the same pool of vesicles released with exhaustive action potential stimulation. Furthermore, because vesicle release is induced both by action potential generation and direct depolarization of the terminal, FM-dye labelling with this protocol is not affected by branch point failures. Given that release probability is estimated by the amount of FM-dye released per action potential (see below), which is affected by action potential failures of propagation, if the initial loading of the terminals was also influenced by this, it would lead to an amplification of any bias due to systematic failure of particular branches. For this reason, high potassium induced FM-dye loading was the preferred method to label the recycling pool. Following an extra 30 s incubation with FM-dye in normal bath solution to allow completion of endocytosis, cells were washed in the FM-dye carrier, Advasep-7, for one min, and in low calcium bath solution for five mins to remove all dye from the membrane surface. For field stimulation a coverslip was placed in a custom made chamber at room temperature and field potentials were generated by passing current between two platinum electrodes lying 1 cm apart. A Grass stimulator was used to deliver the stimulus, which typically consisted of 1 ms 20 V pulses, repeated 30 times at 1 Hz. Excess of FM-dye was removed as for high potassium labelling. During both FM-dye loading procedures, excitatory synaptic transmission was blocked with 20 μM 6-cyano-7-nitroquinoxaline-2,3-dione (CNQX) and 50 μM DL-2-Amino-5-phosphonopentanoic acid (AP5). For FM-dye destaining experiments, a region of interest that included FM-labelled puncta that were likely synaptic contact points between the recorded neurons was selected for imaging. FM-dye destaining was elicited by stimulating the presynaptic cell with 600 APs at 1 Hz, and the loss of fluorescence monitored by acquiring single images every min. This was done at room temperature, because it was found that perfusion of extracellular solution, which was required for temperature control, caused unacceptable drifts in the plane of focus.

Labelling of glutamate receptors

In some control experiments, glutamate receptors were labelled with a mouse antibody directed against the extracellular domain of glutamate receptor subunit-2 (GluR2). The antibody was diluted in the conditioned culture medium (2 μg/mL), and coverslips were incubated with this solution for 45 min at 37 °C, without previous fixation or permeabilization. In this way, the antibody will only label GluR2 receptors present at the cell surface, and the cells will be alive after the labelling procedure, allowing further procedures such as FM-dye loading of presynaptic terminals. After incubation with the primary antibody, cells were washed in fresh culture medium, incubated with a anti-mouse Cy-2 secondary antibody for 30 min at 37 °C and washed again.

2.4 Electron Microscopy

All electron microscopy was done in close collaboration with Dr. Kevin Darcy and Dr. Kevin Staras from the Goda lab and Dr. Lucy Collinson from the MRC LMCB EM unit. Dr. Kevin Staras did the alignment of images and the finding and marking of the regions of interest in the resin. Dr. Lucy Collinson performed the serial sectioning and Dr. Kevin Darcy did all the steps from the osmication to the sectioning. All images were taken by Dr. Kevin Darcy and Dr. Kevin Staras. The majority of image analysis and 3D reconstruction was performed by Dr. Kevin Staras. A detailed description of this protocol has recently been published (Darcy et al., 2006b) and only a brief description will be given here.

Synapses were loaded with FM1-43FX as described above, fixed with 2% paraformaldehyde/2% glutaraldehyde in PBS at room temperature for 15 min, and then washed in 100 mM glycine for 1 h followed by 100 mM NH_4Cl for 1 min. For photoconversion, cells were pre-incubated in 1 mg/mL DAB in PBS for 10 min, and a region of interest was photoconverted by exposure to 475/40 nm light for 10-15 min in the presence of fresh DAB solution. Cells were then treated with 1% osmium tetroxide/1.5% potassium ferrocyanide

Table 2.6: Chemicals / Reagents / Products, used for electron microscopy

Product	*Company*	*Address*
3,3' Diaminobenzidine (DAB)	DAKO	Cambridgeshire, UK
Formvar	Agar Scientific	Essex, UK
Glutaraldehyde 25%	Agar Scientific	Essex, UK
Lead Nitrate	Fisher Scientific	Leicestershire, UK
Paraformaldehyde 16%	Agar Scientific	Essex, UK
Phosphate buffered solution (PBS)	Gibco/Invitrogen	Paisley, UK
Potassium ferrocyanide	Sigma-Aldrich	Dorset, UK
Sodium cacodylate	TAAB Laboratories Equipment LTD	Berkshire, UK
Tannic acid	TAAB Laboratories Equipment LTD	Berkshire, UK

for 1 hr, and stained with a 1% solution of tannic acid. After deionisation and dehydration, samples were embedded in EPON and subsequently serially sectioned. For imaging, sections were placed on formvar coated slot grids, stained with lead citrate and viewed using a Philips CM10 electron microscope. Images were acquired with a cooled-CCD camera (Roper Scientific).

2.5 Activity Manipulations

For long-term manipulation of activity, cells were placed in a custom-made field stimulation chamber and 2 ms long, 5 V pulses at 1-2 Hz were delivered with a Grass stimulator, while maintaining the cultures in the incubator in culture media. When required, drugs were added to the culture medium at the following concentrations: 20 μM CNQX, 50 μM AP5 and 20 μM Bicuculline. When stimulation was not necessary, drugs were added directly to the wells of the 24-well plates in which the cultures were growing. For localised field stimulation, a coverslip was placed on a recording chamber and continuously perfused with extracellular solution at 37 ^{o}C. A pipette was pulled from a theta-glass (TGC 200-10, Harvard Apparatus, Edenbridge, UK), placed on a custom-made holder mounted on a LN 22 Junior micromanipulator and connected to a A360 current stimulator (World Precision Instruments). After selecting a target region, the pipette tip was carefully positioned under visual control using DIC optics, and 5 ms 100 μA current pulses were delivered at 1-2 Hz. All data were obtained in parallel on treated and age-matched sister control cultures.

2.6 Analysis

2.6.1 Electrophysiology

Data were analysed either in Clampfit 9.1 or NeuroMatic 1.71 running on Igor Pro 4.06 (Wavemetrics, Oregon, US), and small custom written routines. Recordings were only accepted for analysis if the access resistance

was <30 MΩ. Prior to analysis, traces were low-passed filtered at 2-5 kHz with a 8-point Boxcar filter. Paired-pulse ratio was calculated using the peak amplitude of the first and second responses. Miniature events were detected semi-automatically using the threshold algorithm in Neuromatic. For recordings in 1 Ca^{2+}/3 Mg^{2+}, the predicted values for the number of quanta released were obtained from the estimated N and p_r for a given cell, using equation 1.2 multiplied by the appropriate number of trials.

2.6.2 Fluorescence Imaging

Images were analysed mainly using custom written routines in Matlab 7.1 (Mathworks), and IgorPro 4.06. When required, digital manipulations of images was done in Photoshop CS2 (Adobe Systems Inc.). ImageJ 1.32j (NIH, US) was used for distance measurements. All quantifications were done in raw images.

Individual synapses mediating a given connection, were selected for analysis based on the apposition of the FM-dye signal with the Alexa-dye filled axon and dendrite. In a number of pilot experiments, ultrastructural analysis was performed after the paired recording and FM-dye loading to confirm the presence of a synapse between the labelled axon and dendrite. Figure 2.1 shows one example of such an experiment, where a synapse can be clearly identified in the electron micrograph at the location marked by the FM-dye.

The general maturity of the synaptic population studied was assessed in separate experiments, by labelling the postsynaptic site with a GluR2 antibody, a AMPA-receptor subunit that is predominantly present in mature synapses in hippocampal cultures (Pickard et al., 2000). As shown in Figure 2.2, >90% of FM-dye labelled synapses were apposed to GluR2 cluster, indicating a high degree of maturation.

Estimation of release probability

The stimulation evoked FM-dye loss was measured by defining a region of interest (ROI) around a punctum, and an equivalent region positioned adjacent

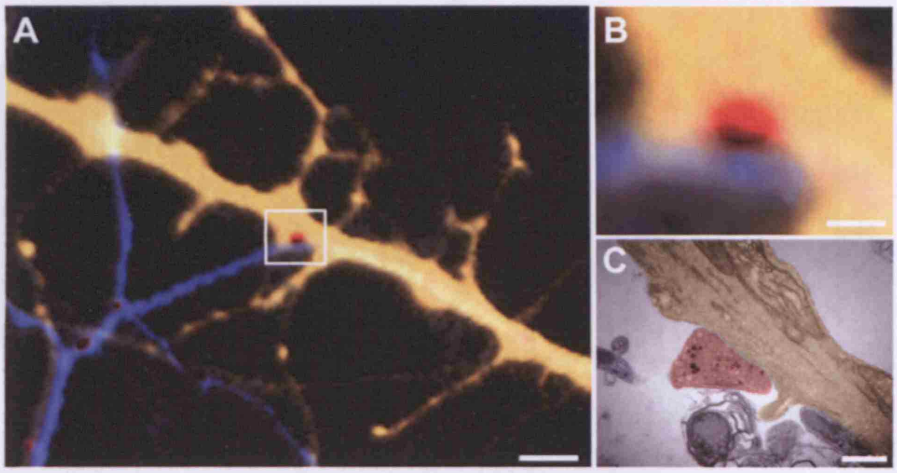

Figure 2.1: Confirming the identity of selected contact points. (A) Epifluorescence image of a dendrite (yellow), axon (blue) and FM-labeled presynaptic terminals (red). Scale bar, 2 μm. (B) High magnification of the boxed area in A, showing a synapse identified as a contact point between the recorded cell pair. (C) Electron micrograph of the same area as in B confirms the presence of a synapse between the Alexa-dye filled axon and dendrite. Scale bar B-C, 0.5 μm.

to it to measure the local background signal (Figure 2.3A). Mean fluorescence was calculated for each region and the background signal subtracted from the synapse signal for every frame. A graph was then constructed by plotting the fluorescence values for each time point acquired (Figure 2.3C, top). Given that the mean punctum fluorescence does not reflect differences in boutton size, to calculate the absolute amount of fluorescence lost upon stimulation, FM-dye destaining curves have to be corrected for differences in the initial recycling pool size. To achieve this, the initial FM-dye puncta fluorescence was measured by averaging the three baseline frames and fitting a 2-D Gaussian to each synapse (Figure 2.3B). The synapse border was defined as 2 SDs from the centre of the fit, and the total fluorescence was quantified by integrating the fit within this limit (Appendix 1). FM-dye destaining curves were then normalized to the average of the first three time points, and multiplied by

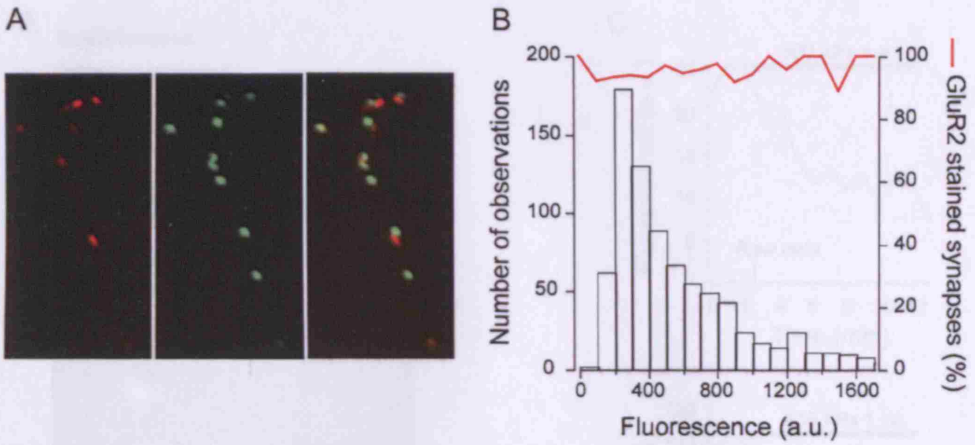

Figure 2.2: Assessing synapse maturity. (A) Example experiment where presynaptic terminals were labeled with FM4-64 (red, left) by field stimulation (30 APs, 1 Hz), and postsynaptic sites were labelled by live antibody staining against GluR2 (center, green). Right panel shows overlap of the two signals. (B) A histogram was constructed with the total FM-dye fluorescence intensity measured for each synapse, and the percentage of FM-dye puncta apposed to GuR2 clusters was calculated for each histogram bin (red line). There was a very high percentage of FM-dye/GluR2 apposition for all synapses analysed.

the estimated total initial fluorescence (Figure 2.3C, middle and bottom). All the curves shown in the following chapters have been processed in this way, and have not been corrected for bleaching. To estimate the FM-dye destaining rate, a simple exponential curve in the form $Ae^{(-\frac{t}{\tau})} + C$ was fit to this data, from the onset of stimulation to the last acquired data point. In this equation, τ is the time constant of the destaining, A is the total initial fluorescence, and C is the fluorescence level at which the curve will reach a plateau phase. All parameters were left free during the fitting procedure. The destaining rate was then calculated by dividing the total fluorescence lost at t = τ (0.63 x $initial fluorescence$) by the number of action potentials at this time point (τ expressed in seconds, given the stimulation frequency of 1 Hz). This yields the amount of FM-dye fluorescence released per action potential.

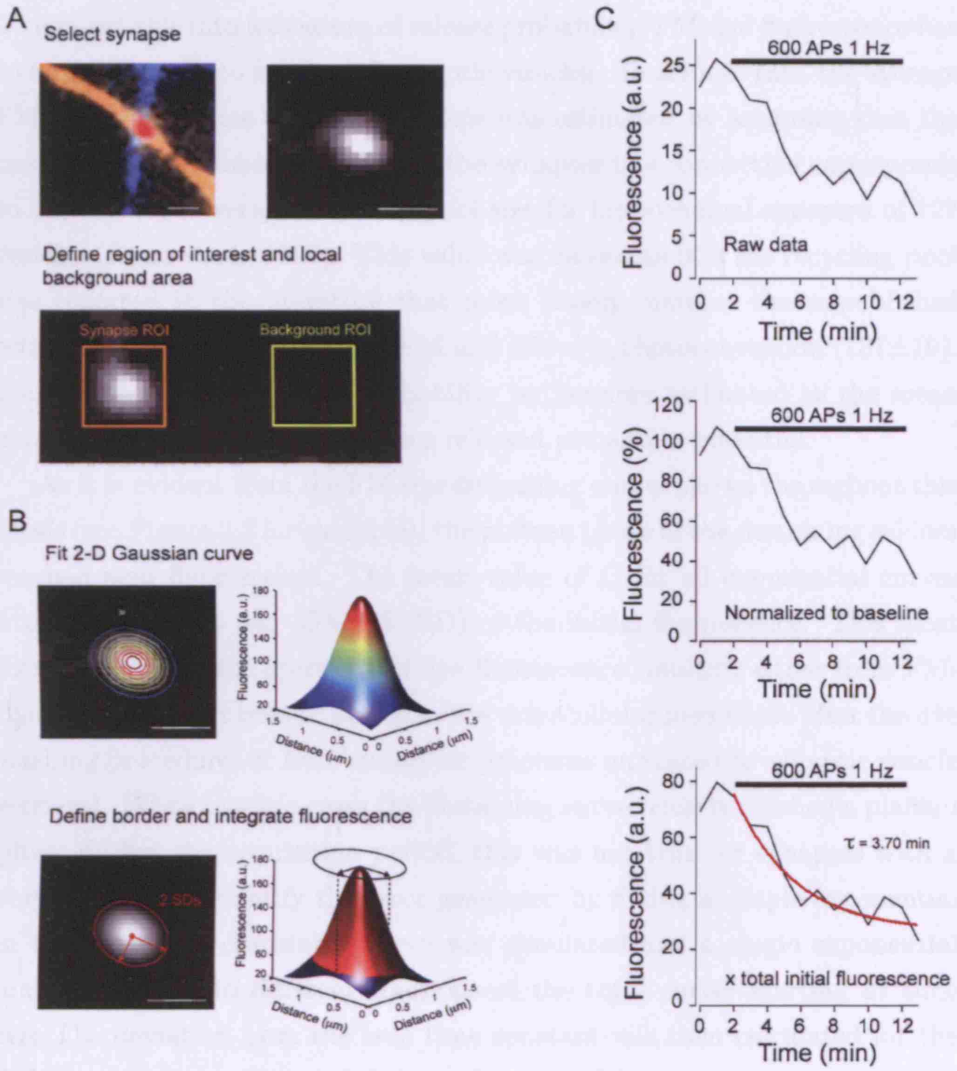

Figure 2.3: Estimating release probability using FM-dye destaining. A) Top, ROI showing axon (blue) and dendrite (yellow) with FM-labelled synapse (red), and raw FM-dye signal from the selected synapse (right). Bottom, ROIs used to measure mean fluorescence. (B) Top, 2-D gaussian curve fitted to the initial FM-dye fluorescence. Bottom, area used to integrate FM-dye fluorescence. (C) Traces showing the loss of FM-dye fluorescence upon stimulation, in raw format (top), or after normalization and correction for initial integrated fluorescence (middle and bottom). Red line is a single exponential fit to the data. Scale bars, 1 μm.

To convert this into a measure of release probability, FM-dye fluorescence has to be converted into number of synaptic vesicles. To achieve this, the average FM-dye fluorescence of a single vesicle was estimated by assuming that the mean integrated fluorescence for all the synapses in a connection corresponds to the reported average recycling pool size for hippocampal synapses of 127 vesicles (Ryan et al., 1997). This value was chosen as it is the recycling pool size reported in the literature that more closely matches the unpublished estimations from the lab, using EM and FM-dye photoconversion (137±19). Using this measure, release probability is therefore estimated as the mean number of FM-dye stained vesicles released per action potential.

As it is evident from the FM-dye destaining curves shown throughout this thesis (see Figure 2.3 for example), the plateau phase of the destaining seldom reached zero fluorescence. The mean value of C for all exponential curves fitted to the data was 30%±25 (SD) of the initial fluorescence. This most likely represents non-specific FM-dye fluorescence resulting either from FM-dye molecules that remain bound to the extracellular membrane after the dye washing procedure, or from endocytic processes unrelated to synaptic vesicle retrieval. While in some cases the destaining curves clearly reached a plateau phase during the acquisition period, this was not true for synapses with a very low p_r. To quantify the error generated by fitting a simple exponential in these cases, a destaining curve was simulated and a single exponential function was fit to different fractions of the total curve, starting at time zero.The deviation from the true time constant was then calculated for the different fractions. Figure 2.4 show that even for synapses with the lowest p_r observed, where the dataset covered only 25-50% of the full curve, the deviation from the true time constant was less than 2%.

The measure of release probability detailed above only takes into account the release of FM-dye stained vesicles, and is therefore an underestimation of the true number of exocytosed vesicles. Once a vesicle is released and loses its FM-dye molecules, it becomes re-incorporated in the recycling pool and will be available for re-release. As more and more vesicles lose their FM-

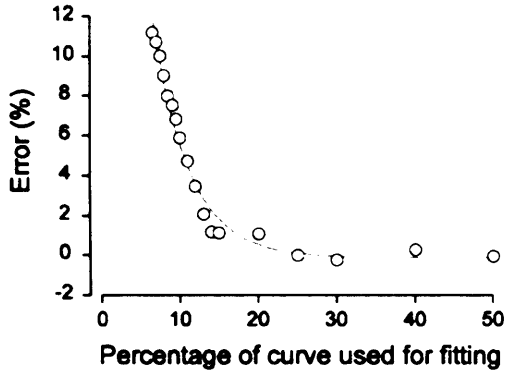

Figure 2.4: Quantification of the error arising from fitting a partial destaining curve. Several time constants were generated by fitting a single exponential to decreasing percentages of the total simulated destaining curve, and the deviation from the true time constant plotted as a percentage.

dye molecules, the probability of releasing a FM-dye stained vesicle decreases, and more unlabelled vesicles are released. If N is the total number of vesicles and n the number of FM-dye labelled vesicles at a given time point, then the probability of releasing a labeled vesicle is $\frac{n}{N}$. The decrease of this probability for every action potential is therefore given by:

$$\frac{dn}{dt} = -\frac{n(t)}{N} p_r \tag{2.1}$$

,where p_r is the probability of a release event occurring. This has the solution (solved using the *Dsolve* function in Mathematica 5.2):

$$n(t) = Ne^{-\frac{t}{\frac{N}{p_r}}} + C \tag{2.2}$$

,which is an exponential function is the same format as the the one fitted to the data to obtain the FM-dye destaining time constant. From here, it is evident that this time constant is a function of both the release probability and the size of the initial recycling pool, decreasing with the first and increasing with the latter. Calculating p_r as $p_r = \frac{N}{\tau}$, yields an average value that, as expected, is higher than what is obtained from the calculations detailed

above, though there is a very good correlation between the two estimates (Figure 2.5A, R = 0.84, P < 0.0001).

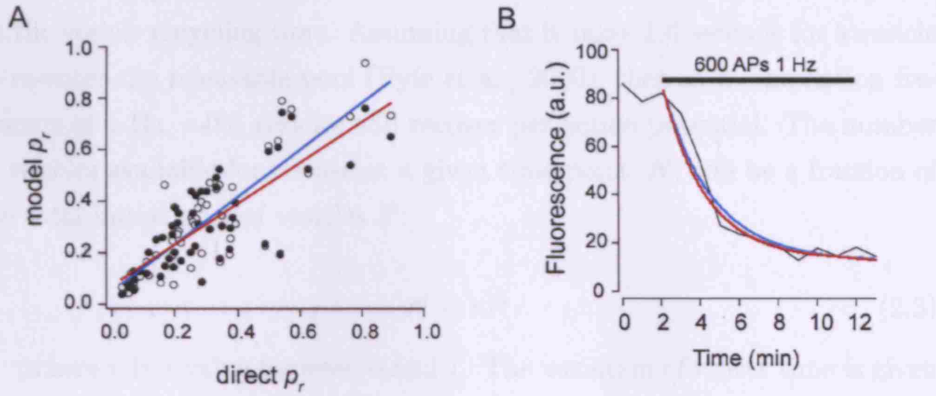

Figure 2.5: Calculating p_r with two different kinetic models. (A) Release probability estimated directly from destaining rates and pool sizes plotted against p_r values obtained by fitting the data with equations 2.2 (open circles, blue line, mean $p_r = 0.32 \pm 0.03$) and 2.7 (closed circles, red line, mean $p_r = 0.30 \pm 0.03$). Lines are linear fits. (B) Same FM-dye destaining curve shown in Figure 3.5, fitted with equation 2.2 (red) and equation 2.7 (blue).

One major assumption of this simple model of FM-dye loss is that N is constant over time. This implies that once a vesicle is released, it repopulates the recycling pool before the next action potential arrives. As the stimulation frequency is 1 Hz, this requires a maximal turnover time of one second. Although the estimates for the rate of vesicle reuse vary amongst the literature, Tsien and colleagues have specifically addressed this issue in hippocampal neurons in culture and suggested that is takes ~1.6 seconds for a vesicle to become available for re-release (Pyle et al., 2000). Such value renders the above model inadequate. A more realistic model has therefore to take into account the vesicle recycling time, where the value of N initially decreases with stimulation, until it reaches a plateau where vesicle release and recycling are balanced. This can be done by attributing two states to each

vesicle: release ready - Rr, and refractory - Rf. For each action potential that arrives to the synapse, the rate of vesicles in pool going from Rr to Rf is the release probability p_r, and the rate of transition back to Rr depends on the vesicle recycling time. Assuming that it takes 1.6 seconds for a vesicle to re-enter the releasable pool (Pyle et al., 2000), then at a stimulation frequency of 1 Hz, ~0.6 vesicles will recover per action potential. The number of vesicles available for release at a given time point, N, will be a fraction of the total initial pool of vesicles P:

$$N = rP \tag{2.3}$$

,where r is a value between 0 and 1. The variation of r over time is given by:

$$\frac{dr}{dt} = \alpha(1 - r) - p_r\, r \tag{2.4}$$

,with α being the rate of vesicle recycling. This has the solution:

$$r(t) = r_\infty(1 - e^{-\frac{t}{\tau}}) \tag{2.5}$$

,where $r_\infty = \frac{\alpha}{\alpha + p_r}$ and $\tau = \frac{1}{\alpha + p_r}$. Substituting N in equation 2.1 for this expression, and correcting it such that r_∞ is approached from an initial value of 1, gives:

$$\frac{dn}{dt} = -\frac{n(t)}{P(r_\infty + (1 + r_\infty)\, e^{-\frac{t}{\tau}})}\, p_r \tag{2.6}$$

,with the solution:

$$n(t) = (1 - r_\infty + e^{\frac{t}{\tau}} r_\infty)^{-\frac{p_r \cdot \tau}{P \cdot r_\infty}} P + C \tag{2.7}$$

This equation can be successfully fitted to the FM-dye destaining data, as shown if Figure 2.5B. The average release probability obtained with this model is lower than with the previous model, reflecting the the lower value of N during stimulation. Comparing with the direct calculations from destaining rate and pool size, this model still yields a slightly higher value, given

that it accounts for the release of unlabeled vesicles (Figure 2.5A). As the values obtained with equation 2.7 are highly dependent on the assumed vesicle recycling rate, throughout this thesis p_r was calculated directly from the pool size and destaining rates. Apart from the assumption that the average recycling pool size is constant between different cells, this measure depends only on experimentally obtained values, and nevertheless agrees very well with the calculations using equation 2.7 ($R = 0.81$, $P < 0.0001$). Though this is likely to constitute an underestimation of the true p_r value, as all synapses should be affected by a similar percentage error, this will not affect the measures of p_r variability used in the next chapters.

In cases that required all FM-dye labeled synapses in a field of view to be analysed, puncta were selected using an automated custom-written algorithm based on edge detection (Appendix 2).

2.6.3 Electron Micrographs

Synapses and neuronal processes were reconstructed using a graphics software package (Xara Xtreme, Xara Ltd, UK) to establish the precise spatial arrangement of axons and dendrites. FM1-43 labeled, photoconverted vesicles were readily distinguishable from unstained vesicles by their dark lumen using the criteria previously described (Darcy et al., 2006a). 3-D reconstructions of processes and presynaptic terminals were made using Reconstruct (Fiala, 2005). Distances between synapses were measured from the centre of the active zone for each presynaptic terminal, along the process of interest. Morphologically docked vesicles were counted in a data subset where the borders of the active zone were clearly visible along all sections where that active zone was present.

2.6.4 Statistics

To compare data sets, non-parametric tests (Mann-Whitney U-test, Wilcoxon rank sum test or χ^2-square test) were used unless otherwise indicated. Tests

for normality and comparison of distributions were made using Kolmogorov-Smirnov tests. Pearson r-test or Spearman r-test were used for correlation analysis. Release probability similarity values were obtained by bootstrapping the relevant data set 10,000 times. For Monte Carlo simulations of δp_r and intersynaptic distance, 20,000 pairs of p_r values were randomly drawn from a Gaussian distribution with the mean fixed at the average pr measured with EM, and the standard deviation adjusted to produce the desired CV as detailed in chapter three. Statistical significance was assumed when $P < 0.05$. In figures, * indicates $P < 0.05$, ** indicates $P < 0.01$ and *** indicates $P < 0.001$. Values in the text and figures represent mean±s.e.m. unless otherwise stated.

Chapter 3

Study of the spatial distribution of release probability in cultured hippocampal neurons

Regardless of what factors are involved in determining the release probability of synapses, the marked variability of p_r described in chapter one indicates that they are not uniformly distributed across a synapse population. Different synapses have different release probabilities and understanding the basis for this may be an important step towards elucidating the determinants of p_r. Thus, an alternative approach to establishing what sets release probability is to ask what makes p_r variable between synapses. To address this problem it is important to study a population of synapses that is as homogenous as possible except for their differences in p_r, so that the underlying factors contributing to p_r variability are limited. The form of synaptic connections that most readily meets these requirements are autapses, where differences in the cellular and molecular composition of both synaptic compartments are reduced to the minimum. However, in autapses the pre and postsynaptic activities cannot be dissociated, which can lead to highly artificial conditions

(i.e.: the evoked release of neurotransmitter is always paired with a postsynaptic spike) and therefore makes experimental results hard to interpret. A more complex alternative is the connection between two neurons mediated by more than one synapse, where all the presynaptic compartments belong to the same axon and interact with the same dendritic tree, therefore constituting a synaptic population with uniform identities. This situation is very frequently observed in primary hippocampal cultures where neurons in small networks form multiple *en passant* synapses on the neighbouring cells. This, together with the disposition of neurons in a mono-layer readily accessible to high resolution imaging of individual synapses, makes hippocampal cultures ideally suited for the study of release probability and they were therefore the system of choice for the work in this thesis.

Although several variables will certainly prove to be important in defining release probability, there seems to be a certain degree of spatial coordination between them, since Murthy et al. (1997) reported that in hippocampal autaptic connections, p_r in immediately adjacent synapses is correlated. This observation was, however, very briefly addressed and there was no information on the dendritic or axonal organisation underlying these neighbouring synapses. In face of this and on the presumption that uncovering some spatial organisational rules of release probability might shed some light on its determinants, the initial approach in this thesis is a detailed study of p_r spatial distribution at the fluorescence and ultrastructural levels. The present chapter describes the experimental paradigms used for this purpose and the results obtained from exploring the spatial organisation of p_r in a connection between two neurons.

3.1 Growing small networks of hippocampal neurons

To successfully limit the study of p_r to the population of synapses connecting two cells, culture conditions were adjusted to favour the development of small

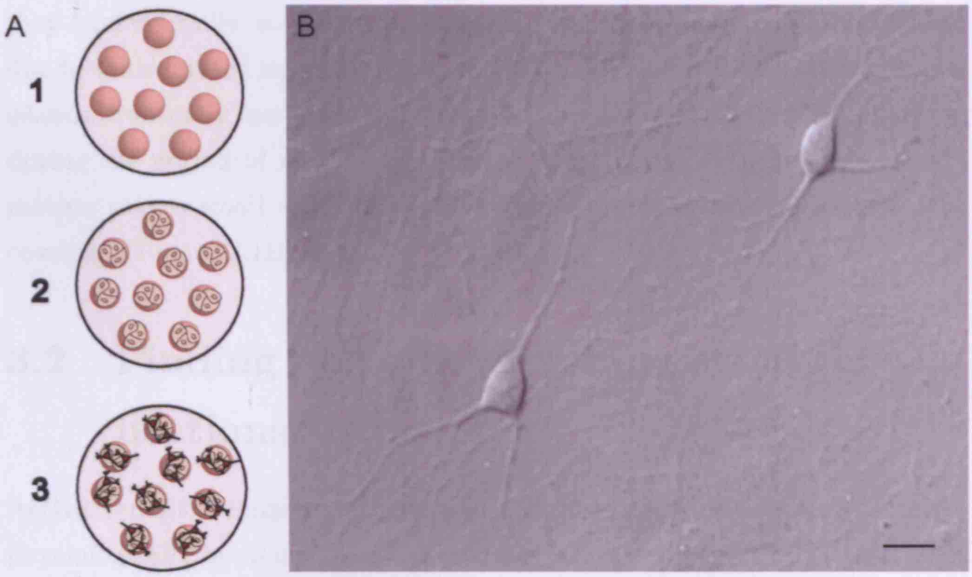

Figure 3.1: Development of small and spatially restricted neuronal networks. (A) Cartoon illustrating the three main steps in the process of growing small networks. 1 - spraying of substrate microdots, 2 - pre-plating glial cells, 3 - plating neurons at low density. (B) DIC image of a typical network of two connected neurons at 12 DIV. Scale bar - 15 μm.

and spatially restricted networks of 2-4 neurons. This not only ensures a high connection rate that greatly improves experimental yield, but also limits synaptic density to facilitate single synapse imaging, while ensuring a certain degree of spatial proximity that allows monitoring of many synapses at the same time. Several methods are available to impose spatial restrictions to cells grown in culture, such as substrate spraying or micropatterning on a bed of agarose that would otherwise prevent cell attachment. These and others were tried, but it was found that cell health was often inferior to unrestrained cultures, and so a protocol was devised that did not rely on imposed physical restrictions. By pre-plating glial cells on coverslips covered with substrate microdots, small astrocyte islands form after 2-3 days (Figure 3.1A). When neurons at appropriate concentrations are then plated onto these coverslips,

they preferentially attach to and develop on the astrocyte islands, which, due to their limited size, will spatially limit neuronal growth. Although glial islands eventually merge with each other, they are sufficiently well separated during the period of more active process growth and branching, so that in mature stages small and healthy discrete neuronal networks populate the coverslip (Figure 3.1B).

3.2 Finding and characterising synaptic connections

Active synaptic connections between two neurons were identified electrophysiologically by double and triple whole-cell recordings. Two or three cells closely placed in a small network were visually identified with DIC optics and the recordings established. To test for the presence of a connection, one cell was held in voltage-clamp mode while the putative presynaptic neuron was stimulated in voltage recording mode. Only monosynaptic connections (i.e.: direct connections between two cells) were considered, as judged by the latency between the peak of the action potential and the 20% rise point of the postsynaptic current (1.87±0.12 ms, N = 26). Because the whole hippocampus was used for preparing the cultures, the final cell population comprises both excitatory and inhibitory neurons. Accordingly, two clearly different types of synaptic currents were recorded and are depicted in Figure 3.2A-B. One group had fast rise and decay kinetics (20-80% rise 472±30 μs, decay tau 1.83±0.13 ms, N = 13), reversed at 0 mV and was completely blocked by CNQX, therefore fulfilling the criteria for a AMPA mediated glutamatergic current (Honore et al., 1988). The remaining connections had comparable rise-times (722±48 μs) but the decay was substantially longer (10.5±0.75 ms), reversed very close to the calculated chloride reversal potential (-69 mV) and were blocked by the broad spectrum gamma-aminobutyric acid (GABA) A receptor blocker Bicuculline (Curtis et al., 1970) thus identifying them as inhibitory GABA-mediated postsynaptic currents (GPSCs, N = 13,

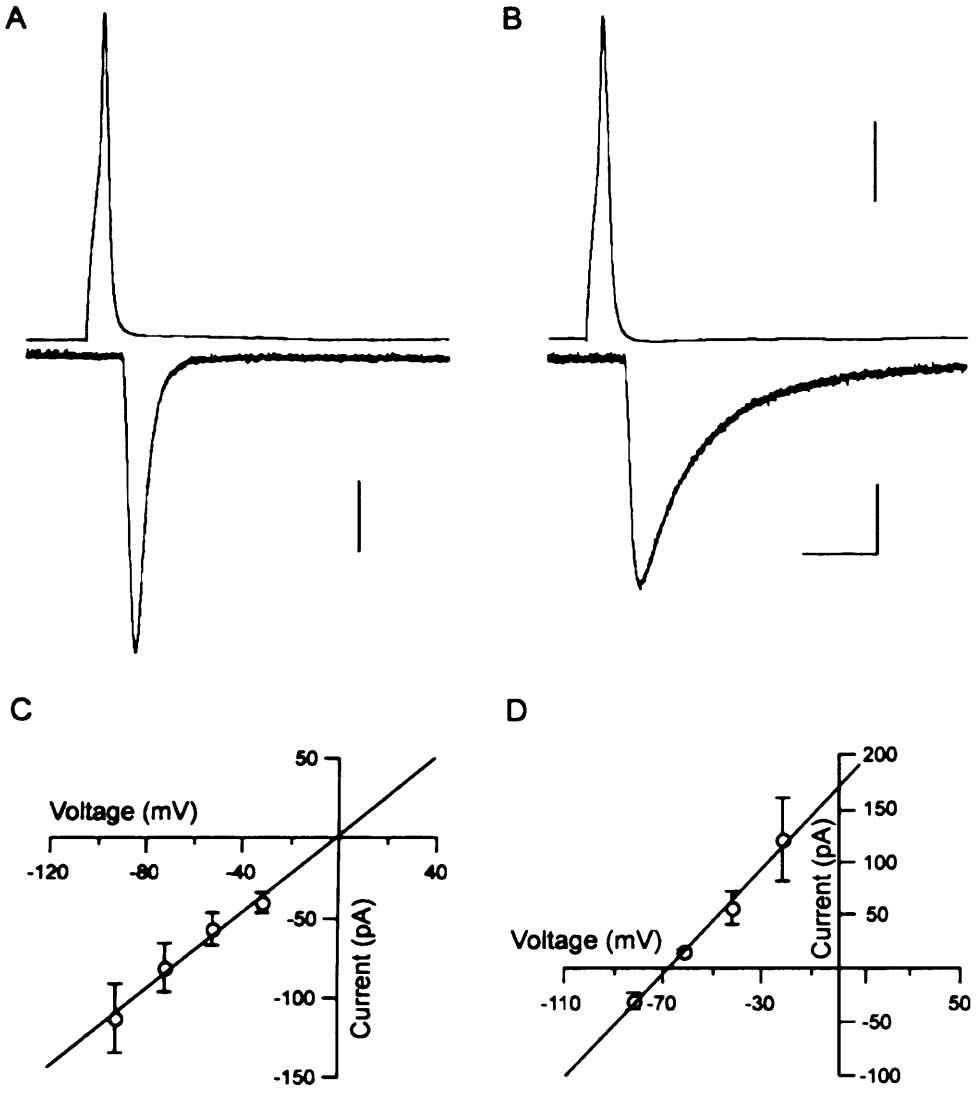

Figure 3.2: Properties of excitatory and inhibitory connections. (A) Representative recording of an excitatory connection with the AP voltage change on top and the time-locked EPSC below. Scale bar, 100 pA. (B) Example of an inhibitory response. Scale bars, top 20 mV, bottom, 30 pA, 10 ms. Traces in A and B are averages of 10. (C) and (D) Average current-voltage relationship for excitatory and inhibitory connections, respectively.

Figure 3.2C-D). The input resistance of both groups was not significantly different (668±81 Vs 898±296 MΩ, P = 0.9787).

Cells were used for experiments between 10-15 DIV, which is generally regarded as the age at which synapses reach maturation (Renger et al., 2001). However, the functional impact of inhibitory synapses is intrinsically linked to the intracellular chloride concentration, which in turn depends on the action of chloride transporters. If high levels of chloride are present inside the cell, the Cl^- reversal potential will be positive relative to the membrane potential and inhibitory synapses will be depolarising, which is the case during development. Full maturation of inhibitory function is only reached with expression of the K^+/Cl^- co-transporter KCC2 (Rivera et al., 1999). To evaluate the maturation stage of inhibitory cultures in this system, perforated patch recordings were achieved with Gramicidin in the internal patch pipette solution, which, when in contact with the cell membrane forms pore channels that are not permeable to Cl^- ions (Rhee et al., 1994). In this way the intracellular Cl^- concentration is not disrupted by the recording procedure and the physiological action of inhibitory synapses can be assessed. Miniature IPSCs were isolated by recording in the presence of AMPA and NMDA receptor blockers, and currents were recorded at different membrane holding potentials to construct a current-voltage curve (Figure 3.3A). As shown in Figure 3.3B, the average reversal potential was -46.5 mV (N = 5). Given the measured average membrane resting potential of -58±0.9 mV, this means that at the age the cultures were used for experiments, GABAergic synapses are either slightly depolarising or just acting as shunting inhibition. This immature phenotype associated with the uncertainty of the resting Cl^- reversal potential relation for individual cells, complicates and undermines the interpretation of experiments with inhibitory synapses and for this reason only excitatory connections were analysed in this thesis.

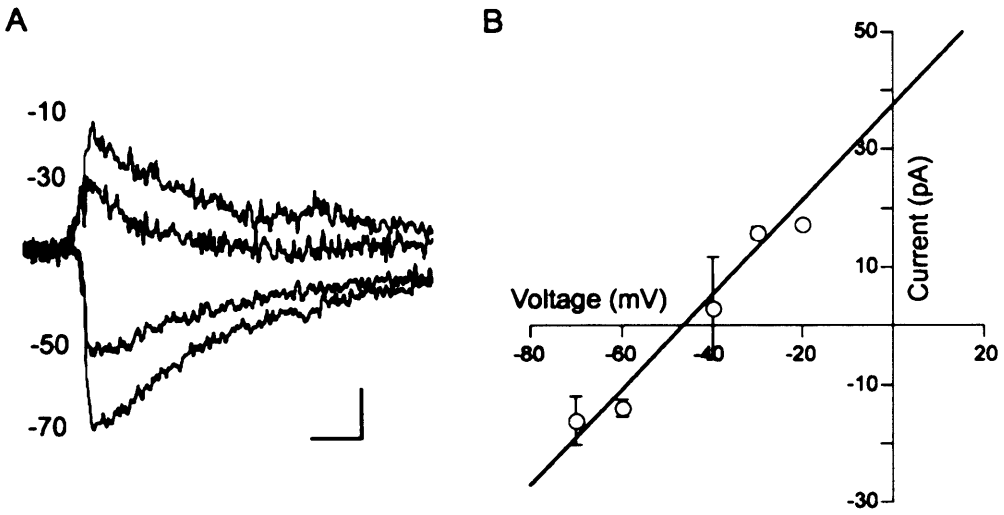

Figure 3.3: Gramicidin perforated-patch recordings of mGPSCs. (A) Average mGPSC traces from one example cell held in voltage-clamp at different membrane potentials (indicated on the left). Scale bars, 5 ms, 5 pA (B) Current-voltage relationship for the cell population studied shows a GPSC reversal potential more depolarised that the average resting potential.

3.3 Visualising axons and dendrites from the recorded cells

Selective visualisation of the processes of the synaptically connected neuron pair is indispensable for any detailed study on spatial organisation of synaptic parameters. Here, this was achieved with Alexa Fluor hydrazides, a class of low molecular weight molecules that consist of an Alexa Fluor dye connected to a hydrazide moiety. This ensures high polarity, which provides great water solubility and cell membrane-impermeability.

Alexa fluor dyes have the advantage over more regular fluorochromes such as fluorescein isothiocyanate (FITC) or Rhodamine that they are more bright and photostable, and they have a well differentiated spectrum that is ideally suited for multicolor detection (Panchuk-Voloshina et al., 1999).

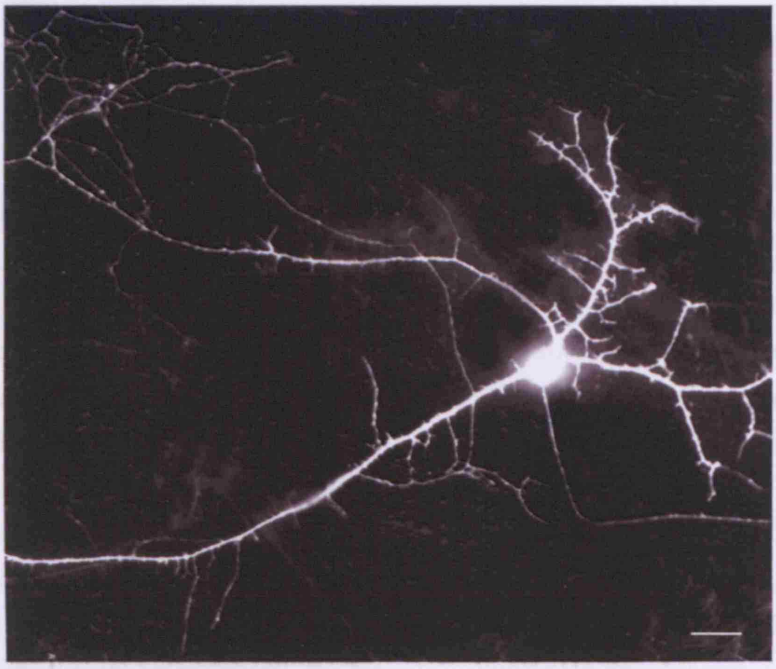

Figure 3.4: Neuron filled with Alexa-dye. A cell was filled with Alexa-488 hydrazide during a whole-cell recording and images taken in an epifluorescence microscope using a FITC filter set. Shown is a montage of several fields of view. Scale bar - 15 μm.

Depending on the experiment, each patch pipette was filled with an internal solution that included a different coloured Alexa-dye, such that the use of standard fluorescence filter sets allowed the independent visualisation of each cell. Labelling of the whole neuron occurred within the first five mins after the whole-cell configuration was established and the dye diffusion and brightness were sufficient to identify even the finer processes as illustrated in Figure 3.4.

3.4 Fluorescence analysis of p_r at identified single synapses

Of the available methods described in Introduction for measuring release probability at individual synapses, a FM-dye based technique was chosen as this is the most direct and versatile. Synapses were labelled with FM4-64 by bulk stimulating the whole coverslip with a 90 mM KCl solution in the presence of the dye. Hyperkaelemic solutions induce neuronal activity by depolarising both the AP initiation site above threshold and the presynaptic terminal directly, and are a standard procedure to label all the recycling pool (Harata et al., 2001a). After stimulation, the culture was washed and kept in a low Ca^{2+}/high Mg^{2+} solution to minimise dye loss from the terminal due to spontaneous activity. A paired whole-cell recording was then obtained usually in the following 5-10 mins and the extracellular solution changed to the physiological Ca^{2+}/Mg^{2+} ratio. If a synaptic connection was present, neurons were left to fill with alexa-dyes for ~5 mins and a region that contained both overlapping labelled axonal and dendritic branches, and FM-stained puncta that were likely synaptic contact points between the recorded neurons, was selected for live imaging (Figure 3.5A). To measure p_r the presynaptic cell was stimulated in voltage-recording mode by eliciting 600 AP, and vesicle fusion was monitored by imaging fluorescence loss from the FM-labelled synapses. Action potentials were delivered at 1 Hz to prevent dynamic changes in p_r due to short-term plasticity, but even at this frequency range a slow and progressive reduction in release probability is known to occur (Larkman et al., 1997b) and will lead to underestimation of the absolute p_r value. During the stimulation, excitatory synapses were blocked with CNQX and APV to prevent recurrent network activity. In this way, the number and timing of APs delivered to the presynaptic cell are precisely controlled and no other cells in the network are allowed to spike. This ensures that only synapses belonging to the axon of the stimulated cell will lose FM-dye, which combined with the Alexa-dye fills identifies those synapses as putative contacts between the cell

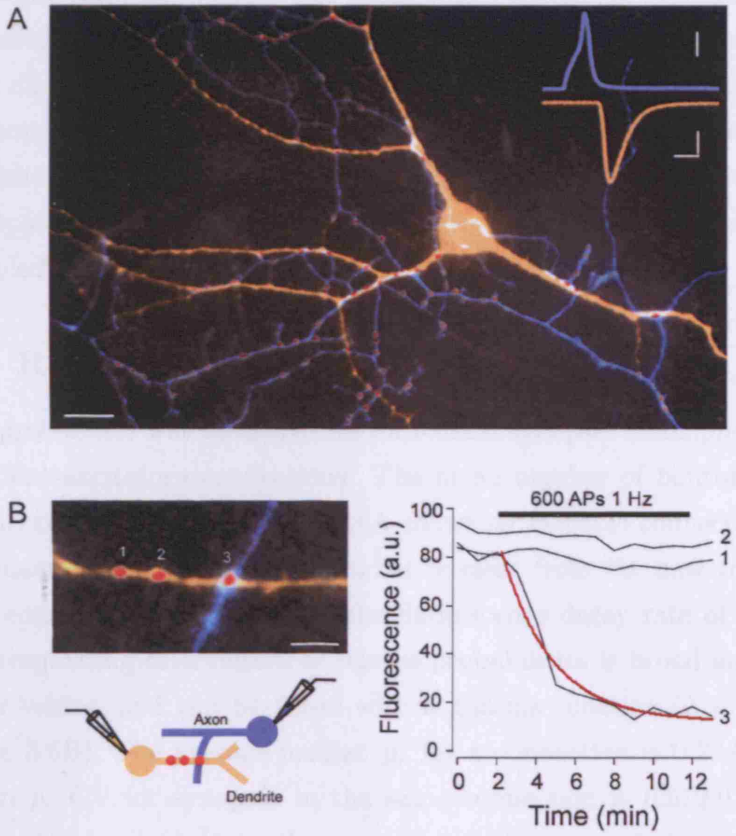

Figure 3.5: Measuring p_r at identified synapses using FM-dye. (A) Epifluorescence image of a selected region of interest showing an axon (blue) making multiple synaptic contacts (red, FM4-64) with a postsynaptic cell (orange). Whole-cell recording confirmed the presence of an excitatory connection between the two neurons (inset). Scale bars, 15 μm, inset, 2 ms, 20 mV (top), 200 pA (bottom). (B) Example of a putative synapse between the labelled axon and dendrite, next to two synapses presumably belonging to different presynaptic cells (left). Selective stimulation of the presynaptic neuron exclusively destains FM4-64 fluorescence from the synapse belonging to the labelled axon (right). Red line is a single exponential fit . Scale bar, 5 μm. Images have been pseudocoulored for clarity.

pair of interest (Figure 3.5B). Release probability was estimated for each imaged synapse from the fluorescence decay time constant as mentioned above and detailed in the Methods chapter. Because at the end of the destaining protocol all synapses from the stimulated axon have lost their fluorescence, p_r measurements are only possible for the synapses in the chosen field of view. Although probably not all synaptic contact points are monitored, the limited spatial spread of the network ensures that the majority of boutons are sampled.

3.4.1 Release probability is not uniform

Release probability was measured for individual synapses belonging to seven independent excitatory connections. The mean number of boutons imaged per connection was 7.9±2. Figure 3.6A shows an example connection where p_r was measured at 19 synapses, and it is clear from the raw traces that there is considerable variability in the fluorescence decay rate of each one. The corresponding distribution of release probabilities is broad and skewed to larger values, and can be fitted with a gamma function (λ = 5.8, n = 3, Figure 3.6B). The average median p_r for a connection is 0.22±0.04 and the mean p_r CV for synapses in the same connection is 0.51±0.13. This variability is also evident in the recycling pool sizes and destaining time constants alone, as illustrated by the histograms in figures 3.6C and 3.6D. For synapses belonging the same connection, the mean CV for recycling pool size is 0.35±0.07, and for destaining time constants 0.41±0.05. This description is in full accordance with previous studies in cultured hippocampal neurons (Murthy et al., 1997; Slutsky et al., 2004; Granseth et al., 2006), and shows that in the chosen paradigm of one axon making synapses in one dendritic tree there is indeed a great amount of variability in release probability.

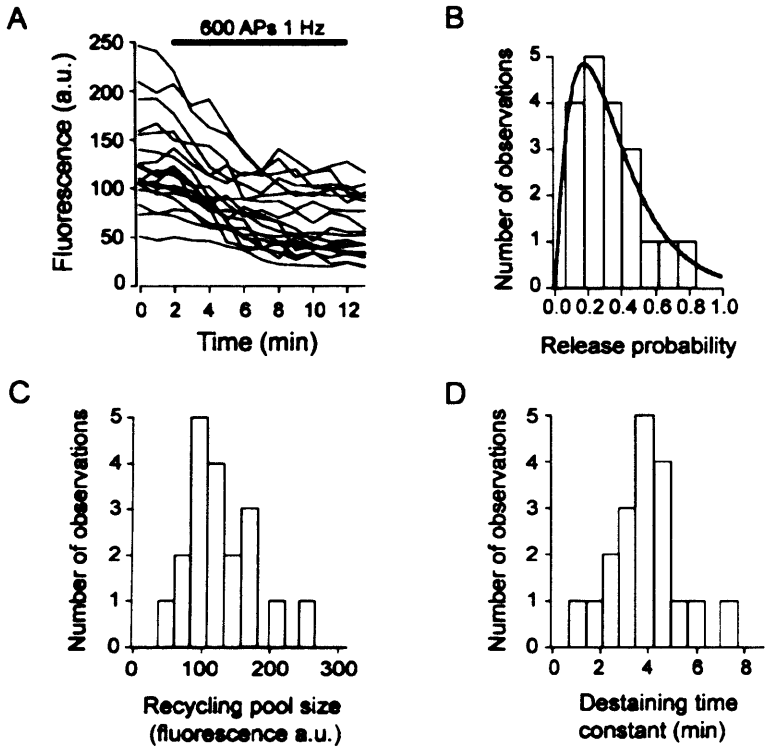

Figure 3.6: Variability of release probability. (A) FM-dye destaining traces from one connection mediated by 19 individual synapses. (B) Corresponding release probability frequency histogram. Solid line is a gamma function fit. (C,D) Frequency histograms for recycling pool sizes and destaining time constants, respectively, for the same connection.

3.4.2 There is no relation between p_r and distance to the soma

A previous study has reported that, in CA1 pyramidal neurons, the quantal size of synapses made on the main dendritic trunk increases with distance to the soma (Magee and Cook, 2000). To determine if the same is true for release probability in hippocampal cultures, distance from the FM-dye labelled synapses to the soma of the putative postsynaptic cell was measured along the dendrite and p_r plotted against it. As is evident from Figure 3.7, no correlation was found between these two parameters (R = 0.1005, P = 0.5015). When the same analysis was done for distance along the presynaptic cell axon, the same lack of correlation was observed (R = -0.07192, P = 0.6053). This was also true for both the recycling pool sizes (R = -0.03735, P = 0.8010 for dendrite, R = -0.2342, P = 0.1131 for axon) and destaining time constant (R = 0.09927, P = 0.5020 for dendrite, R = -0.06736, P = 0.6528 for axon, see Figure 3.7). This result indicates that in these conditions there is no apparent relation between release probability and the physical distance to the soma.

3.4.3 Release probability is dendritically segregated

The same axon can develop a variety of release probabilities in the same dendritic tree. However, axons and dendrites in vivo and in vitro exhibit multiple branches that interact with various configurations of input or output convergence and divergence. To investigate if the spatial organisation of synapses has any impact on their release probability, the degree of variability was independently determined for two different situations: i) axonal branches that contact different dendritic branches and ii) dendritic branches that are contacted by different axonal branches. Branches were defined as the short segment between two successive branchpoints, and no distinction was made for different branching orders. Axonal and dendritic branches running in parallel to each other were excluded from this analysis. Variability was mea-

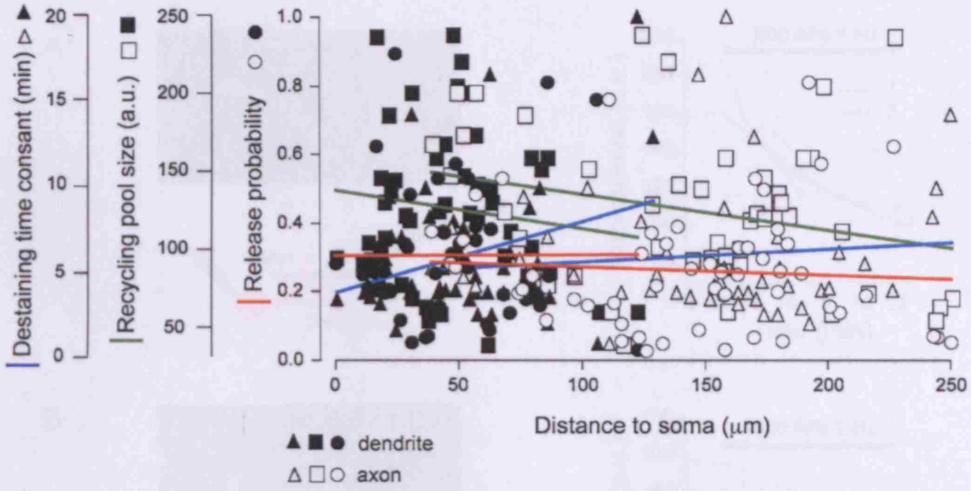

Figure 3.7: Distance to soma and release probability. Physical distance of single synapses to the soma, measured along the dendrite of the postsynaptic cell, or axon of presynaptic neuron, plotted against p_r, recycling pool size and destaining time constant. Coloured lines are linear fits to the data and show no relationship between p_r and along the dendrite (short line) or axon (long line).

sured as the CV for each segment and as the p_r ratio between synapses in the same segment. For the latter, each synapse was compared to all the others in the branch and the ratio calculated with the highest p_r as the denominator. In this way the ratio becomes a measure of similarity between two synapses and can be conveniently expressed as a percentage. An example of the situation where one axon branch makes two synapses in two different dendritic branches is illustrated in Figure 3.8A . The release probability of both synapses was markedly different, and for all the population the mean CV was 0.48 ± 0.09, which is not different from the overall p_r CV ($P > 0.9999$). The mean similarity between synapses in the same axon branch was $49\pm3\%$. To better understand the significance of this value, a bootstrap was used to predict the expected similarity due to random sampling of the p_r distribution. The obtained value was 53%, which is not significantly different from the value obtained for this first situation ($P = 0.1331$, Wilcoxon rank sum test,

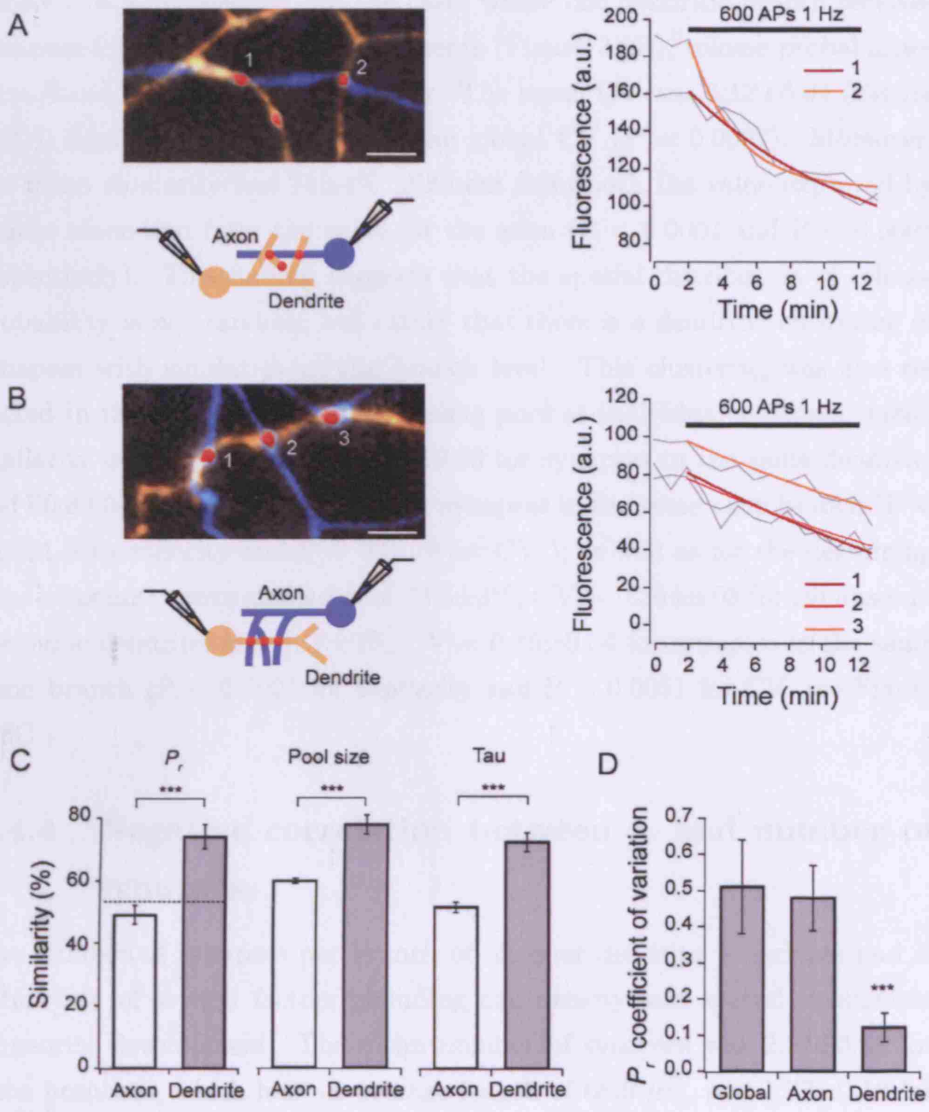

Figure 3.8: Spatial analysis of release probability. (A-B) Example images (left) and destaining curve fits (right) for synapses on different (A) or on the same dendritic branch (B). Scale bars, 5 μm. (C) Summary of similarity comparisons between synapse pairs for p_r, recycling pool sizes and destaining time constants. Dashed line indicates expected similarity due to chance calculated by bootstrap. (D) Release probability CV for all synapses in a connection (global) compared to synapses in the same axon or dendritic branch.

Figure 3.8C). In contrast, for the cases where one dendritic branch receives synapses from different axonal segments (Figure 3.8B), release probabilities were found to be remarkably similar. The mean CV was 0.12±0.04 (Figure 3.8D), significantly different from the global CV (P = 0.0007). Moreover, the mean similarity was 74±4%, different from both the value expected by chance alone and from the value for the axon (P < 0.0001 and P < 0.0001 respectively). This finding suggests that the spatial distribution of release probability is not random, but rather that there is a dendritic clustering of synapses with similar p_r at the branch level. This clustering was also reflected in the sizes of the total recycling pool at individual synapses: mean similarity of 77.4±3%, CV = 0.18±0.03 for synapses in the same dendrite, and 60.8±0.9%, CV = 0.35±0.06 for synapses in the same axon branch (P < 0.0001 for similarity and P = 0.0116 for CV); as well as for the destaining time constant: mean similarity of 73.3±3%, CV = 0.20±0.03 for synapses in the same dendrite, and 51.7±2%, CV = 0.36±0.04 for synapses in the same axon branch (P < 0.0001 for similarity and P = 0.0051 for CV, see Figure 3.8C)

3.4.4 Negative correlation between p_r and number of synapses

The number of synapses per branch of axon or dendrite is variable and is a function of several factors including cell density and spatial constraints to neurite development. The mean number of synapses was 2.57±0.51 for axon branches, which had an average length of 68.9 μm, and 1.77±0.18 for dendrite branches with a mean length of 28.9 μm. The mean intersynaptic distance was 8.5±0.7 μm in the axon and 5.9±1.7 μm in the dendrite, not significantly different from each other (P = 0.1406, N = 55 synapses).To investigate if there is a relationship between the number of synapses in a branch and the individual release probabilities, the mean p_r for synapses in one branch was plotted against their number (Figure 3.9).

This plot summarises data from different connections that belong to net-

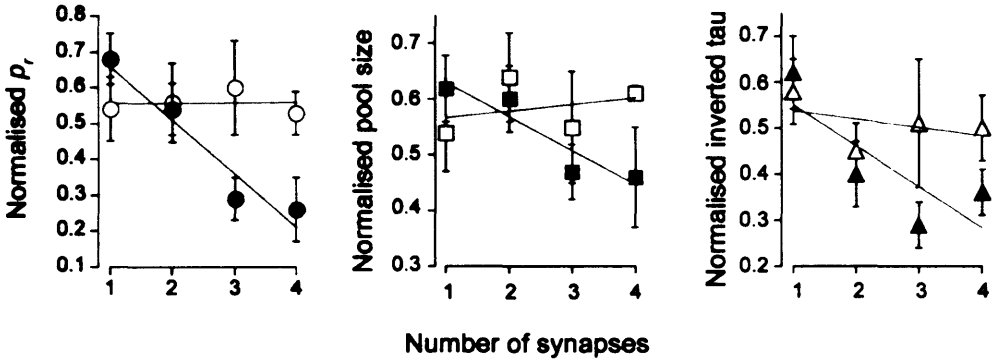

Figure 3.9: Synapse number and release probability. Normalised p_r (left), recycling pool size (middle) and destaining time constant (right), plotted against the number of synapses in the branch of the axon (white symbols) or of the dendrite (black symbols). The destaining time constant has been inverted so that smaller values indicate slower destaining rates. Lines are linear fits to the data.

works with probably different levels of activity. Given the complex relations between p_r and activity described in the first chapter, different connections might have different overall release probabilities, and therefore individual values of p_r were normalised to the maximum p_r value of the connection they belong to. As is evident from Figure 3.9, although there was no relation between p_r and the number of synapses made by axon branches contacting different dendrites (R = 0.01, P = 0.9349), there was a very significant negative correlation for release probability and the number of synapses in the dendritic branch (R = -0.53 , P < 0.001). The same result was obtained for the recycling pool sizes (R = 0.06, P = 0.7238 for axon, R = -0.29, P = 0.0482 for dendrite) and for the rate of FM-dye destaining (R = -0.09, P = 0.5532 for axon, R = -0.42, P = 0.0032 for dendrite, see Figure 3.9B, middle and right). This suggests that release probability adapts to the environment in the dendrite, but is independent of the disposition of synapses along the axon.

3.4.5 There is no correlation between p_r and the overall synapse density

One possible explanation for the above finding would be a sampling bias arising from the fact the population of cell included in the study is mixed. If, for example, different cell types attract axons onto common dendritic fragments with different avidity, branches with higher number of synapses for a connection will also have more synapses from other axons, generating differences in the overall axon-dendrite contact area. In the event that release probability is negatively regulated by some secreted factor that diffuses extracellularly, synapses in branches with high synaptic density would systematically have a lower p_r due to interactions with other synapses, an not necessarily due to differences in the activity they impinge on the dendrite. To verify if the population of cells analysed had a constant synaptic density, the number of synapses per branch of dendrite and axon was counted for every connection. This was done by counting the number of all FM-dye puncta overlapping a filled process, before the onset of stimulation. As shown in Figure 3.10A, there were no differences between synaptic density for the dendrite (population mean = 5.16, P = 0.6703 ANOVA) nor for the axon (population mean = 6.06, P = 0.1073 ANOVA). Furthermore, there was no systematic correlation between the mean overall synapse density and release probability for individual connections (R = -0.006, P = 0.9906 for density in the dendrite, R = 0.22, P = 0.6321 for density in the axon, see Figure 3.10B). This indicates that the distribution of synapses in the population of cells studied is homogeneous, and that the release probability of a connection is not related to the overall synapse density of the pre or the postsynaptic cell.

A similar bias could also occur at the level of individual dendrites within a given connection. If due to particular geometric arrangements of the culture, some dendrites are more favored than others to received synaptic input, the above argument could still apply, and the bias would not be detected in the plot of Figure 3.10B. To investigate if this was the case, dendritic branches from experiments where p_r was estimated by loading synapses with FM-dye

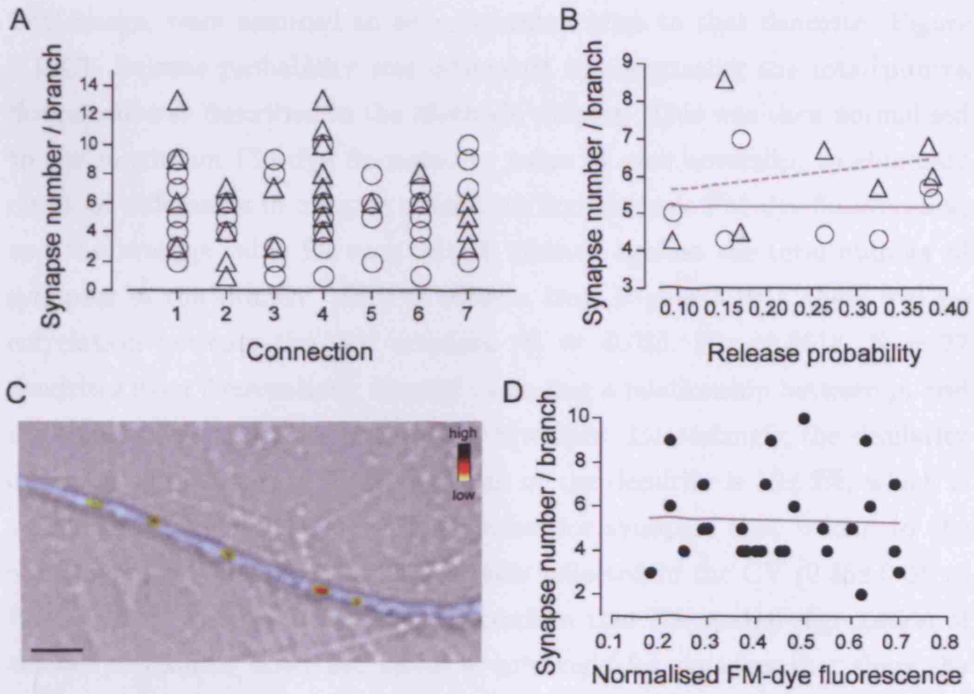

Figure 3.10: Overall synapse density and release probability. (A) Number of synapses per branch of dendrite (circles) or axon (triangles) for all connections analysed. Each symbol represents one branch. (B) Average number of synapses per branch of dendrite (circles) and axon (triangles) for a connection, plotted against its average release probability. Each symbol represents one connection. Lines are linear fits to the data, solid line is fit to dendrite data and dashed line to axon data. (C) DIC image of a dendritic branch (coulored in blue for clarity) with superimposed FM4-64 measure of p_r (pseudocoulored). FM-dye puncta in the field of view that were not in contact with the highlighted dendrite were digitally removed for clarity. Scale bar, 5 μm. (D) Average integrated FM-dye fluorescence against for individual branches, plotted against synapse density for the branch. Line is a linear fit to the data.

using 30 APs delivered by field stimulation (see below) were analysed. All FM-labelled puncta in contact with a branch of interest, as identified by a DIC image, were assumed to be presynaptic sites to that dendrite (Figure 3.10C). Release probability was estimated by integrating the total puncta fluorescence as described in the Methods chapter. This was then normalised to the maximum FM-dye fluorescence value of each coverslip, to eliminate eventual differences in imaging conditions and intrinsic FM-dye fluorescence, and the average value for each branch plotted against the total number of synapses in the branch. As it is evident from Figure 3.10D, there was no correlation between the two variables (R = -0.035, P = 0.8618, N = 27 dendrites from 7 coverslips), thereby excluding a relationship between p_r and the total synaptic density of dendritic branches. Interestingly, the similarity of p_r for all synapses in a given branch of the dendrite is 59±2%, which is significantly lower than the 74±4% value for synapses that belong to the same axon (P = 0.0083), and this is also reflected in the CV (0.45±0.04 vs 0.12±0.04, P = 0.0002). These data confirm that the spatial segregation of release probability described above is only valid for synapses that share the same presynaptic cell.

3.5 Ultrastructural analysis of release probability

In the experiments at fluorescence light microscopy level described above, synaptic contact points between the cells of interest were identified as FM-dye labelled puncta that overlapped with Alexa-dye filled axons and dendrites, and that lost fluorescence upon stimulation. Although only synapses belonging to the stimulated axon will destain, it is however, impossible to guarantee that in all cases their postsynaptic target was the apposed labelled dendrite. Even in these culture conditions of very low cell and neuronal process density, the possibility remains that on some occasions synapses are formed with an unlabelled dendrite that crosses the identified presynaptic

site. Unequivocal identification of single synapses and the axonal and dendritic processes they belong to can only be achieved at the ultrastructural level. Electron microscopy and FM photoconversion were therefore used to confirm and complement the findings of p_r spatial distribution at the fluorescence level.

3.5.1 Measuring p_r with FM1-43 photoconversion and EM

Photoconversion is a process whereby fluorescent molecules are excited in the presence of a reducing agent such as DAB, and give rise to an electron dense reaction product that is visible in EM once treated with osmium tetroxide. Photolabile fluorophores such as FM-dyes are more likely to emit free radicals, and this makes them a very good substrate for an efficient photoconversion. Synaptic vesicles labelled with FM are readily identifiable in electron micrographs as they have a very electron dense core when compared to non-labelled vesicles (Henkel et al., 1996; Harata et al., 2001b; Darcy et al., 2006a). This makes FM-dye photoconversion an ideal method for counting the number of vesicles exocytosed in response to stimulation and an attractive technique to estimate release probability. If a terminal is stimulated by a defined number of APs, p_r can be measured directly by the ratio of vesicles labelled to the number of APs. To implement this, synapses were first labelled with the fixable form of FM1-43 (FM1-43FX) by delivering 30 APs at 1 Hz using field stimulation, while blocking AMPA and NMDA receptors to prevent recurrent network excitation. To ensure that this was a reliable method of eliciting APs, the stimulation parameters were initially calibrated by field stimulation while simultaneously monitoring action currents with whole-cell recordings in individual cells (see Figure 4.5). After FM-dye loading, cells were kept in a low Ca^{2+}/high Mg^{2+} external solution to minimise FM-dye loss and a region of interest was selected at the fluorescence level. After fixation with glutaraldehyde/paraformaldehyde and incubation with DAB, the selected region was illuminated with maximal light intensity in

the 455 nm to 495 nm range to induce photoconversion of the FM-labeled synapses. The samples were then embedded, serial sectioned, imaged with an electron microscope and fully reconstructed. The details of both FM1-43 photoconversion and EM protocols used have been recently published by the researchers I collaborated with for this part of the thesis (Darcy et al., 2006b,a) and will not be discussed here.

3.5.2 Confirming p_r variability

Serial sectioning and full 3D reconstruction was possible for 35 synapses. Only boutons with an apparently single active zone, an identifiable postsynaptic site and at least one FM-dye labelled vesicle were accepted for analysis (Figure 3.10A-B). The vesicle cluster size was variable across synapses and the median total pool size was 277 vesicles (Interquartile range, IQR = 290), with an average of 11±2 morphologically docked vesicles. Release probability, as estimated by the number of photoconverted vesicles per AP, had a median of 0.37 (IQR = 0.91) and a broad distribution skewed to larger values (Figure 3.10C). Of all the synapses analysed, 9 had more than 30 photoconverted vesicles, which yields a p_r above one. The potential reasons for this are varied and are discussed below, but nevertheless the distribution of release probabilities obtained with this method matched what was found at the fluorescence level and is compatible with a great degree of p_r heterogeneity. As a further validation of this measure, the number of FM-dye labelled vesicles was plotted against the number of morphologically docked vesicles for each synapse, a proposed physical correlate of p_r (Schikorski and Stevens, 2001). As shown in Figure 3.10D there was a good correlation with release probability estimated by counting photoconverted vesicles (R = 0.80, P = 0.0002).

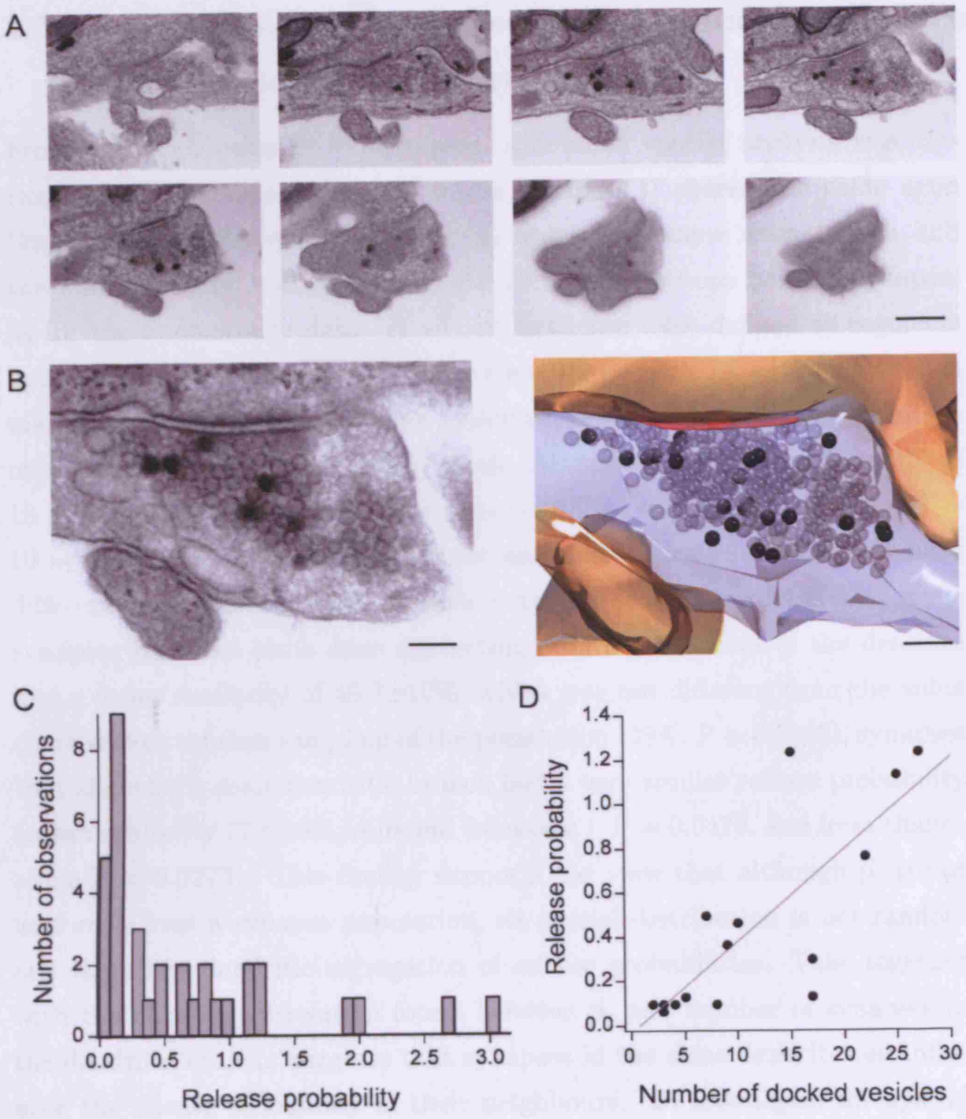

Figure 3.11: Measuring release probability with EM. (A) Consecutive electron micrographs showing a complete serial section series of a representative synapse. Scale bar 300 nm. (B) 3D reconstruction of the same series, with photoconverted vesicles in black and active zone in red (right). One electron micrograph in the same orientation and scale is shown on the left. Scale bar, 100 nm (C) Histogram of release probabilities for 35 synapses that have been fully reconstructed. (D) Plot of release probability against the number of morphologically docked vesicles.

3.5.3 Confirming p_r spatial segregation and dependence on the dendritic environment

From this population of 35 synapses, a detailed spatial analysis was carried out by examining all cases where synapses i) shared the same axon branch but a different dendrite, or ii) shared the same axon branch and the same dendrite, and calculating the similarity between pairs of synapses as for the fluorescence data. Similarly, branches were defined as segments between branchpoints. Figure 3.11 shows an example of one axon branch making two synapses in the same dendritic branch and one synapse in another branch. The mean intersynaptic distance was 5.28±1.37 μm (N = 18 synapses) for synapses in the same dendrite and 7.69±1.48 μm (N = 10 synapses) for synapses in different dendritic branches (not significantly different P = 0.2051). In agreement with the previous experiments, while synapses from the same axon contacting different branches of the dendrite had a mean similarity of 40.7±10%, which was not different from the value derived from random sampling of the population (49%, P = 0.5140), synapses that shared the same dendritic branch had a very similar release probability (mean similarity 77.6±8%, different from case i, P = 0.0478, and from chance alone P = 0.0273). This finding supports the view that although p_r is not uniform across a synapse population, its spatial distribution is not random and there is a dendritic segregation of release probabilities. This, together with the negative correlation found between p_r and number of synapses in the dendritic branch, suggests that synapses in the same dendrite can influence the release probability of their neighbours. To investigate the spatial extent of this interaction, all pairs of synapses that a) shared the same axonal and dendritic branches, and b) were not apparently separated by intervening synapses, were analysed further. Plotting the absolute difference in p_r for each pair against the distance between their active zones yielded a very strong positive correlation (R = 0.9298, P = 0.0003). Using the measured distribution of release probabilities, the average Δp_r expected by randomly selecting any two synapses was calculated by bootstrap. As indicated by the

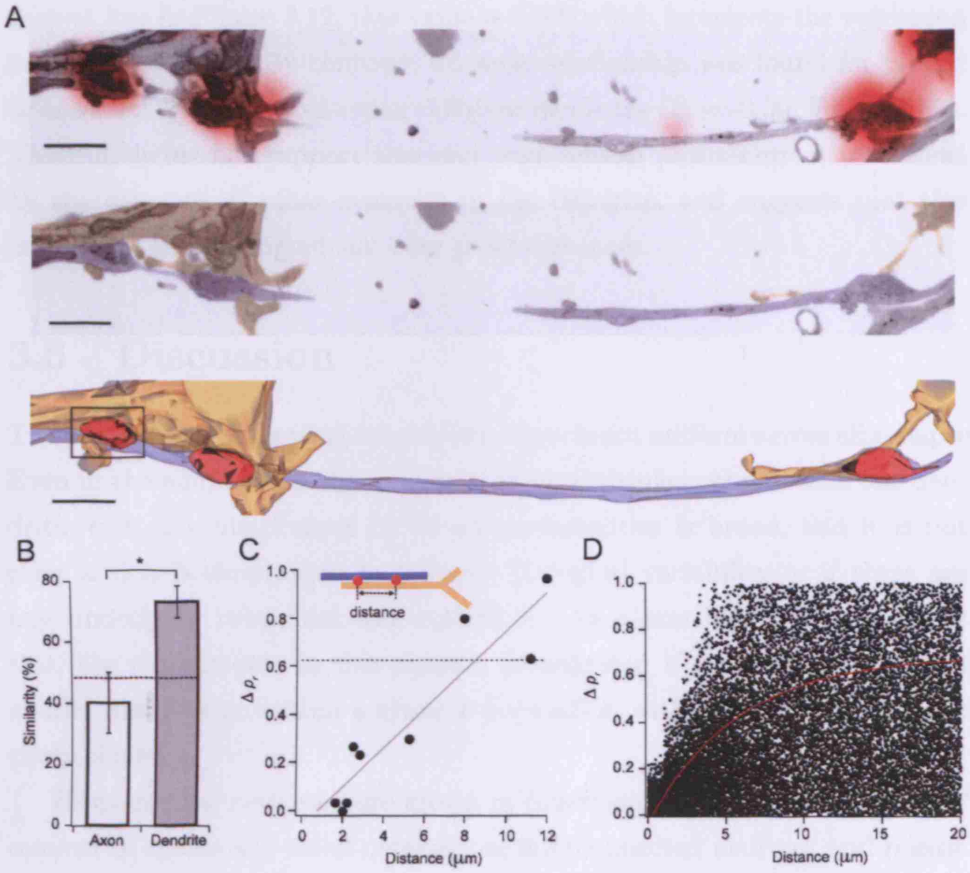

Figure 3.12: Ultrastructural spatial analysis of p_r. (A) Representative experiment showing one axon (blue) making synapses (red) with two different dendrites (orange). Top panel shows a low magnification electron micrograph with the FM-dye fluorescence overlaid, and the middle one the same micrograph with the axon and dendrite coloured for clarity. Bottom panel shows the full 3-D reconstruction, with the vesicle clusters in red. Scale bar, 1 μm. (B) Summary of similarity comparisons. Dashed line indicates the expected similarity due to chance calculated by bootstrap. (C) Absolute difference in p_r for pairs of synapses on the same dendrite, plotted against the distance between them. Dashed line indicates the expected Δp_r by randomly selecting any two synapses from the measured p_r distribution. (D) Simulation of the theoretical relationship between Δp_r and intersynaptic distance when synapses close together influence the release probability of each other. Red line is an exponential fit to the datapoints.

dashed line in Figure 3.12, this value is 0.63, which intersects the regression line close to 9 μm. By contrast, no such relationship was found for p_r and distance for synapses contacting different dendrites (R = -0.30, P = 0.6186). These data further support the idea that release probability is influenced by the presence of other synapses in the dendrite, and suggests that this interaction is more significant over short distances.

3.6 Discussion

The probability of releasing neurotransmitter is not uniform across all synapses. Even in the simple case of one axon making multiple contacts with one dendritic tree, the distribution of release probabilities is broad, and it is not clear if this is simply due to intrinsic biological variability or if there are any underlying rules that can explain it. As a starting point to address this, the experiments in this chapter investigated if there is an organized spatial distribution within a synapse population with heterogeneous release probabilities.

Hippocampal neurons were grown in conditions that favoured the development of sparse and small networks of interconnected neurons, and release probability at single synapses was studied at the fluorescence and ultrastructural levels. In fluorescence experiments, glutamatergic connections between two neurons were confirmed electrophysiologically and p_r at visually identified synaptic contact points was estimated by the rate of FM-dye fluorescence loss upon stimulation. As explained above, the time constant of the destaining curve is inversely proportional to release probability and constitutes a relative measure of p_r. The conversion to an absolute p_r value relies on the assumption that the average recycling pool size for all synapses in the connection is similar to the value reported in previous studies (Ryan et al., 1997), and that pool sizes for each synapse can be estimated from the relation between the individual integrated initial FM-dye fluorescence and the population mean. These assumptions, together with errors associated

with measuring the total integrated fluorescence for each puncta and fitting the destaining curve, can potentially diminish the accuracy of p_r estimation. Also, it has been reported that synaptic stimulation at the frequency range used to evoke FM-dye destain will result in a progressive reduction in release probability over time (Larkman et al., 1997b), thus leading to an underestimation of p_r. Even so, the distribution of release probabilities obtained matches very well what has been previously reported for hippocampal synapses in culture (Murthy et al., 1997; Slutsky et al., 2004; Granseth et al., 2006). This distribution was broad with a high CV, indicating great variability in p_r amongst different synapses of the same connection.

A simple analysis of p_r of individual synapses and their distances to the soma revealed no relationship both along the axon and the dendrite, which suggests that this is not an important variable in defining p_r. However, given the random and sparse placement of synapses in these cultures, it is not possible to exclude that in more organized synaptic circuits, such as the ones found in vivo, this might be different. Nevertheless, the finding that there is no relation between the axon branching order and p_r in particular, is a technically useful one, as it indicates that there are no progressive branchpoint failures of AP propagation. If this were the case, synapses in higher order branches would systematically have lower p_r values.

The analysis of p_r spatial distribution at axonal and dendritic branch level showed that synapses made on the same branch of the dendrite have a high degree of similarity. This was evident from i) the CV of the mean p_r on dendritic branches, which is significantly lower than the CV for the overall connection and ii) the high similarity ratio between synapses on the same branch of the dendrite. Bootstrap was used to predict the expected p_r similarity between two synapses with release probabilities randomly drawn from the measured p_r distribution, and this confirmed that the similarity obtained for synapses in the same dendritic branch is higher than that expected by chance. Furthermore, the CV and similarity values found for synapses made by the same axon branch onto different dendrites were not significantly dif-

ferent from the values obtained by bootstrapping the measured population of release probabilities. Because this analysis was restricted to segments of axon, branchpoint failures of AP propagation, as described above, cannot explain the observation of high p_r variability in the axon. Moreover, the same result was obtained for the recycling pool size of individual synapses, a correlate of p_r. Together, these results suggest that release probability is actively biased to acquire a particular value at individual dendritic branches. Two previous studies of release probability have briefly addressed the relation between p_r and the relative spatial disposition of synapses along the dendritic tree. In hippocampal autapses, Murthy et al. (1997) reported that any two neighbouring synapses had highly correlated release probabilities, and that this correlation was only valid if immediately adjacent synapses were considered. Given that in this study there was no information on the morphological pattern of cell processes, the results are difficult to interpret. Nevertheless, since the reported mean intersynaptic distance was 3 μm, it seems likely that on most occasions the compared pairs of synapses belonged to the same dendritic branch. However, when more distant synapses were compared this was probably not the case. If this assumption is correct, the observations of Murthy et al. are consistent with the results presented in this chapter. The other study was made on synapses from layer 2/3 cortical pyramidal cells (Koester and Johnston, 2005). The authors reported an estimated p_r CV <0.20 for synapses between two cells, and a very good correlation of release probabilities for pairs of synapses in different dendritic branches. This clearly contrasts with the findings in this chapter. However, the difference could simply be due to the different identity of the cells analysed and the different circuits they belong to. If indeed the overall p_r CV is low, then the distribution of release probabilities will be narrow and a correlation between the p_r value of any two synapses is expected. Nevertheless, in this study the CV was not measured directly but only estimated statistically, and both this work and a recent one in the same circuit (Hardingham et al., 2007) were only able to describe the statistics of release with uniform p_r in

50% of the cases. Moreover, Koester and Johnston et al used a very small number of synapse pairs and pooled data from different cell types to conclude homogeneity in p_r in single connections. Only measurements of p_r at all contact points between layer 2/3 cortical pyramidal cells will elucidate if release probability is uniform across all synapses and if the findings described in this thesis do not apply to these cells.

It was found that p_r is inversely correlated with the number of synapses made on the same branch of the dendrite. Because action potential firing in cultured neurons is likely to be random due to lack of external input, the level of activity of any given part of the dendritic tree will be proportional to the number of synapses. Thus, the relationship between synapse number and p_r becomes a relationship between activity in the dendrite and release probability. The fact that no such correlation was found for synapses along an axon contacting different dendrites, cannot be explained by a systematic difference in disposition or density of boutons, since the intersynaptic distance and process length in both cases were not significantly different. This relationship cannot also be explained by systematic differences in synaptic density of different dendritic branches, given that the overall number of synapses per branch was similar for all connections, and there was no correlation between overall synapse density and release probability. Taken together, these data suggest that release probability homeostatically adapts to the level of activity in the dendrite, and since different branches have a different mean p_r, such regulation must be implemented locally. Furthermore, these results also imply that release probability is independent of synapse density in the axon, and that it is mainly coordinated by the dendrite.

At the ultrastructural level p_r was estimated at single synapses by directly counting the number of FM-labelled vesicles after stimulation. Regions of interest were selected at the fluorescence level, and all synapses with a discrete vesicle cluster and a single active zone were imaged with EM. Two fundamental assumptions underlie this technique. First, that there is a one-to-one coupling of exo and endocytosis, and second, that the photocon-

version process is 100% effective and specific. While several studies support the first (Cowan et al., 2001; Gad et al., 1998), the latter was tested in a number of control experiments during the development of the protocol in the lab, by using different photoconversion times and experiments where FM-dye was omitted (Darcy, 2006). The fact the p_r distribution obtained with this method was similar to that measured in the fluorescence experiments and other previous reports, and furthermore, that there was a good correlation between the measured p_r and the number of docked vesicles, indicates that this is a valid method for estimating release probability. There was however a higher median p_r and a small subset of synapses with release probabilities above one. Several explanations can account for this. Although the time that FM-dye was left in contact with the cells was reduced to a minimum of 2 mins, spontaneous release could have occurred during this period and increased the number of labelled vesicles. The presence of multivesicular release, which has been described for hippocampal excitatory synapses in culture (Tong and Jahr, 1994), could also explain the high synaptic p_r measured. Also, errors in identifying photoconverted vesicles and the fact that it cannot be definitely excluded that some of the synapses analysed had more than one functional active zone despite their apparent uniformity, could also contribute to the prevalence of high p_r in some synapses. Another possibility is that even though selected synapses had the morphological features of excitatory synapses, it is impossible to exclude that this was the case for all boutons analysed. Thus, the possibility remains that some synapses which were included in the analysis were inhibitory, and these have been shown to have a high prevalence of multivesicular release in the hippocampus (Biro et al., 2006). A further point, as mentioned above, is that while fluorescence p_r measurements are likely to be an underestimation due to low frequency pulse train depression, this will be less prominent in the EM estimation given that only 30 APs were used to load the synapses with FM-dye.

Spatial analysis at EM level confirmed the dendritic clustering of release probabilities found in the fluorescence experiments. Notably, the mean sim-

ilarity values for synapses in the same dendrite and in different dendrites were very close to the ones obtained with FM-dye destaining, and similarity for the latter case was also not significantly different from what is predicted by random sampling of the population. As above, this finding cannot be explained by a different array of synapse disposition since the mean intersynaptic distance for each case was not significantly different. For this analysis, only synapses that shared the same branch of the axon were included. This differs from the analysis of the fluorescence data, in which synapses on the same dendritic branch could come from different axonal branches. The reason for this is that while in the first experiments filling of the axon with Alexa-dye allowed different branches to be identified as belonging to the same cell, in the EM experiments it was technically difficult to reliably trace the axonal branch of interest back to the cell of origin. Therefore, to ensure that synapses analysed belong to the same connection, only boutons in the same segment of one axon were selected for analysis. This also guarantees that branchpoint failures of AP propagation do not confound the results.

Analysis of synapses on the same dendrite at different intersynaptic distances showed that there is a positive correlation between differences in release probability and distance to the nearest neighbour. To isolate the intersynaptic distance as the single independent variable of this relationship, only pairs of synapses were considered, as the presence of more than one close neighbour will generate complex interactions and add confounding variables. Apart from this relation between similarity and distance, it would be interesting to analyse the effect of the latter on the absolute value of release probability. Given the negative correlation for p_r and number of synapses in the same dendritic branch found above, it would be expected that p_r would increase with distance to the closest synapse. Unfortunately, because the plot in Figure 3.11C was obtained from pairs of synapses from different cells and preparations, the fact that global p_r might vary considerably between different connections invalidates any comparison of absolute p_r values. This would only be possible if all the synapses in the plot came from the same

connection, or if it was possible to normalise each p_r to the maximum of the connection they belong to (this was done for FM-dye destaining experiments because p_r was measured for the great majority of synapses for each connection). Nevertheless, the finding that synapses in the same dendrite separated up to 5 μm have similar release probabilities, indicates that over this distance they can influence each other's p_r. This agrees well with the idea that the local environment in the dendrite plays a role in determining release probability. Also, the fact at the mean intersynaptic distance for synapses along the dendrite is 5.28±1.4 μm, is in accordance with these data. Over longer intersynaptic distances, each of the synapses in the pair will be more likely to be influenced by different local conditions, and differences in their release probability are therefore expected. In theory, if the distribution of synapses along the dendritic tree is random, then the p_r difference for a pair separated by a long distance should on average be the value expected by random population sampling. The theoretical relationship between Δp_r and intersynaptic distance shculd thus be exponential in the form $f(x) = y0 - Ae^{-\frac{x}{\tau}}$, with y0 being the Δp_r expected by random sampling of the population. To simulate such a relationship, a Monte Carlo simulation was performed, where pairs of synapses were randomly drawn from a population which had a CV that increased with intersynaptic distance. In the simulation, CV was 0.1 for distances < 1μm, and increased linearly to the measured CV of 0.56 until 9 μm, after which it remained stable. Figure 3.11D shows the simulation results for 20,000 synaptic pairs. Over short distances Δp_r is very small and tightly clustered, and as distance increases both the average Δp_r and dispersion from the mean value increase. As predicted, an exponential function in the above format provides a very good fit to the datapoints, with y0 = 0.68, very close to the value of 0.63 obtained by bootstrap. The strongly linear correlation shown in Figure 3.13 is most likely a result of finite sampling. The fact that there is no relation between differences in p_r and distance for synapses in the same axon contacting different dendrites, suggests that geometrical proximity between synapses by itself is not a determinant factor

of release probability. Rather, for this to be the case, geometrical proximity has to be translated into proximity of synaptic input in the dendrite.

Taken together, the fluorescence and ultrastructural observations suggest that some form of dendritically-coordinated homeostatic adaptation contributes to locally setting release probability. The next chapters test the validity of this hypothesis.

Chapter 4

Characterisation of homeostasis of release probability

The results discussed in the previous chapter suggest that release probability of individual synapses adapts homeostatically to the level of activity in the dendrite. As described above, it has been shown that in hippocampal cultures, as in other systems, release probability can respond homeostatically to changes in neuronal activity (Bacci et al., 2001; Thiagarajan et al., 2005, 2002; Murthy et al., 2001; Burrone et al., 2002). In most of these studies, activity was globally reduced by blocking either AP generation or excitatory synaptic transmission, and this lead to compensatory increases in p_r. However, these manipulations cause a simultaneous reduction in activity of both the pre and postsynaptic sites, and it is not clear what triggers the homeostatic increase in p_r. The experiments described in this chapter test the hypothesis that homeostatic adaptations of release probability are mainly dependent on dendritic activity. A paradigm to induce presynaptic homeostatic plasticity was first set up, and the exclusive dependence of this process on postsynaptic activity was then tested.

4.1 Electrophysiological estimation of release probability

Release probability was estimated using whole-cell paired recordings performed at near physiological temperatures. Three different approaches were used, which in combination gave a robust description of the mean release probability for each connection analysed. These methods were favoured to the optical techniques used in the previous chapter because single synapse resolution was not required at this stage. Since the overall p_r for the connection is an average of the individual release probabilities of each synapse, the findings of these experiments will be a reflection of the mean outcome of mechanisms operating at all the synapses belonging to the same connection. Furthermore, the use of several different techniques to measure p_r provides a more comprehensive and solid description of release probability and its determinants in hippocampal neurons.

4.1.1 Paired-pulse ratio

As explained above, the paired-pulse ratio is generally inversely proportional to release probability. After a stable paired recording was obtained, two APs separated by 50 ms were elicited in the presynaptic cell and EPSCs recorded in the postsynaptic neuron. This was repeated at least 30 times every 10 s, and the PPR calculated from the peak amplitude of the first and second responses. Although there was some variability between cell pairs, the majority of the connections in control conditions showed paired-pulse depression with an average PPR of 0.71±0.05 (N = 15, Figure 4.1). This value is in good agreement with previous reports of paired-pulse ratio in hippocampal neurons in culture (Mennerick and Zorumski, 1995).

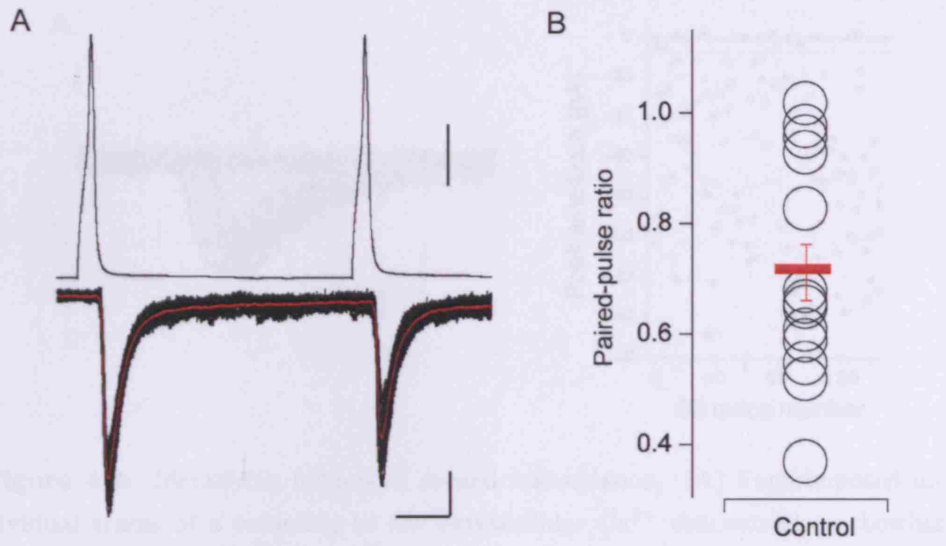

Figure 4.1: Paired-pulse ratio in control conditions. (A) Individual traces of a representative response in voltage-clamp to the paired-pulse protocol (bottom), with the average AP trace on top. Red line is average of 20 consecutive traces. Scale bars, top 20 mV, bottom 10 ms , 100 pA. (B) Graph showing the PPR variability in the population of cells analysed. Red bar is the population average.

4.1.2 Failure rate

At the physiological extracellular Ca^{2+} and Mg^{2+} concentrations used during whole-cell paired recordings, excitatory synaptic transmission never exhibited failures on any of the connections analysed. While the failure rate is a function of both release probability and the total number of synapses that mediate the connection, the absence of failures is more likely dominated by the presence of many contacts between two cells under the culture conditions chosen for this thesis. To overcome this, the Ca^{2+}/Mg^{2+} ratio was adjusted to reduce release probability to the point where failures of evoked release could be detected. Paired recordings were first established in normal extracellular solution, and after a connection was identified, cells were perfused with the reduced Ca^{2+} solution. As shown in Figure 4.2A, failures

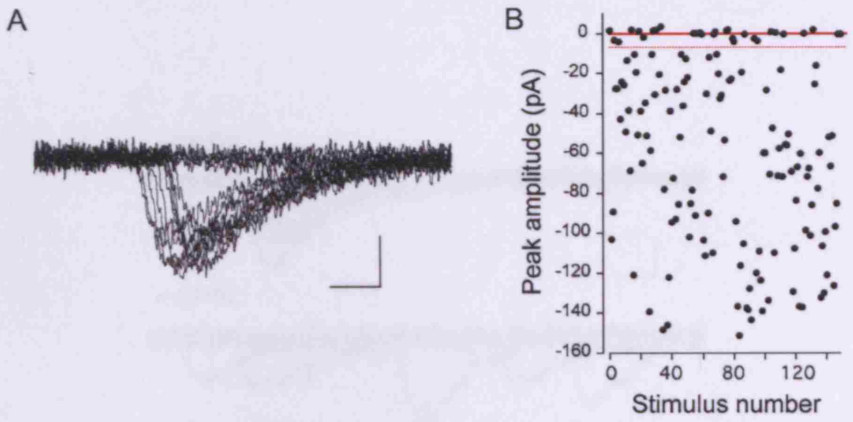

Figure 4.2: Identifying failures of evoked transmission. (A) Superimposed individual traces of a recording in low extracellular Ca^{2+} concentration, showing a clear distinction between failures and successes. Scale bar, 2 ms, 20 pA. (B) Plot of EPSC peak amplitude against stimulus number. Solid red line is the mean baseline noise, and dashed line marks 2 SDs from this level.

were clearly identifiable by visual inspection of the recordings, and evoked responses were constantly resolved over two standard deviations below the baseline recording noise (Figure 4.2B). Under these conditions the failure rate obtained from traces of more than 100 recorded responses was 32±3% (N = 7).

4.1.3 Counting quanta

Under the low p_r recording conditions described above, it was found that release events were markedly asynchronous and that successful responses were sometimes composed of more than one individualised component. To investigate if these components correspond to the release of single quanta of neurotransmitter, spontaneous events that occurred during the inter-stimulus interval were first analysed (Figure 4.3A). Because under these recording conditions synaptic activity is never sufficient to elicit action potentials, spon-

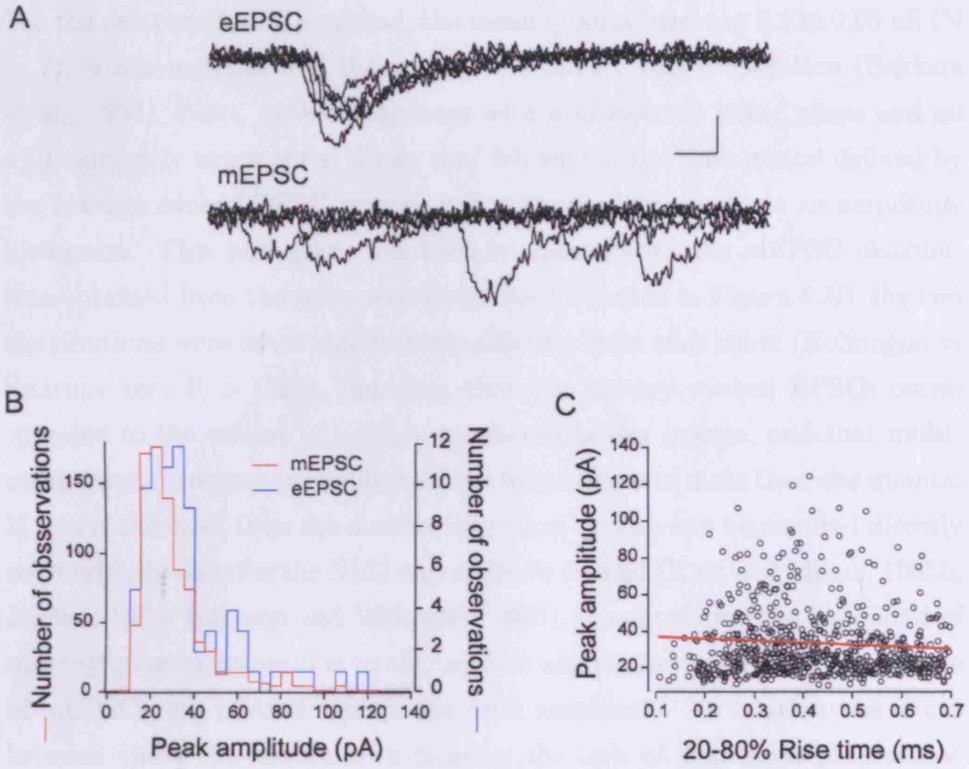

Figure 4.3: Evoked unitary EPSCs are single quantal events. (A) Superimposed traces from recording in 1 Ca^{2+} / 3 Mg^{2+}, showing stimulus-aligned unitary evoked EPSCs (eEPSC) and spontaneous miniature events (mESPSC) during the inter-stimulus interval. Scale bars, 1 ms, 20 pA. (B) Frequency histograms for mEPSCs and eEPSCs from one example connection show the same underlying distribution with medians of 25.9 (IQR = 27.9) and 30.1 (IQR = 30.5 respectively. (C) 20 - 80% rise time of mEPSCs plotted against the peak amplitude shows no correlation between the two variables (R = -0.042, P = 0.2903)

taneous events are effectively mEPSCs and thus constitute a measure of the quantal size. Figure 4.3B shows a mEPSC frequency histogram from a typical recording, where the characteristic skewed distribution can be observed. For the cell population analysed, the mean quantal size was 0.53±0.06 nS (N = 7), which matches well the values reported for this preparation (Bekkers et al., 1990). Next, evoked responses with a monotonic rising phase and an approximately exponential decay that fell within the time period defined by the average evoked EPSC time course, were used to construct an amplitude histogram. This histogram was then compared with the mEPSC distribution obtained from the same recording. As illustrated in Figure 4.3B, the two distributions were never significantly different from each other (Kolmogorov-Smirnov test $P > 0.05$), implying that the unitary evoked EPSCs corresponded to the release of a single neurotransmitter quanta, and that multicomponent responses probably resulted from release of more than one quanta. If this is the case, then the number of evoked quanta can be counted directly as previously done for the NMJ and endbulb of Held (Katz and Miledi, 1965b; Zucker, 1973; Isaacson and Walmsley, 1995). To determine the likelihood of missing quantal events due to electrotonic attenuation, the 20-80% rise time of mEPSCs was plotted against the peak amplitude. No relation was found between these two variables, indicating the lack of significant electrotonic filtering of the recorded currents (Figure 4.3C). In the face of these observations, the mean quantal content and quantal variance were measured directly by counting the number of quanta evoked by each trial (Figure 4.4A). From these two values, assuming simple binomial release, release probability for the connection is given by the relationship $p = 1 - \frac{\sigma^2}{m}$. The mean quantal content in control conditions was 1.18±0.09 and the average release probability 0.163±0.02 (N = 7). Calculating the predicted values for the number of quanta released using the Binomial theorem (equation 1.2) and comparing them to the observed counts revealed a very good agreement in all cases (χ^2 test, P = 0.32 to 0.96), validating the use of this method to estimate release probability (Figure 4.4B).

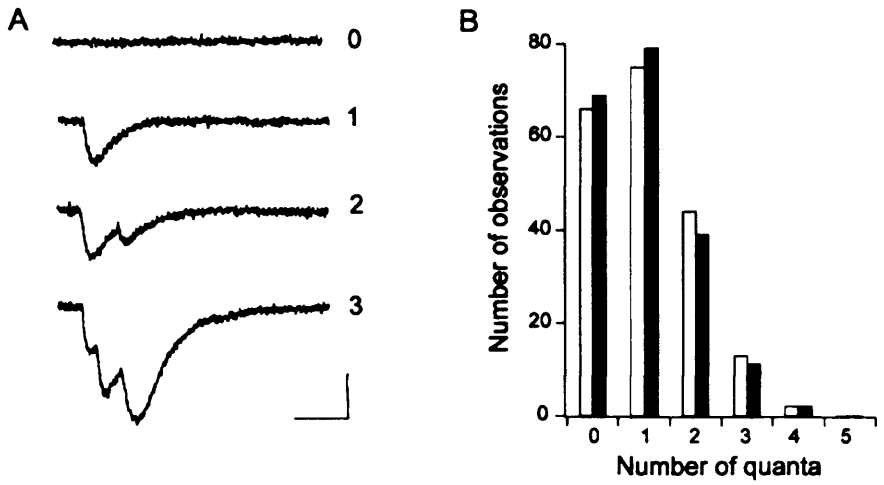

Figure 4.4: Measuring quantal content directly. (A) Example traces illustrating the marked asynchrony in evoked release under low extracellular Ca^{2+}, which allows individual quanta to be identified and counted directly. Numbers on the right indicate number of quanta released. Scale bars, 2 ms, 50 pA. (B) Frequency histogram for one representative connection shows a good agreement between the observed counts (white bars) and the prediction from simple binomial statistics (black bars).

4.2 Increased network activity causes a reduction in p_r

To study homeostatic changes in release probability, network activity was increased using field stimulation. Parameters of stimulation were calibrated by simultaneously stimulating and making whole-cell recordings in voltage-clamp mode. Figure 4.5A-B shows that it was possible to consistently elicit both TTX-sensitive currents and synaptic currents that were blocked by CNQX and AP5. Particular care was taken to ensure that synaptic activation was action potential driven and not a result of direct depolarization of the presynaptic terminals, which was confirmed by the lack of a synaptic component when TTX alone was added to the extracelullar recording solu-

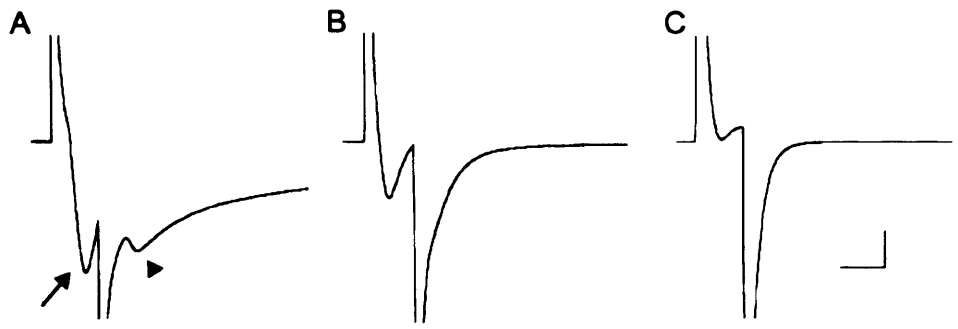

Figure 4.5: Calibration of field-stimulation parameters. (A) Voltage-clamp trace shows that delivery of a 2 ms, 2 V pulse across the field stimulation chamber elicited a sodium current (arrow) followed by a synaptic current (arrowhead). (B) Stimulation in the presence of CNQX and AP5 does not trigger the synaptic component of the response. (C) TTX alone abolishes both the sodium current and the synaptic response. Traces are averages of 10. Scale bars, 2 ms, 500 pA.

tion (Figure 4.5C). To globally increase network activity, action potentials were delivered at 1-2 Hz for two hrs at 37 °C, and changes in p_r monitored immediately after.

It was found that after stimulation, the PPR was increased to 23±5% above control values (P = 0.0394, N = 8), consistent with a homeostatic decrease in release probability. Recordings under low Ca^{2+} conditions showed a very significant 107±12% increase in the failure rate (P = 0.0061, N = 4), and a corresponding 69.7±7.7% decrease in the binomial p_r (P = 0.0061, N = 4). Accordingly, the mean quantal content decreased by 63 ±5%. These observations demonstrate that release probability can respond homeostatically to elevated network activity, confirming the findings of others (Bacci et al., 2001; Thiagarajan et al., 2005, 2002; Murthy et al., 2001; Burrone et al., 2002) and validating the chosen method as a means to study homeostatic plasticity (Figure 4.6).

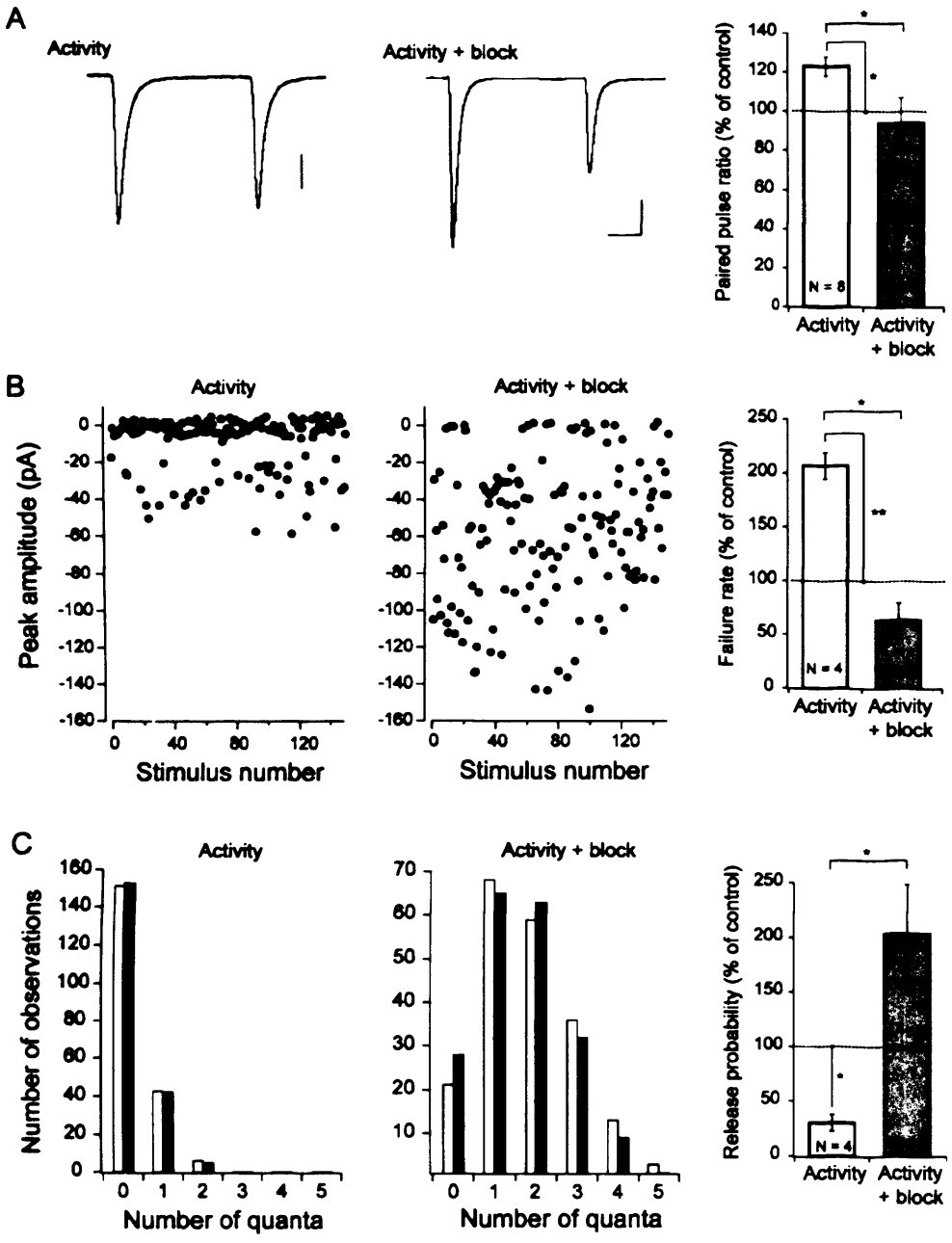

Figure 4.6: Homeostatic changes of release probability. Cultures were stimulated for 2 hrs in normal culture media (Activity) or with added synaptic blockers (Activity + block). A-C show examples of the paired-pulse ratio (A, scale bars 15 ms, 200 pA left, 100 pA right), failure rate (B) and number of quanta released (C) in both conditions. Population summary for all measures is given on the right.

4.3 Block of synaptic transmission prevents the homeostatic reduction of p_r

Homeostatic plasticity of release probability could be a response to increased AP firing of the axon, increased activity in the dendrite, or a combination of both. To distinguish between these possibilities it is necessary to selectively manipulate either pre or postsynaptic activity. One way of achieving this is by eliciting action potentials while blocking excitatory synaptic transmission. Here, the axon and presynaptic terminals are stimulated and evoke neurotransmitter release as usual, but postsynaptic activity is selectively silenced. Because modulations of neurotransmitter release mediated by presynaptic AMPA and NMDA receptors have been previously reported in some classes of neurons (Engelman and MacDermott, 2004), it was first tested if block of glutamatergic synaptic transmission acutely changed the basal release probability. This was achieved by analysing paired-pulse responses before and after perfusion of the individual blockers. As shown in Figure 4.7, the PPR did not change significantly after blocking NMDA receptors with AP5 (P = 0.0994, N = 4), or AMPA receptors with a sub-saturating concentration of CNQX (P = 0.2822, N = 6). These observations argue against a direct effect of NMDA or AMPA receptor signalling on release probability. Therefore, field stimulation of the network in the presence of AP5 and CNQX will elicit action potentials and normal neurotransmitter release with no synaptic activity in the dendrite (see Figure 4.5B). Blocking excitatory synaptic transmission while stimulating the network abolished the homeostatic decrease in p_r, as evident from the lack of increase in the PPR of evoked responses (P = 0.0377 vs activity, N = 6), a decrease in the failure rate (P = 0.00286 vs activity, N = 5) and an increase in binomial p_r (p = 0.0159 vs activity, N = 5, see Figure 4.6) and quantal content (P = 0.0066 vs activity, N = 5). Moreover, the last three measures show a clear tendency for release probability to be higher than control, consistent with a homeostatic adaptation to reduced activity despite enhanced presynaptic stimulation. These experiments

strongly support the hypothesis that p_r can be adjusted homeostatically by a mechanism that is dependent on postsynaptic activation, and that release of neurotransmitter by itself is not sufficient to downregulate p_r.

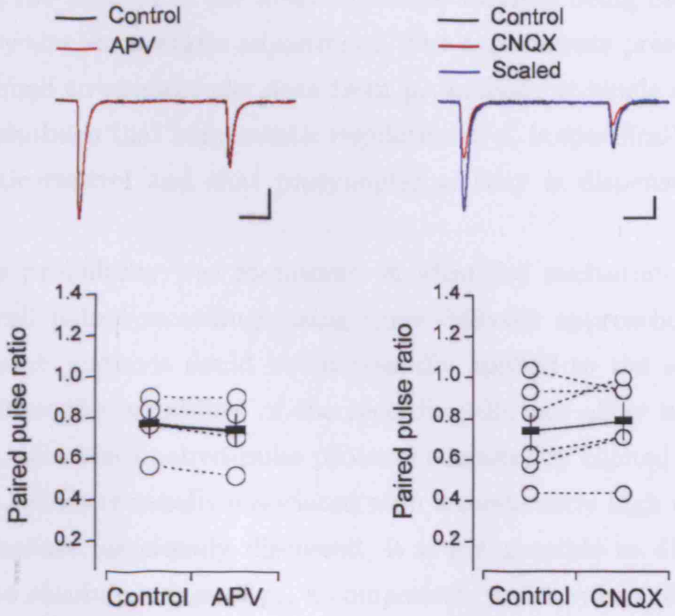

Figure 4.7: Testing for the presence of presynaptic NMDA and AMPA receptors. (A) Top, superimposed paired-pulse example traces before and after perfusion of 50 μM AP5. Bottom, summary plot showing no change in PPR (control - 0.77±0.07, AP5 - 0.74±0.08. Scale bars, 10 ms, 200 pA. (B) Top, example traces of paired-pulse responses in control and after perfusion of a 400 nM CNQX. Blue trace is the EPSC in CNQX peak-scaled to control to illustrate lack of change in kinetics. Bottom, data summary showing no change in PPR (control - 0.74±0.09, CNQX - 0.79±0.09). Scale bars, 10 ms, 100 pA. Traces are average of 20.

4.4 Discussion

The study of p_r spatial distribution has suggested that the basal release probability at single synapses is coordinated by activity in the dendrite in

a homeostatic manner. Consistent with this hypothesis, previous studies have demonstrated that p_r can indeed respond homeostatically to changes in the network activity. However, they have not clearly distinguished between activity in the axon or in the dendrite as the variable being monitored and targeted by the homeostatic adjustment. The experiments presented in this chapter aimed to support the data from p_r analysis at single synapses, by trying to establish that homeostatic regulation of p_r is specifically dependent on dendritic control and that presynaptic activity is dispensable for this process.

Release probability was monitored in identified excitatory connections by whole-cell paired recordings using three different approaches. While in some cases all methods could be successfully applied to the same connection, in others the instability of the recording did not allow it. In control conditions a standard paired-pulse protocol consistently elicited paired-pulse depression, which is usually associated with a moderately high release probability. Because, as already discussed, it is not possible to directly relate the PPR to absolute values of p_r, a comparison to the values obtained from the FM-dye studies cannot be made. One difference to note between these two approaches is that the FM-dye data were obtained at room temperature and the recordings in this chapter at near physiological temperatures. By changing the Ca^{2+}/Mg^{2+} ratio of the extracellular recording solution it was possible to observe failures of evoked responses and use the failure rate to infer changes in the probability of release. While with this method alone it is impossible to distinguish modifications of p_r from changes in the number of release sites, the ability to identify failures with exceptional resolution confers a minimal measurement error to this approach. As a third technique to estimate release probability, the number of quanta released after stimulation was counted directly and p_r calculated from the mean quantal content and quantal variance. This was possible because of i) large quantal sizes that allowed unequivocal identification of a release event, ii) minimal electrotonic attenuation that ensured successful detection of events from all

over the dendritic tree, and iii) a marked asynchrony in the release process which permitted the distinction between individual quanta released. While the counting process was straightforward, two sources of error are present in this measurement. The first is from the occurrence of spontaneous events that can fall in the time window defined after stimulation and be mistakenly interpreted as evoked events. Given the average low frequency of spontaneous events observed, it can be estimated that <3% of the evoked responses were contaminated by spontaneous release (Isaacson and Walmsley, 1995). The second source of error is the impossibility of distinguishing two quanta that are released exactly at the same time, which has been rigourously described by Zucker (1973) and shown to not significantly distort the measured distribution of quanta. One other assumption that this method relies on is that the release process can be described by simple binomial statistics. Although with normal Ca^{2+}/Mg^{2+} ratio this is clearly not the case given the high p_r CV obtained in the previous experiments, there is no information on the distribution of release probabilities at low extracellular Ca^{2+} concentrations. The fact that the binomial prediction of the number of quanta released matched the observed number suggests that simple binomial statistics may be used as an aproximation in these conditions. In combination, these three measures of release probability provide a very good description of the average p_r in a population of connections, and allow for robust relative comparisons between the different experimental conditions tested.

Continuous low frequency delivery of action potentials to the whole network caused a significant decrease in release probability that was reflected in all p_r measures used. Manipulations of network activity to induce homeostatic plasticity have, to date, mostly relied on a long term (24-48 hrs) global activity block (Bacci et al., 2001; Thiagarajan et al., 2005, 2002; Murthy et al., 2001) and reported increases in release probability. The finding that increased network activity leads to a compensatory decrease in p_r, confirms for the first time the prediction that homeostatic plasticity of p_r is bidirectional, and reinforces that view that release probability is indeed a parameter

balanced homeostatically by the global state of the network. One difference is that in the experiments discussed here, homeostasis was induced after only two hrs of activity manipulation, whereas in the previous studies homeostatic plasticity was only seen after at least 12 hrs. Several explanations can account for this. One is that inducing APs at 1-2 Hz might be a stronger manipulation than activity block, and therefore more efficient in recruiting homeostatic mechanisms. Another one relates to the measure of release probability used. Most of the work done to date used the frequency of mEPSCs to infer changes in p_r. Because this parameter is highly variable between cells, a dramatic change in release probability has to occur before any significant changes from control conditions are measurable. By the same line of argument, the culture conditions used here favour the development of very homogenous networks, with similar numbers of cells and synapses, which together with the sampling of single connections, minimises population variability and allows detection of more subtle changes. In agreement with a fast homeostasis of release probability, a recent study in the Drosophila NMJ has reported increases in p_r after only 10 mins of AMPA receptor block (Frank et al., 2006). The implications of such a fast acting homeostatic mechanism are discussed later.

Eliciting action potentials while blocking excitatory synaptic transmission allowed the dissociation of pre and postsynaptic activity, and also offered the opportunity to test the locus of homeostatic plasticity induction. It was found that under these conditions release probability failed to be down-regulated, and consistently displayed values above control. One assumption underlying the interpretation of this experiment is that there are no AMPA or NMDA receptors on the presynaptic terminal that regulate neurotransmitter release directly. This is supported by the lack of change in PPR after receptor block with CNQX or AP5. It is important to note that stimulating the network while blocking synaptic transmission is a different situation to blocking receptors alone. While in the former, evoked neurotransmitter release still occurs, in the latter the lack of excitatory input abolishes network AP firing. The fact

that with synaptic transmission block, release probability did not decrease despite enhanced axonal activity, indicates that homeostasis of p_r cannot be explained either by a direct action of neurotransmitter on the presynaptic terminal (via mGlu receptors for example), or by the average level of depolarization in the presynaptic compartment. Rather, neurotransmitter has to depolarise the dendrite for homeostatic mechanisms to be activated. Burrone et al. (2002) reported that synapses made onto a cell that had been selectively hyperpolarised, developed an increased p_r over time that restored the cell's AP firing rate to normal. Although consistent and supportive of the experimental results discussed in this chapter, the authors interpretation was that the variable responsible for inducing retrograde changes in p_r was the firing rate of the postsynaptic cell. Given that the stimulation protocol used here evokes spikes in both pre and postynaptic cells, the data obtained indicate that action potential firing and backpropagation alone cannot account for the observed homeostatic decrease in release probability. More likely, a stronger depolarization, triggered either directly by glutamate receptors or secondary to local activation of voltage-gated ionotropic channels is necessary to induce homeostasis. This interpretation is consistent with a recent study in the Drosophila NMJ, where spontaneous miniature events were sufficient to elicit compensatory changes of release probability (Frank et al., 2006), emphasising the proposed view that localised depolarisations of the postsynaptic site are the main trigger of presynaptic homeostasis.

Chapter 5

Manipulations of the spatial organisation of release probability

The experiments presented so far support the hypothesis that release probability is determined by a homeostatic mechanism coordinated by dendritic activity. The observation that synapses on different dendritic branches have different release probabilities, and that similarity of p_r between synapses decays with distance along the dendrite, suggests that this might be implemented with a degree of spatial constraint. If this was indeed the case, then it would provide an explanation for the observed heterogeneity of p_r. Since both in the intact brain and in hippocampal cultures, inputs are not uniformly distributed throughout the dendritic tree, spatially-distinct parts of the dendrites will receive different inputs, both in quantity and in quality. This will generate a non-uniform distribution of activity levels across the neuron, and a local adaptation of p_r to dendritic activity would therefore produce a broad distribution of release probabilities. In this case, one prediction is that local external manipulations of activity should be sufficient to induce local p_r changes. Another prediction is that by forcing inputs to be uniform over the entire dendritic tree, the variability in p_r should become very small.

This chapter describes the attempts to determine if release probability is set by a spatially localised mechanism. First, activity was manipulated in a restricted part of the dendrite and the consequences of this on p_r analysed. Second, the effect of uniform activity on p_r was tested experimentally.

5.1 Local synaptic stimulation

As a means of depolarising the dendrite in a spatially restricted area, a technique was established to locally stimulate neurotransmitter release from a group of synapses in a single dendritic branch. This was achieved by generating a highly localised field potential with a theta-glass pipette with an aperture of ~5 μm, placed next to the target synapses and connected to a current stimulator. To calibrate the positioning of the pipette and the current intensity needed to elicit neurotransmitter release, synapses were first

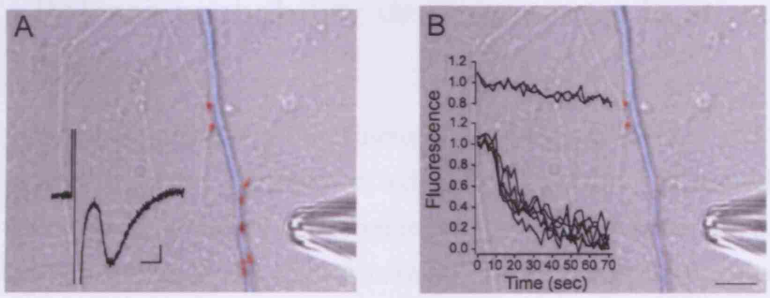

Figure 5.1: Selective stimulation of synapses. (A) DIC image of a dendrite (coloured in blue for clarity) with superimposed FM4-64 labelled synapses (red). A theta-glass pipette was placed next to the synapses and current pulses were delivered. Inset show the synaptic response elicited by the stimulation. Scale bars, 2 ms, 10 pA. (B) The same synapses were stimulated with a train of APs and FM-dye fluorescence imaged. The inset graph shows that only the synapses directly in front of the pipette destained. The FM-dye image after full destain is superimposed on the DIC image. Scale bar, 5 μm.

labelled with FM4-64 and stimulation was carried out while simultaneously monitoring the elicited currents with a whole-cell recording.

As shown in Figure 5.1A, placing the pipette within ~5 μm of the dendrite and delivering a 5 ms 100 μA pulse consistently elicited a synaptic response. The recorded EPSC was very sensitive to the placement of the pipette, which had to be directly in front of the target synapses, and it was completely blocked by CNQX and AP5. To verify the spatial selectivity of the stimulation, 1200 stimuli were delivered at 20 Hz while monitoring FM-dye destaining. Figure 5.1B shows that only the synapses next to the pipette lose their FM-dye fluorescence, confirming the highly local nature of this stimulation procedure. Even though the spatial extent of the stimulus was not precisely mapped, pilot experiments indicated that it was generally restricted to an area of 10-15 μm, as judged by the differential destaining of neighbouring boutons.

5.1.1 Release probability decreases only in stimulated synapses

In the previous chapter, a global increase in network activity for two hrs elicited a compensatory decrease in release probability. To establish if a similar change in p_r could be triggered locally, a group of synapses was stimulated for two hrs at 2 Hz, and release probability measured immediately after by globally loading synapses with FM4-64 with 30 APs at 1 Hz using field stimulation (Figure 5.2A). Although this measure of release probability does not yield an absolute value, it allows relative comparisons to be made between stimulated and non-stimulated synapses. Also, though it would have been convenient to identify the exact location of synapses by initially labelling them with FM-dye, the incomplete FM-dye destain observed even after exhaustive stimulation would severely bias any estimate of p_r by FM-dye reload. For this reason, using DIC optics, areas along the dendrite which were likely sites for synapses were identified owing to the presence of an axon in an appropriate orientation. As illustrated in Figure 5.2C, after the stim-

ulation protocol, release probability decreased to 59±4% exclusively in the stimulated synapses when compared to unstimulated neighbouring boutons ($P < 0.0001$, $N = 5$ cells, Figure 5.2B). When the same stimulation was performed in the presence of CNQX and APV, the decrease in p_r was abolished (113 ±10%, $P = 0.1872$, $N = 3$ cells). This observation shows that individual synapses can adjust their release probability in response to local changes in dendritic activity, and suggests that this mechanism operates in a spatially restricted manner.

5.2 Imposing spatially uniform inputs to the dendritic tree

To test if the variability of release probability arises from local adaptations to dendritic activity such as the ones described above, inputs to the dendrite were manipulated to be uniformly distributed. The ideal way to achieve this would be to cover all dendrites equally with evenly spaced synapses, and activate them synchronously. As this is not experimentally feasible, one alternative is to bypass the synapse and manipulate the level of dendritic depolarization directly. This approach was chosen and implemented in two different ways to generate two extreme and opposite situations. First, AMPA, NMDA and GABA-A receptors were completely blocked. Even though the presence of metabotropic glutamate and GABA receptors was not verified, block of these three classes of ionotropic receptors abolished all synaptic inputs as verified by whole-cell recordings, making all dendrites silent and therefore uniform in their membrane potential. In the second condition, 20 mM KCl was added to the cells while blocking synaptic transmission as above. Even though the raised concentration of extracellular KCl triggers neurotransmitter release, because postsynaptic receptors are blocked, the net result is a direct depolarization of the dendrite that is spatially uniform. Both of these manipulations are expected to induce homeostasis of release probability, albeit in opposite directions. While the first has been used several

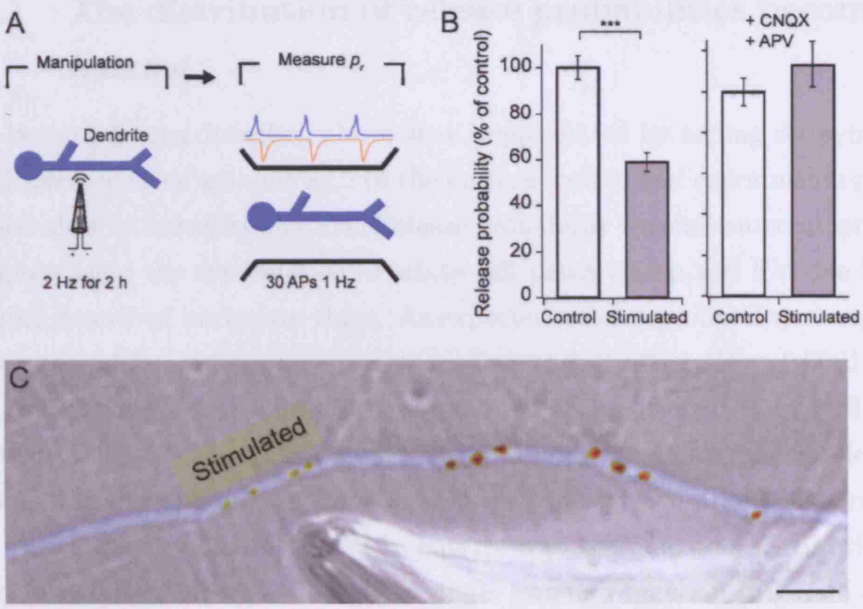

Figure 5.2: Changing release probability locally. (A) Cartoon illustrating experimental scheme. (B) Data summary showing that p_r decreases only in synapses that have been stimulated. (C) Representative example of the selective change in p_r. The DIC image shows the selected dendritic branch (coloured in blue) and the FM4-64 measure of p_r after prolonged synaptic stimulation has been superimposed. FM-dye labelling is pseudocoloured and red indicates higher intensities. Only the four stimulated synapses show an homeostatic decrease in release probability. Scale bar, 5 μm.

times before for this purpose (Bacci et al., 2001; Thiagarajan et al., 2005, 2002; Murthy et al., 2001), raising the KCl concentration should work equally well, based on the suggestion from the previous chapter that the trigger for p_r homeostasis is a strong enough depolarization in the dendrite. In fact, Leslie et al. (2001) successfully used a similar protocol to elicit homeostatic plasticity of the quantal size in cortical cultures.

5.2.1 The distribution of release probabilities becomes narrow

The two conditions described above were implemented by adding the synaptic blockers with or without KCl to the culture media, and experiments performed after 24 hrs of incubation. Release probability was measured at single synapses using the combination of whole-cell patch clamp and FM-dye live imaging described in chapter three. As expected, release probability changed homeostatically, reaching an average median of 0.41±0.01 ($P < 0.0001$, $N = 5$ connections, 66 synapses) in synaptic block and 0.07±0.01 in KCl ($P < 0.0001$, $N = 5$ connections, 25 synapses). Building a histogram of release probabilities for single connections showed that, in both conditions, the broad and skewed distribution observed in control was lost, and the distributions could be satisfactorily described by a single gaussian function (Figure 5.3A, top).This change was also reflected in the recycling pool sizes, that showed a slight increase to 138±5 (not significantly different from control, $P = 0.2000$) in block and a marked decrease to 70±8 in KCl ($P < 0.0001$), and in the destaining time constants (3.69±0.15 min in block, $P < 0.0001$, 11.02±1.48 min in KCl, $P = 0.0139$, see Figure 5.3A, middle and bottom). Furthermore, individual distributions were markedly narrow, with a mean CV of 0.17±0.03 for activity block and 0.19±0.06 for KCl, which is significantly different from control values ($P = 0.0087$ and $P = 0.0303$, respectively). Notably, the global CV for individual connections in both conditions was not significantly different from the dendritic CV measured in the control situation ($P = 0.5773$ for activity block and $P = 0.4565$ for KCl, Figure 5.3B, top). The individual measures of recycling pool size and destaining rate also showed a clear trend towards a decrease in CV, albeit the change was not significantly different from control values (pool size CV 0.22±0.06 in block, 0.12±0.11 in KCl; tau CV 0.22±0.08 in block, 0.19±0.17 in KCl, see Figure 5.3B, middle and bottom). These observations are compatible with the predicted overall reduction in p_r variability.

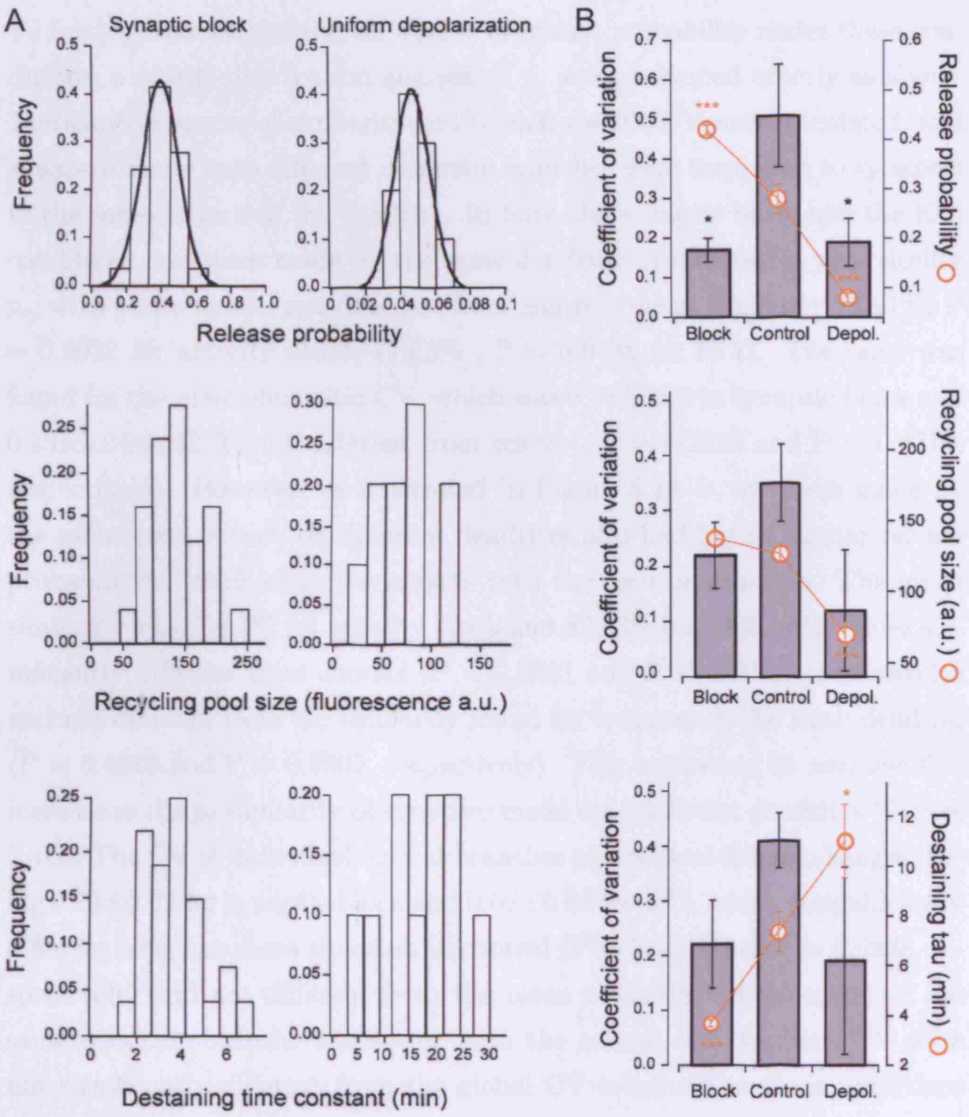

Figure 5.3: p_r distribution after activity manipulations. (A) Frequency histograms for two example connections show opposite changes in p_r for each condition, and a change in the distribution shape. Lines are Gaussian fits. (B) Data summary for changes in release probability and CV.

5.2.2 Dendritic organisation of p_r is lost

To further characterise the variability of release probability under these conditions, a spatial distribution analysis of p_r was performed exactly as above. The same measures of similarity and branch specific CV were calculated, and synapses made onto different dendritic branches were compared to synapses in the same branch of the dendrite. In both the synaptic block and the KCl conditions, synapses made on the same dendritic branch had a very similar p_r, with mean values not different from control (mean similarity 77±1%, P = 0.9022 for activity block, 77±3% , P = 0.9158 for KCl). The same was found for the mean dendritic CV, which was 0.18±0.02 in synaptic block and 0.15±0.04 in KCl (not different from control, P = 0.2396 and P = 0.8713, respectively). However, as illustrated in Figure 5.4A-B, synapses made by the same axon branch on different dendrites also had highly similar release probabilities, which clearly contrasts with the control situation. The mean similarity was 75±2% for activity block and 82±3% for KCl, both values significantly different from control (P < 0.0001 and P < 0.0001, respectively) and not different from the similarity found for synapses in the same dendrite (P = 0.4645 and P = 0.2962, respectively). This represents an average 30% increase in the p_r similarity of synapses made onto different dendrites (Figure 5.4C). The CV of individual axonal branches also reflected these changes, being 0.15±0.02 for synaptic block and 0.09±0.04 for KCl, which is significantly different from the same situation in control (P = 0.0107 and P = 0.0238, respectively) and not different from the mean similarity for synapses on the same dendritic branch. Moreover, both the axonal and dendritic CV were not significantly different from the global CV measured in these conditions (P = 0.6923 and P = 0.5443 for activity block, P = 0.3929 and P = 0.4981 for KCl, respectively). Also, recycling pool sizes of individual synapses mirrored the observed changes in p_r, becoming spatially uniform (similarity for axon 76.2±0.5%, in block and 77.6±2% in KCl, P = 0.4260 and P = 0.9985 versus similarity for dendrite in control, respectively), as well as destaining time constants (similarity for axon 72.5±2%, in block and 72.9±5% in

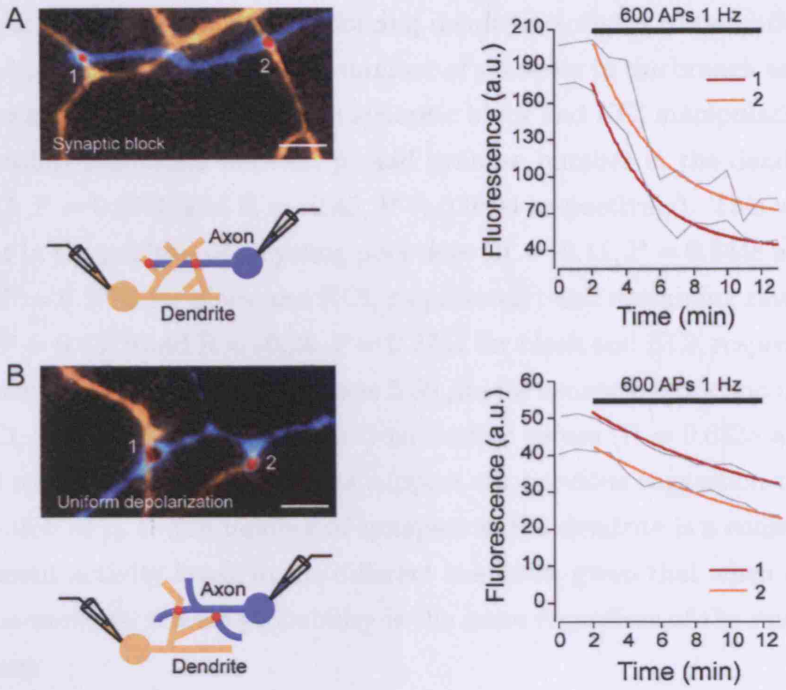

Figure 5.4: Spatial analysis of p_r after activity manipulations. (A-B) Representative examples of synapses on different dendrites (left) and respective FM4-64 destaining curves (right) after 24 hrs of synaptic block (A) and uniform depolarization (B). Scale bars, 5 μm.

KCl, P = 0.9365 and P = 0.9594 versus similarity for dendrite in control, respectively). These data confirm that when the levels of depolarization are uniform across the dendritic tree, p_r variability becomes very small, and the spatial organisation of release probabilities is lost.

5.2.3 Loss of correlation between p_r and the number of synapses

In the control condition there is a negative correlation between release probability and the number of synapses in a dendritic branch. To investigate if

this relation is maintained after forcing dendritic activity to be uniform for 24 hrs, p_r was plotted against the number of synapses in the branch as above. As shown in Figure 5.4D, for both synaptic block and KCl manipulations, no relationship was found between p_r and synapse number in the dendrite (R = -0.03, P = 0.8746 and R = -0.45, P = 0.0804 respectively). This was also evident in the analysis of recycling pool sizes (R = -0.11, P = 0.5448 and R = -0.14, P = 0.5792 for block and KCl, respectively) and destaining rates (R = -0.03, P = 0.8579 and R = -0.24, P = 0.2751 for block and KCl, respectively). The mean intersynaptic distance was 5.39 μm for synaptic block and 6.45 μm for KCl, not significantly different from control values (P = 0.6325 and P = 0.6558 respectively). These results support the previous suggestion that the adaptation of p_r to the number of synapses in the dendrite is a consequence of different activity levels in the different branches, given that when activity is made uniform, release probability is the same regardless of the number of synapses.

5.3 Discussion

One feature of the hypothesis that release probability is homeostatically determined by activity in the dendrite, is that this mechanism is implemented locally. This is suggested by the p_r similarity of synapses in the same dendritic branch and by the fact that this similarity is higher for smaller intersynaptic distances. Also, the observation that postsynaptic cell spiking alone is not sufficient to trigger presynaptic homeostasis, indicates that a more local and probably synaptically induced depolarization is required for the effect. The results presented in this chapter tested the local nature of release probability regulation.

Small groups of synapses were locally stimulated with a theta-glass pipette. Whole-cell recordings verified the synaptic origin of the responses evoked by the stimulus, and its spatial selectivity was monitored by imaging FM-dye fluorescence loss during stimulation. A relative measure of release proba-

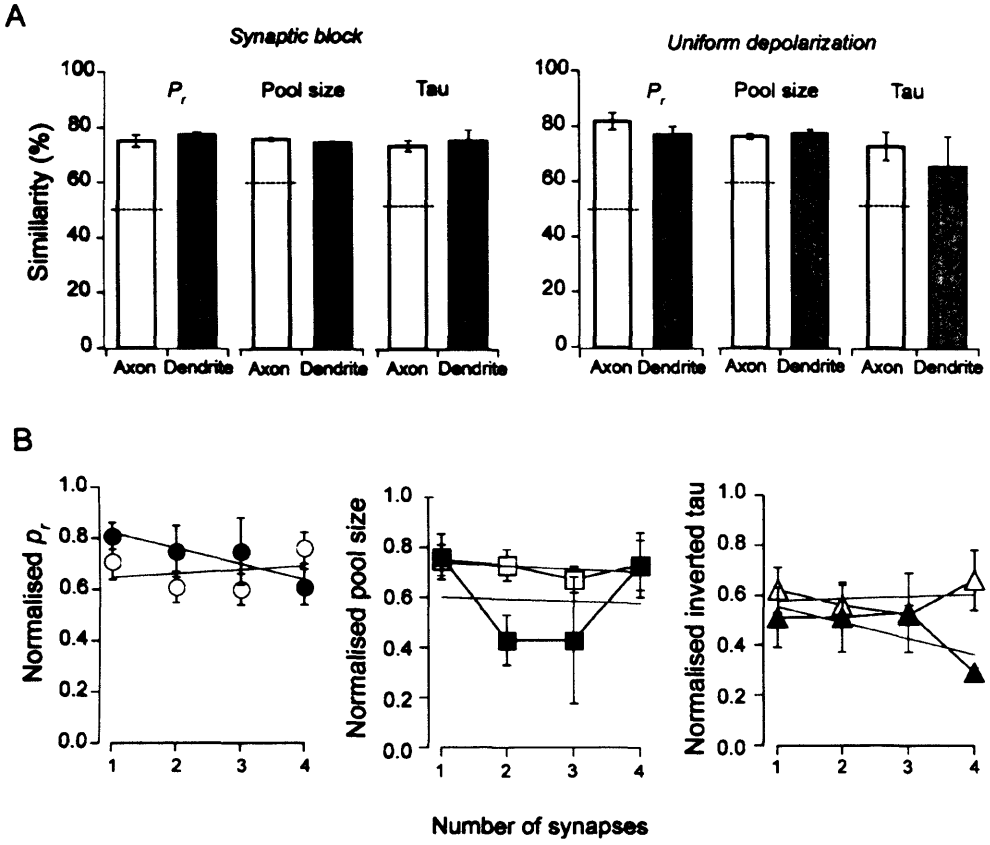

Figure 5.5: Summary of spatial analysis after activity manipulations. (A) Similarity comparisons in both conditions, for release probability, recycling pool size and destaining time constant. Dashed lines indicates control values. (B) These three measures were normalized for each connection as in Figure 3.9, and plotted against the number of synapses in the dendrite for synaptic block (open symbols) and uniform depolarization (filled symbols).

bility at individual synapses was obtained by globally loading boutons with FM-dye using the procedure described for the EM experiments, and quantifying the total fluorescence. Using this method, continuous low frequency stimulation of selected synapses resulted in a homeostatic decrease in release probability. This confirms that small, localised depolarisations of the dendrite can trigger an homeostatic adaptation of p_r. Notably, only synapses in the stimulated area show a decrease in release probability. Since the exact spatial extent of the stimulation was not measured, only cases where the group of stimulated synapses was separated by at least 10 μm from control boutons were included in the analysis. While this ensures that only non-stimulated synapses are selected as control, it precludes a precise mapping of the spatial spread of the elicited changes in p_r. Also, it is not possible to know if only the stimulated synapses undergo changes, or if release probability would also decrease in very close neighbouring synapses. Nevertheless, this result shows that even for synapses along the same dendritic branch, pr can be independently modified by a highly localised mechanism.

If such local adaptations of release probability operate during the normal functioning of the neuron, and if there is indeed a direct and spatially confined relation between p_r and dendritic activity, then local p_r differences should arise from local differences in activity. In this case, having uniform inputs across the dendritic tree that generate a uniform depolarization, should produce very similar release probabilities. To test this, spatially uniform depolarization levels were achieved by either blocking excitatory and inhibitory synaptic input, or by increasing the culture medium KCl concentration while blocking postsynaptic receptors. Maintaining these manipulations for 24 hrs resulted in a homeostatic change in release probability, as measured by the FM-destaining technique used in chapter three. In agreement with the literature and with the previous results, activity block increased release probability, while KCl reduced the mean p_r. It is important to note that while blocking synaptic receptors selectively manipulates the activity in the postsynaptic site, globally raising the KCl concentration will act both on the pre and post-

synaptic compartments. However, the experiments on global p_r homeostasis discussed above have excluded increased activity in the axon and presynaptic terminals as a homeostatic trigger. This allows changes in p_r that arise from uniform depolarization to be interpreted as a consequence of changes in the postsynaptic site. Increasing the extracellular KCl concentration while blocking synaptic receptors, dissociates postsynaptic depolarization from receptor activation. The fact that under this condition release probability is down-regulated, further supports the view that the homeostatic trigger is the depolarization of the dendrite, regardless of how this depolarization is initiated.

Measures of p_r at single synapses showed that in both conditions tested, the histogram of release probabilities for a given connection changed from a broad and skewed distribution to a Gaussian one with a very low CV. This is compatible with a central dominant value of p_r, associated with some scatter possibly due to intrinsic biological variability and measurement noise, and indicates very uniform release probabilities amongst synapses. The contrast with the control p_r distribution is clear, and is a sign of a marked decrease in the heterogeneity of release probability. In addition, the fact that the global CV in these conditions is not different from the dendritic CV in control, implies that the overall uniformity in p_r is very close to what is observed for single dendritic branches. Analysis of similarity ratios showed that synapses have very similar release probabilities regardless of their spatial arrangement, the mean values being the same for synapses in the same or different dendritic branches. This confirms a very small variability of pr after the manipulations with synaptic block or KCl. The fact that in these conditions, CV and similarity values for synapses in the same dendrite are the same as in control, suggests that the changes elicited by the manipulations are within physiological ranges and are not taking the system to artifactual limits. These results show that two opposite but spatially uniform manipulations of the postsynaptic membrane potential result in loss of release probability variability, despite opposing changes in the overall p_r. This unequivocally links p_r het-

erogeneity to non-uniformities of inputs to the dendritic tree, and supports the idea that the homeostatic response of release probability is implemented at a local level.

After prolonged synaptic block and KCl incubation, the relationship between release probability and the number of synapses on the same branch of the dendrite was lost. This is in full agreement with the hypothesis that p_r adjusts to the regional depolarizations in the dendrite. Because in both conditions the dendritic levels of depolarization are the same regardless of the number of synapses, each individual synapse will try to adapt to the same average membrane potential. No matter how many or how close synapses are in a dendritic branch, blockage of postsynaptic receptors prevents them from having an impact on activity in the dendrite. This shows that the difference in the number of synapses has to be converted into a difference in activity, for a relation with p_r to be established, emphasising that p_r dissimilarity between dendrites indeed results from an adaptation to local depolarization.

Together, the experiments discussed in this chapter confirm that under basal conditions the set point of release probability in cultured hippocampal synapses is determined by a local homeostatic adaptation to the level of activity in the dendrite. Such local operation of homeostatic plasticity has been already suggested to maintain the balance of inhibition and excitation on individual dendritic branches (Liu, 2004) and to mediate GluR1-dependent quantal size scaling after prolonged activity block (Ju et al., 2004; Sutton et al., 2006). Moreover, theoretical simulations of homeostatic plasticity in CA1 pyramidal neurons indicate that synapse-specific homeostasis can successfully counterbalance persistent, cell-wide perturbations of dendritic activity (Rabinowitch and Segev, 2006).

Chapter 6

Theoretical simulations of release probability and dendritic activity

The experimental work in this thesis shows that release probability dynamically adapts to the local level of activity in the dendrite. It is not immediately clear however, what are the functional consequences of having such homeostatic and branch specific regulation of p_r. Is there an advantage to regulating release probability in this way, rather than allowing all synapses in a connection to adopt the same p_r? What would be the impact on basal synaptic transmission and its plastic changes if p_r is set independently of the activity level in the dendrite? To answer these questions, it would be necessary to directly manipulate release probability at individual synapses, and test the impact of imposing a variety of p_r values to a given level of dendritic activity. This requires the natural mechanisms of p_r adaptation found in the previous chapters to be overcome. Since the biological details of the proposed homeostatic process are not known, it is currently not possible to simply block this process in order to achieve independence between p_r and postsynaptic activity. Furthermore, modifying p_r at selected single synapses would be technically very difficult to implement. Thus, such manipulations

are experimentally not feasible at present. Alternatively, theoretical models of realistic neurons can be used to perform virtual experiments where p_r and dendritic activity can be freely dissociated and chosen values assigned. In the present chapter, theoretical simulations were used to gain insight into the physiological significance of the negative feedback regulation of release probability by activity in the dendrite, described in the previous chapters.

6.1 Modelling a CA1 pyramidal neuron and excitatory synaptic input

Neurons from different areas of the brain can have markedly different morphologies and biophysical properties. Since the experiments performed in this thesis were done in hippocampal neurons, a CA1 pyramidal neuron was chosen as the model cell. While this might not be a completely accurate representation of all cells used experimentally, it serves as a good general approximation, and allows the relationship between p_r and dendritic activity to be explored in a neuron model with characteristics very close to what is found in more intact systems. Furthermore, the vast knowledge on the membrane properties of this class of neurons allows the construction of very precise models. All simulations were performed using the NEURON simulation program (Hines and Carnevale, 1997) and the realistic model of a CA1 pyramidal neuron was the same as in Gasparini et al. (2004), in which the cell morphology was obtained from reconstruction of a biocytin-filled neuron (Migliore et al., 1999, Figure 6.1A-B). In general, all biophysical parameters in the model are based on the available experimental data. The passive membrane properties were kept the same as inGasparini et al., as was the incorporation of active conductances in the dendritic tree, which included sodium, delayed rectifier, A-type potassium and non-inactivating, non-specific cation currents. Given that the main variable of interest in this study is the level of depolarization in the dendrite, the presence of dendritic voltage-gated channels in the model is of particular importance, as they can significantly modify the shape and du-

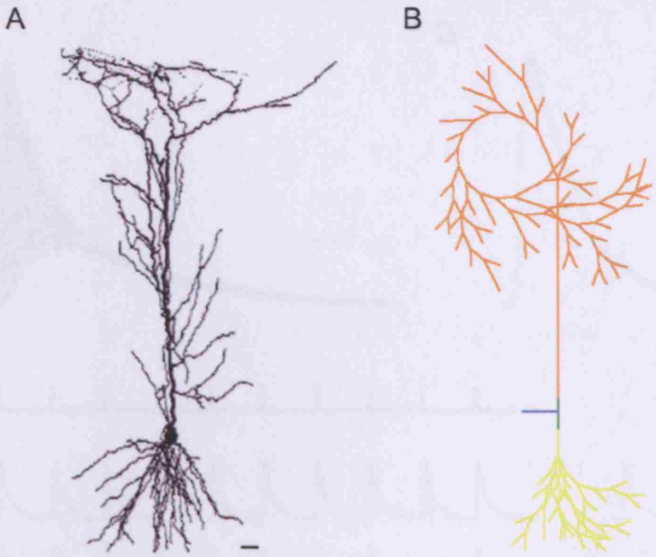

Figure 6.1: Model cell morphology. (A) Neurolucida reconstruction of a byocitin-filled CA1 pyramidal cell, which served as a template to build the cell used in the simulations. Scale bar, 15 μm. (B) Schematic representation of the model cell morphology, showing the 202 different compartments used to recreate the original neuron, with soma (green), axon (blue), basal (yellow) and apical dendrites (orange).

ration of a depolarising signal. Excitatory synapses were modelled as AMPA conductances using a single exponential function, with a 1 ms time constant, a reversal potential of 0 mV and a peak conductance of 1.5 nS. Figure 6.2A shows traces of the membrane potential recorded at the soma obtained after sequentially activating 60 different synapses distributed over the dendritic tree. The average amplitude and kinetics of the EPSPs obtained, match well the average spontaneous EPSP from whole-cell recordings. This exponential function was then modified to include an adjustable release probability to the stimulus (Appendix 3), and used in all simulations below. Figure 6.2B illustrates the effect of changing p_r on a single synapse.

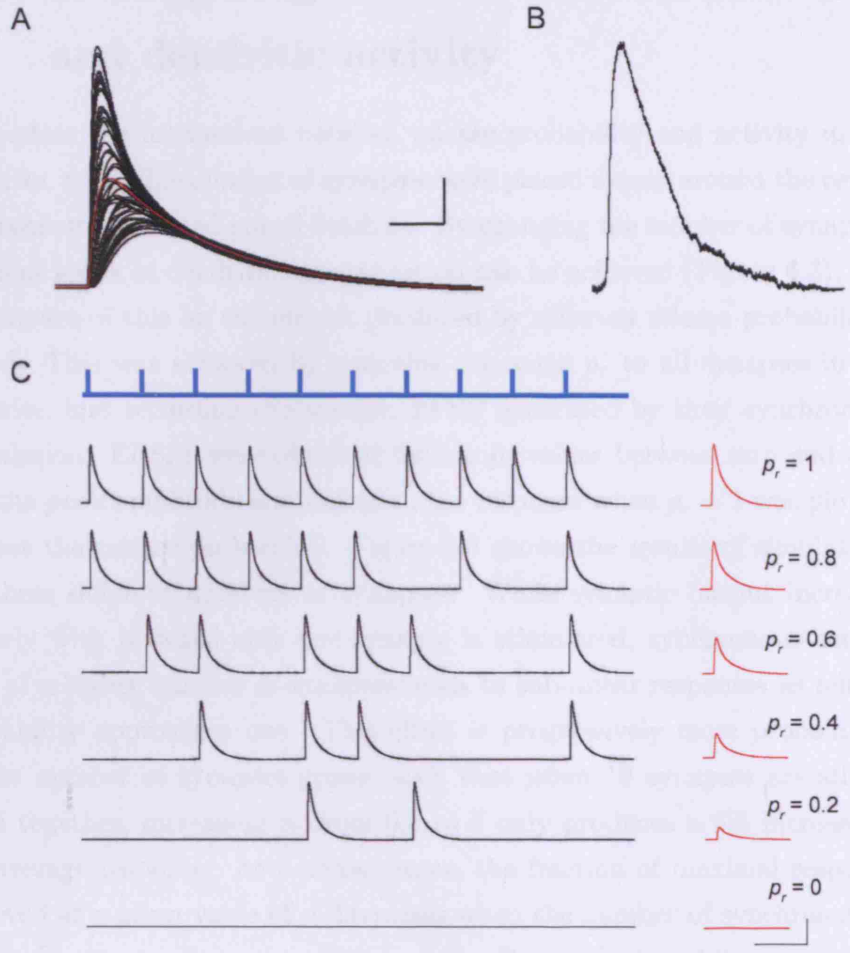

Figure 6.2: Modelling synaptic input. (A) Somatic voltage traces of simulated EPSPs. Each black trace corresponds to activation of a single synapse in a different branch of the dendritic tree. Red trace is average of all synapses. (B) Real EPSP obtained from voltage recording at the soma in a cultured neuron. Trace is average of 15 miniature events. Scale bars for A and B, 5 ms, 0.2 mV. (C) One synapse was stimulated 10 times every 40 ms (top scheme, vertical bars indicate time of stimulation) and the resulting somatic voltage is shown (traces below). As p_r is decreases the number of EPSP successes decreases as expected. Traces on the right are average EPSPs for a given p_r, including failures. Scale bars, 40 ms, 0.4 mV.

6.2 Investigating different combinations of p_r and dendritic activity

To explore the interactions between release probability and activity in the dendrite, a variable number of synapses were placed evenly around the centre of a randomly selected apical dendrite. By changing the number of synapses, different levels of dendritic depolarization can be achieved (Figure 6.3), and the impact of this on the output produced by different release probabilities tested. This was achieved by assigning the same p_r to all synapses in the dendrite, and recording the somatic EPSP generated by their synchronous stimulation. EPSPs were obtained for ten p_r values between zero and one, and the peak amplitude normalised to the response when $p_r = 1$ was plotted against the release probability. Figure 6.3 shows the results of simulations for three different numbers of synapses. While synaptic output increases linearly with p_r when only one synapse is stimulated, synchronous activation of a higher number of synapses leads to sub-linear responses as release probability approaches one. This effect is progressively more pronounced as the number of synapses grows, such that when 10 synapses are stimulated together, increasing p_r from 0.5 to 1 only produces a 6% increase in the average response. As a consequence, the fraction of maximal response achieved at a given value of p_r increases when the number of synchronously activated synapses increases (Figure 6.3). For example, while stimulating one synapse with a p_r of 0.4 naturally leads to an average response that is 40% of what is obtained when $p_r = 1$, if four synapses are stimulated this number changes to 72%. This means that by increasing the level of activity in the dendrite, each synapse will operate closer to the saturation of its dynamic range. Therefore, to prevent saturation, release probability should decrease as the average dendritic depolarization increases. Figure 6.4 shows the necessary decrease in p_r required to maintain three different saturation levels when the synapse number increases from one to four. These values were obtained from the equations of simple exponential fits to plots similar

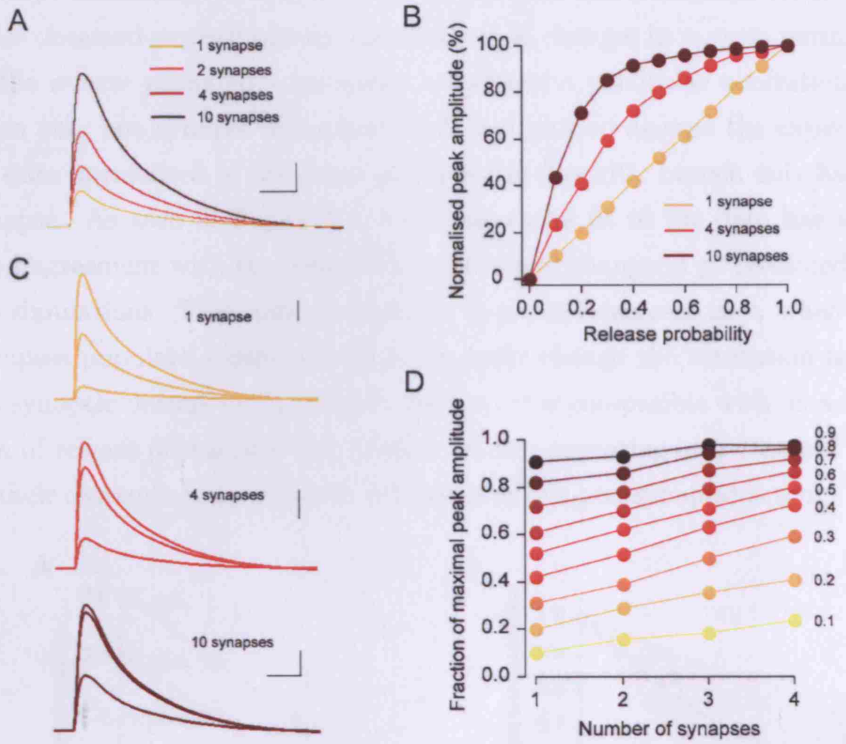

Figure 6.3: Effect of changing p_r and number of stimulated synapses. (A) EPSP traces obtained by activating an increasing number of synapses with $p_r = 1$. Scale bars, 5 ms, 0.5 mV. (B) Plot of peak EPSP amplitude normalised to the response when $p_r = 1$ against release probability, for three different numbers of synapses in the dendrite. (C) Traces show the average EPSPs for the three conditions in B, when $p_r = 0.1$, 0.5 and 1. Scale bars, 5 ms, 0.1, 0.4 and 0.5 mV (top to bottom). (D) Fraction of maximal peak amplitude (obtained when $p_r = 1$) for different release probabilities (coloured line, value of p_r indicated for each one), plotted against the number of stimulated synapses in the dendritic branch.

to the one in Figure 6.3, and bear a close resemblance to the negative correlation between p_r and number of synapses in the dendritic branch found with FM-dye destaining (see Figure 3.9). To compare the simulation results with those obtained experimentally, the theoretical changes in p_r were normalised to the release probability necessary to achieve a particular saturation level when only one synapse was stimulated, and plotted against the experimental data normalised to the mean p_r when the dendritic branch only had one synapse. As seen in Figure 6.4, the exponential fit to the data has a very good agreement with the magnitude and rate of change in p_r predicted from the simulations. This suggests that the measured decrease in p_r when more synapses populate a dendrite does not really change the saturation level of the synaptic output to the branch. Rather, it is compatible with an adaptation of release probability that keeps synapses operating at a constant point in their dynamic range, despite variations of the postsynaptic activity level.

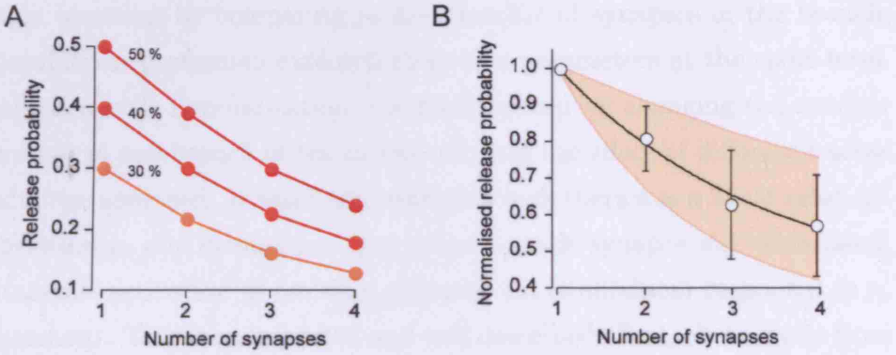

Figure 6.4: Decreases in p_r prevent synaptic saturation. (A) Plot shows the necessary adaptive change in p_r required to maintain three different levels of saturation (indicated by different coloured lines) as the number of stimulated synapses increases. (B) Shaded area show the theoretical changes in p_r to maintain saturations between 10% (lower limit) to 90% (upper limit) with increasing number of synapses. Open circles are experimental data and solid line is a single exponential fit to the data.

6.3 Discussion

The results presented in the previous chapters described an inverse relationship between the average level of dendritic depolarization and the probability of neurotransmitter release. In this chapter, to explore what are the major functional consequences of such a relationship, theoretical simulations were performed where p_r and postsynaptic activity could be artificially dissociated from each other.

A multicompartmental model of a CA1 pyramidal cell was used, incorporating a number of active conductances in all compartments, including the dendritic tree. Excitatory synapses were modelled as a single exponential function, and their peak conductance was chosen to match the experimental data, as judged by comparing the average mEPSP recorded at the soma in the model with real whole-cell voltage recordings. Given that the relationship described above between p_r and dendritic activity was found at the level of single branches by comparing p_r and number of synapses in the branch, the simulations performed explored these two parameters at the same level. Average dendritic depolarization was manipulated by changing the number of synapses in one branch of the model cell, and the effect of different release probabilities analysed. It was found that although there was a linear relationship between p_r and synaptic output when a single synapse was stimulated, simultaneous activation of multiple synapses led to sublinear responses as p_r was increased. This is an expected and well described effect, that results from two different mechanisms: 1) a reduction in the driving force, since with increasing number of activated synapses the dendrite will be more depolarised and closer to the AMPA reversal potential of 0 mV, and 2) a decrease in input resistance due to opening of more channels, which leads to less voltage being generated per unit of current (Rall and Rinzel, 1973; Rinzel and Rall, 1974).

Although no background synapses were included in the present model, the effect of globally distributed synapses activated randomly can be modelled as a global increase in conductance. In such a case, the impact of

the conductance change produced by a synaptic event represents a smaller fraction of the total conductance. This means that the synaptic saturation that results from decreases in input resistance will be less pronounced, but it would not change the overall finding. The particular case analysed in this chapter, in which the number of synapses is increased in the same branch of the dendrite, is expected to produce the maximal effects of synapse saturation. This is because these branches have a length much smaller than the space constant (Rall and Rinzel, 1973; Rall, 1969a,b; Jack and Redman, 1971), and therefore, the voltage changes that underlie synaptic interaction and saturation propagate very efficiently throughout the whole length of the branch. Although it has not been explored in this chapter, these interactions will occur to a much lesser extent if synapses are distributed over different branches, instead of being placed all in the same one. The degree of interaction will depend on several well known parameters related to the morphology and biophysical properties of the neuron, such as the dendrite branching pattern, branch diameter, membrane and internal resistance (Rall and Rinzel, 1973; Rall, 1969a,b; Rinzel and Rall, 1974; Jack and Redman, 1971).

The synaptic saturation described can have very detrimental consequences for the functioning of the neuron. Namely, it will decrease its sensitivity to increases in the number of stimulated inputs, and it will compromise p_r changes as an efficient means of changing the gain of a synapse. If a high number of synapses are present, increases in p_r will have a very small effect on the actual voltage change produced. By testing different combinations of release probability and number of stimulated synapses, it was found that an exponential decrease in p_r can prevent this synapse interaction and maintain a constant level of saturation. Notably, the rate of change in p_r obtained from the simulations matched very well the experimental data, with a single exponential fit to the data falling close to the predicted change required to maintain a 50% saturation. The results of these simulations therefore indicates that one advantage of having a negative feedback between dendritic activity and release probability, is that it ensures that synapses operate close to the cen-

ter of their presynaptic dynamic range in the face of different postynaptic environments.

Chapter 7

Concluding remarks

The probability of neurotransmitter release is one of the three classic quantal parameters used by Bernard Katz to describe synaptic transmission. It defines the strength of a synapse and is uniquely linked to activity-dependent short-term adaptations of transmission, thereby profoundly shaping the efficiency of information transmission between neurons. In this thesis, fluorescence imaging, electron microscopy and electrophysiology were combined to study the determinants of release probability at single synapses. A new retrograde negative feedback model is proposed, whereby depolarization of the dendrite locally and constitutively down-regulates the probability of neurotransmitter release. This model raises several considerations about our current understanding of homeostatic regulations of synaptic strength. In this last chapter these considerations will be addressed, while integrating the findings of this thesis with the current literature and giving insight into possible molecular mechanisms for implementing the negative feedback regulation of p_r.

A form of homeostatic control of release probability by dendritic depolarization was established by the finding that neighbouring synapses on the same dendritic segment have a very similar p_r, and that release probability is negatively correlated with the number of synapses made by the axon onto the dendrite. This was confirmed by the observation that globally in-

creasing network activity elicited a compensatory decrease in p_r that was dependent on glutamatergic synaptic transmission. Although the full time course of this adaptation was not explored, it was observed as early as following 2 hrs of increased neuronal activity. This is a considerably shorter time period than is generally associated with homeostatic changes of synaptic function, which are typically reported after at least one or two days of activity manipulations (Turrigiano et al., 1998). However, recent evidence from experiments in hippocampal cell cultures (Sutton et al., 2006) and in the Drosophila NMJ (Frank et al., 2006) suggests that such homeostatic changes might develop over time periods as small as 15 mins. Interestingly, both in the experiments in this thesis and in other studies, paradigms used to induce homeostatic changes (Turrigiano et al., 1998), increase network activity to 1-2 Hz, which is very similar to LTD protocols that use low-frequency stimulation. While LTD usually develops instantaneously after the induction protocol, its readout is normally the size of synaptic responses of the same population of synapses before and after induction. On the other hand, the readout of homeostasis comes normally from comparing spontaneous synaptic events on a population of control cells versus a population of cells exposed to activity changes. This has the disadvantage that any detectable effects have to overcome the intrinsic population variability and therefore is a much less sensitive approach. Is it thus possible that if the same population of synapses was used to assess the effects of protocols designed to induce homeostasis, changes would be detected much earlier. In such a case, the functional distinction between LTD and homeostatic down-regulations of synaptic transmission becomes blurred, as they both serve the same purpose: a long-lasting negative feedback between increased low frequency activity and synaptic strength. Thus, a better understanding of the cellular and molecular mechanisms of homeostatic changes, as well as a more complete description of its time course, will be required to establish if this phenomenon is actually mechanistically distinct from LTD.

A basic requirement of the proposed model of p_r regulation is the action of

a retrograde signal, that is triggered by dendritic depolarization and acts on the presynaptic terminal to down-regulate release probability. Although the nature of such a signal was not pursued in this thesis, many mechanisms have been described in the literature where postsynaptically derived signals influence presynaptic neurotransmitter release. A particularly attractive class of molecules are endocannabinoids, whose production and release from the postsynaptic terminal is triggered by depolarization of the dendrite, and which then cross the synaptic cleft to decrease release probability of excitatory and inhibitory synapses. Although this effect can be short-lived, endocannabinoids have been proposed to mediate some forms of LTD, namely in the striatum, nucleus accumbens and layer 5 pyramidal cells (Alger, 2002; Sjostrom et al., 2004). The involvement of this signalling pathway in the p_r regulation described in this thesis, could be tested by increasing network activity in the presence of endocannabinoid receptor blockers, and assessing the impact of this on release probability adaptation. Another type of retrograde signalling that could be important for p_r regulation is direct transsynaptic signalling via cell adhesion molecules. For example, in one scenario, decreases in synaptic strength are induced and expressed postsynaptically via removal of AMPA receptors, leading to a decrease in the overall size of the PSD (Schnell et al., 2002). This change in size could then be communicated to the presynaptic site via the neuroligin-neurexin complex to decrease release probability (Futai et al., 2007), possibly by reducing the size of the active zone and the number of vesicles available for release. This hypothesis could be tested by knocking down the function of neuroligin in the postsynaptic cell, via transfection of a dominant-negative form for example, and investigating the effects of this on the homeostasis of p_r.

The clear spatial segregation of p_r found in this thesis contrasts with the findings of Koester and Johnston (2005) for synapses of layer 2/3 cortical pyramidal cells. Here, it was reported that synapses from the same connection had very similar release probabilities, even if the synaptic boutons were located in different parts of the dendritic tree. However, as discussed in

chapter three, given that the estimated CV for release probability was very small, it is not surprising that p_r is correlated between any two synapses, regardless of the distance between them. Interestingly, Koester and Johnston state that *we are left with the conclusion that the normalisation could arise from the unique pattern of pre and postsynaptic activity that is similar for all contacts of a given connection.* While there is no speculation on how such unique patterns of activity arise and implement the observed normalisation of p_r, the authors interpretation of the data is in excellent agreement with the model of p_r regulation proposed in this thesis. Indeed, if all the synaptic connections between a pair experience the same amount of activity in the dendrite, then this model predicts that they will all have the same release probability. This could arise, for example, if there were no systematic differences in the activation of the inputs to a given dendritic branch, so that synapse activation in a given location follows a Poisson distribution. Under these conditions, synapses that belong to the same axon will experience not only the same amount of activity produced by the firing rate of their axon, but will also be exposed to a similar level of local background activity, thus adopting similar release probabilities.

Ultrastructural analysis of the spatial distribution of p_r confirmed that synapses close together on the same dendritic branch have a very similar release probability. At first sight, this is in apparent contradiction with EM studies of the hippocampus from native tissue (Harris and Sultan, 1995). In these studies, release probability was inferred from the size of the active zone and number of docked vesicles, and no correlation was reported for synapses along the same dendrite. However, the spatial correlations of release probability found in this thesis are only valid for synapses that belong to the same axon. Although it was not systematically quantified, it was clear from the EM analysis performed here that there was no such correlation for boutons with different origins. This implies that what underlies the correlation in p_r between any two synapses is the systematic synchronicity of their activation. This synchronicity results in both synapses experiencing very similar levels of

postsynaptic activity over time, provided that they are close enough together on the dendrite, and in this way, they will adopt a very similar p_r. Thus, a clear correlation between release probabilities is to be expected with either synapses from the same axon or synapses from different axons systematically activated at the same time. In the EM studies referred to above there was no information about the source of inputs, and therefore these most likely arise from different axons with different activity histories. In this case, the lack of correlation between morphological correlates of p_r is expected.

A point of particular interest is how synapse specific and locally restricted the modulation of release probability is. Investigating this could be achieved by adjusting the theta-glass stimulation technique established in chapter five to stimulate and elicit a decrease in p_r in only one synapse, and measuring release probability in immediate neighbours to check for any spread of the induced homeostatic change. Nevertheless, the apparent ability of the proposed p_r regulation model to influence only activated synapses, implies the need for some kind of coincidence detection, whereby synapses that have released glutamate are tagged for potential p_r modifications. Such a mechanism has been described for example for LTD of layer 5 pyramidal cells, where LTD expression requires signalling through presynaptic NMDA receptors, which serves to ensure synapse specificity of this plastic change (Sjostrom et al., 2004). Although the paired-pulse ratio experiments presented here did not support the presence of presynaptic NMDA receptors, coincidence detection could, for example, be implemented via metabotropic glutamate receptors. This could be readily tested by targeting a candidate receptor with blockers or agonists and assessing their capability to compromise the induction of release probability homeostasis or its synapse specificity, respectively. If this were the case, the spatial spread of p_r modulations could then be determined by the degree of glutamate spillover between neighbouring synapses.

The local nature of the mechanism involved in setting release probability was evident not only from the differences between boutons in different dendritic branches, but also from the local stimulation experiments, where only

the group of stimulated synapses showed a decrease in p_r. However, in addition to the synapse specificity discussed above, the exact spatial extent over which two synapses activated at the same time can interact to influence each other's release probability, was not measured. This question could be investigated by using two independent theta-glass pipettes to stimulate pairs of individual synapses separated by different distances, and using this approach to establish the maximum intersynaptic distance that generates a decrease in p_r stronger than stimulation of one synapse by itself. The fact that the EM data shows that for intersynaptic distances over $\sim$ 10 μm the similarity in p_r was not different from that expected by chance, should not be taken to imply that interactions between synapses do not occur over this distance. Because the pairs of synapses analysed were not isolated in the dendrite, it is likely that interactions with other synapses occur over $\sim$10 μm, in which case release probability of each of the synapses in a given pair will be no longer a strict reflection of the interaction between them. Furthermore, the theoretical simulations presented, suggest that a potential functional role for this model of p_r regulation would be to prevent voltage interactions that lead to synapse saturation. As voltage spreads very efficiently over a single dendritic branch (Rall and Rinzel, 1973; Rall, 1969b), the underlying cellular mechanism that mediates synapse interactions responsible for p_r correlations has to spread as much as voltage. The fact that there is a significant drop in voltage spread between dendritic branches, is consistent with the observation of branch specific release probabilities. Although the identity of the activity sensor responsible for translating dendritic depolarization into the biological events that lead to changes in p_r was not investigated, a likely candidate is calcium. Activation of NMDA receptors and GluR2-lacking AMPA receptors allows direct entry of calcium to the dendrite via the postsynapse, and this can be amplified by voltage-gated calcium channels and release from internal stores. Calcium in the dendrite would then spread locally to guarantee interaction with neighbouring synapses (Lohmann et al., 2005), and would trigger the activation of a retrograde signalling cascade. This potential role for cal-

cium ions could be tested by chelating calcium exclusively in the postsynaptic cell while trying to induce homeostatic changes in release probability.

The local operation of release probability homeostasis described here is in conflict with the general view of homeostatic plastic changes. These are usually described as cell-wide modifications that scale synaptic function up or down, without changing the relative synaptic weights. However, the evidence that supports this view comes from experiments where activity was uniformly modulated across the entire cell, and therefore did not directly test the potentially local nature of this phenomena. By contrast, the local stimulation experiments in this thesis clearly show that release probability can be modified homeostatically in restricted groups of synapses. Such local implementation of homeostasis has been recently shown theoretically to be as effective as global changes (Rabinowitch and Segev, 2006), and experimental evidence points to a similar local form of homeostatic control of postsynaptic receptors (Liu, 2004; Liu and Tsien, 1995; Sutton et al., 2006).

Blocking postsynaptic excitatory receptors, and therefore breaking the link between neurotransmitter release and dendritic depolarization, led to a compensatory increase in release probability, even if presynaptic terminals were continuously stimulated. This demonstrates that for a homeostatic decrease in p_r to develop, dendritic depolarization is required. Interestingly, in the experiments where network activity was increased by field stimulation while blocking AMPA and NMDA receptors, APs were elicited both on the pre and postsynaptic cells. The fact that p_r did not decrease under these conditions, indicates that the depolarization produced by the backpropagating action potential alone is not sufficient to elicit such change. Furthermore, the fact the p_r actually increases with activity block implies that apart from the negative feedback model explored in this thesis, a concurrent mechanism operates to increase release probability. This could be implemented by action of glutamate in presynaptic metabotropic autoreceptors, for example, such that glutamate release would trigger two opposing mechanism to regulate p_r. The balance between these two mechanisms would then determine the

release probability of a synapse. Experiments where candidate receptors are blocked and postsynaptic activity abolished would test this hypothesis.

While the work in this thesis led to a model for setting release probability at individual synapses, it did not explore how changes in p_r might be implemented. The finding that the individual sizes of the recycling pool follow the same spatial distribution of p_r, and that they are modulated by changes in activity, suggested that changes in the number of vesicles available to release contribute to adjusting of p_r. However, given the complexity of the process of neurotransmitter release, it is equally likely that many other factors, such as the density of voltage-gated calcium channels or the efficiency of calcium buffering on the presynaptic terminal, are involved in modifications of release probability. Only carefully designed and specifically directed experiments will dissect the mechanisms that synapses use to dynamically change their p_r. It will also be very interesting to explore if this negative feedback regulation of release probability is a conserved mechanism across the many different types of synapses in the brain. In particular, the question remains if the model proposed here could account for the target-cell dependence observed in many brain circuits. Although, in this case, differences could arise during synapse development due to different cues and genetic programs, it is also possible that they can be explained by systematic differences in the activity of specific types of cell in a given circuit. This could be initially assessed by trying to correlate release probability and spontaneous postsynaptic activity for different types of cells, as measured globally by the firing rate or locally by calcium imaging, for example.

The fact that the basal release probability of synapses is set in an homeostatic manner, implies that there is a target level of dendritic depolarization that drives adjustments in p_r. Different synapses over the dendritic tree will adopt a given release probability based on the local synapse density and activity. If this mechanism is fully successful, then all dendrites will have, on average, the target membrane potential and the dendritic tree will be isopotential. Making p_r uniform by postsynaptic receptor blockage should

disrupt this balance, and lead to a non-uniform distribution of voltages, such that in the culture system used, the average voltage of a dendrite will be simply proportional to the number of synapses. It would be interesting to test this prediction directly, which could be done by combining FM-dyes and voltage-sensitive dye imaging.

Theoretical simulations of release probability in a multicompartmental neuronal model, suggest that a potential role for the negative feedback model of p_r regulation is to prevent synaptic saturation. If p_r is very high in all synapses, then stimulation of increasing number of inputs will lead to progressively smaller increases in the elicited voltage changes, due to a reduction in the driving force and shunting. This means that beyond a certain point, the neuron cannot detect the activation of more synapses, and this will be highly detrimental to the transfer of information. By adjusting release probability to the level of dendritic activity, it is ensured, presynaptically, that this point is not reached. As the voltage change produced by a synapse is partially dependent on the combination of voltage-gated channels present in the dendrite, another functional consequence of setting p_r in this way is that synaptic strength will be matched to the degree of dendritic excitability. This can again prevent saturation of voltage responses, and also ensure that inputs onto less excitable areas of the dendritic tree are not disadvantaged. Given that single dendritic branches can behave as individual compartments that perform independent computations (Polsky et al., 2004), it is therefore fundamental that, as proposed in this thesis, the balance between synaptic strength and dendritic activity is achieved at the level of individual branches.

Appendices

Appendix 1 - MATLAB/IGOR code for integrating FM-dye puncta

```
%For MATLAB

%load and display image
i=imread('/path/image_name.tif');
clear image
figure; imshow(i); colormap(jet(100));

%manually select synapses to analyse and convert image
%matrix into a linear array that can be read by IgorPro
for num=1:10
        clear x y z index linear_matrix
        figure;
        [i_crop, rect]=imcrop(i);
        index=[1:(size(i_crop,1)*size(i_crop,2))]; index=index';
        [x, y]=ind2sub([size(i_crop,1) size(i_crop,2)],index);
        for n=1:length(index)
            z(n)=i_crop(x(n),y(n));
        end
        z=double(z');
        linear_matrix=[x y z];
        i_crop=double(i_crop);
        file_number=mat2str(num);
        save_string_linear=['synapse_' file_number '.txt'];
        save_string_matrix=['synapse_m_' file_number '.txt'];
        save(save_string_linear, 'linear_matrix', '-ascii');
        save(save_string_matrix, 'i_crop', '-ascii');
end


%For IGOR

#pragma rtGlobals=1 // Use modern global access method.

Function syn_fit()

Variable n

for (n=1;n<10;n+=1)

%load and display individual  synapse image selected in MATLAB
string load_string_1 = "path:synapse_" + num2istr(n) + ".txt"
string load_string_2 = "path:synapse_m_" + num2istr(n) + ".txt"
LoadWave /G /N load_string_1
LoadWave /G /M /N=matrix load_string_2
```

```
Display;AppendImage matrix0
Display;AppendXYZContour wave2 vs {wave0,wave1}

%fit a 2D-gaussian curve
CurveFit Gauss2D wave2 /X={wave0,wave1} /D
Display;AppendImage fit_wave2

%store the fit coefficients
WAVE W_coef
Variable x=W_coef[2]+W_coef[3]*2
Variable y=W_coef[4]
Variable cutoff_level

%calculate 2SDs from the center of the fit
cutoff_level=W_coef[0] + W_coef[1]*exp((-1/(2*...
(1-W_coef[6]^2)))*(((x-W_coef[2])/W_coef[3])^2+...
((y-W_coef[4])/W_coef[5])^2-((2*W_coef[6]*...
(x-W_coef[2])*(y-W_coef[4]))/(W_coef[3]*W_coef[5])))

%display the cutoff level
AppendMatrixContour fit_wave2
ModifyContour fit_wave2 rgbLines=(52428,1,1),labels=0,...
manLevels={cutoff_level,0,1}
Print cutoff_level

string save_string = "path:synapse_fit_" + num2istr(n) + ".txt"
Save/G /O  W_coef as save_string

endfor
End

%For MATLAB

clear integral z

for n=1:10

%load and read fit coefficients
load_string = ['path/synapse_fit_' num2str(n) '.txt'];
coef = load(load_string);
xi=coef(3)+coef(4)*2;
yi=coef(5);

%calculate 2SD cutoff level
cutoff_level = coef(1) + coef(2)*exp((-1/(2*(1-coef(7)^2)))*...
    (((xi-coef(3))/coef(4))^2+((yi-coef(5))/coef(6))^2-...
    ((2*coef(7)*(xi-coef(3))*(yi-coef(5)))/(coef(4)*coef(6)))));
```

```
%generate a 2D gaussian with the fit parameters
i = 1;
for x = (coef(3)-2*coef(4)):0.1:(coef(3)+2*coef(4))
    j = 1;
    for y = (coef(5)-2*coef(6)):0.1:(coef(5)+2*coef(6))
        z(i,j) = coef(1) + coef(2)*exp((-1/(2*(1-coef(7)^2)))*...
        (((x-coef(3))/coef(4))^2+((y-coef(5))/coef(6))^2-...
        ((2*coef(7)*(x-coef(3))...*(y-coef(5)))/(coef(4)...
        *coef(6)))));
        j = j+1;
    end
    i = i+1;
end

figure; imshow(uint8(z))

%integrate the fit above the cutoff level
index = find(z > cutoff_level);
integral(n) = sum(z(index));
z(index)=255;
figure; imshow(uint8(z))

end
```

Appendix 2 - MATLAB code for detecting FM-dye puncta

```
function IdentifyPuncta(im, preferences)

Io=imread('path/imagename.tif');
I=imresize(Io,2);
Io=I;

% offset the image by the mean pixel intensity
limit=mean2(I);
I=double(I);
I=I-limit;
I=uint8(I);

% apply Laplacian of Gaussian filter
sigma=preferences.LoGsigma;
s=round(6*(2^(1/2))*sigma);
g=fspecial('gaussian', s, sigma);
A=[0, -1, 0; -1 4 -1; 0 -1 0];
c=conv2(A,g);
Ic=conv2(double(I),double(c));
Ic=uint8(Ic);

% apply Canny filter
t=[preferences.CannyLT preferences.CannyUT];
bin=edge(Ic,'canny',t,preferences.CannySigma);

% crop borders
extra=(size(bin,1)-size(I))/2;
for n=1:extra
    bin(n,:)=[];
    bin(:,n)=[];
    bin((size(bin,1)-(n-1)),:)=[];
    bin(:,(size(bin,2)-(n-1)))=[];
end

% select the closed edges by bridging, filling and
% opening the image
bin=bwmorph(bin,'bridge');
bin=imfill(bin,'holes');
se=strel('disk',1,0);
bin=imopen(bin, se);

% fit a gaussian to each region and eliminate bad fits
% based on rsquare
c=1;
for t=1:(n-1)
```

```
    [i,j]=find(L==t);
    if length(min(j):max(j))>length(min(i):max(i))
        x=min(j):max(j);
        y=min(i)+round((max(i)-min(i))/2);
        vector=Io(y,x); vector=double(vector);
    else y=min(i):max(i);
        x=min(j)+round((max(j)-min(j))/2);
        vector=Io(y,x); vector=double(vector);
    end
    vector=vector(:);
    l=length(vector); x=[1:l]; x=x(:);
    [cf,gof] = fit(x,vector,'gauss1');
    if gof.rsquare<preferences.rsquare
       index=find(L==t); L(index)=0;
    else SigmaValues(c)=cf.c1/sqrt(2);
        c=c+1;
    end
end
index=find(L~=0); L(index)=1;

% constrain the size to max intensity -2SD
[L,n]=bwlabel(L);
for k=1:(n-1)
    index=find(L==k); m=max(Io(index)); m=double(m);
    scaleF=m/(1/(SigmaValues(k)*sqrt(2*pi)));
    limit=(1/(SigmaValues(k)*sqrt(2*pi)))*exp(-...
    (SigmaValues(k)*preferences.AreaSigma)^2/(2*SigmaValues(k)^2));
    limit=limit*scaleF;
    index=find(L==k);
    Oindex=find(Io(index)<limit);
    L(Oindex)=0;
end

% erase puncta out of area limit
c=1;
for k=1:n
    if area(k)>preferences.AreaLimit || area(k)<5 %SlimitArea
       index=find(L==k); L(index)=0;
    else Farea(c)=area(k);
         c=c+1;
    end
end
index=find(L~=0); L(index)=1;

% plot the result over the original image
global punctamask
global subtraction
```

```
Io=imresize(Io, 0.5);

Isize=size(Io);
index=find(Io>254)
Io(index)=253; % keep i255 for color
set(gcf,'unit','pixels');
initialposition=get(gcf,'position')
figure; image(Io)

punctamask=imresize(L, 0.5);
AlphaMatrix=punctamask;
AlphaMatrix=double(AlphaMatrix);
index=find(punctamask==1); punctamask(index)=255;
hold on;
overlay=image(punctamask);
alpha(overlay, AlphaMatrix);

set(gcf,'unit','pixels','position',[initialposition(1)+50 ...
initialposition(2)-50 Isize(2)+30 Isize(1)+30], 'resize',...
'off','MenuBar','none');
set(gca,'unit', 'pixels','position',[15 15 Isize(2)...
Isize(1)],'Visible','off');
colors=gray(254);
colors(255,1)=1; colors(255,2)=0.6; colors(255,3)=0;
colormap(colors);

RemoveButton=uicontrol('style','pushbutton','string',...
'Manually Remove Puncta','position', [20 20 135 20],...
'callback', @RemoveButton_callback);

subtraction=punctamask;

% ------------------------------------------------------------
% function to remove puncta
function RemoveButton_callback(obj, eventdata)

global punctamask
global subtraction
global Io
global Farea
global finalpuncta

size(Farea)
size(finalpuncta)

subtraction=uint8(subtraction);
```

```
punctamaskLabel=bwlabel(subtraction);
puncta2remove=bwselect;
puncta2remove=uint8(puncta2remove);
punctamask=uint8(punctamask);
index=find(puncta2remove==1); puncta2remove(index)=255;
subtraction=imsubtract(subtraction, puncta2remove);

set(gcf,'unit','pixels');
initialposition=get(gcf,'position')
hold off;
Isize=size(Io);
image(Io)
AlphaMatrix=subtraction;
AlphaMatrix=double(AlphaMatrix);
index=find(AlphaMatrix==255); AlphaMatrix(index)=1;

hold on;
newoverlay=image(subtraction);
alpha(newoverlay, AlphaMatrix);

set(gcf,'unit','pixels','position',[initialposition(1)...
 initialposition(2) Isize(2)+30 Isize(1)+30], 'resize', 'off');
set(gca,'unit', 'pixels','position',[15 15 Isize(2)...
 Isize(1)],'Visible','off');
colors=gray(254);
colors(255,1)=1; colors(255,2)=0.6; colors(255,3)=0;
colormap(colors);

[puncta2removeLabel,n]=bwlabel(puncta2remove);
for i=1:n
    index=find(puncta2removeLabel==i);
    punctanumber=punctamaskLabel(index(1));
    finalpuncta(punctanumber)=[];
    Farea(punctanumber)=[];
end
```

Appendix 3 - NEURON code used in the simulations

```
%MOD file for ExpSyn with adjustable release probability
NEURON {
POINT_PROCESS myExpSyn
RANGE tau, e, i, p
NONSPECIFIC_CURRENT i
}

UNITS {
(nA) = (nanoamp)
(mV) = (millivolt)
(uS) = (microsiemens)
}

PARAMETER {
tau = 0.1 (ms) <1e-9,1e9>
e = 0 (mV)
p = 0.5 (1) <0,1>
}

ASSIGNED {
v (mV)
i (nA)
}

STATE {
g (uS)
}

INITIAL {
g=0
}


LOCAL r
LOCAL s

BREAKPOINT {
SOLVE state METHOD cnexp
i = g*(v - e)
}

DERIVATIVE state {
g' = -g/tau
}

NET_RECEIVE(weight (uS)) {
```

```
s = 1
r = scop_random()
printf("r = %g\n", r)
if (r>p) {
s = 0
}
printf("s = %g\n", s)
state_discontinuity(g, g + weight*s)
}

%HOC file

//preceded by the first 157 lines of code in
//the file forfig5A.hoc of Gasparini et al (2004)
//downloaded from http://senselab.med.yale.edu

SYNE    = 0         // Driving force of excitatory synapses
SYNG    = 0.0015          // Initial synaptic conductance (uS)
P = 1
SYNTAU = 1

tstop = 20

///add stimulator///
objref ns
ns = new NetStim(0.5)
ns.interval = 0
ns.number = 1
ns.start = 1
ns.noise = 0

///add synaptic input///
intersyn_d = 1       //in microns
nsyn_T = 0
dend_i = 47     //chose dendrite
dend_e = 47

for d = dend_i, dend_e {
nsyn_t = apical[d].L/intersyn_d
nsyn_T = nsyn_T + nsyn_t
}

objref syn[nsyn_T], nc[nsyn_T]
counter = 0

for d = dend_i, dend_e {
dend_n = d
```

```
nsyn = 1  //variable number of synapses
Pinit = 0.5 - ((nsyn-1)*(intersyn_d/apical[dend_n].L)/2)
access apical[dend_n]
nseg = apical[dend_n].L/1

for i=0,nsyn-1 {
Pi = Pinit + i * (intersyn_d/apical[dend_n].L)
syn[counter] = new myExpSyn(Pi)
syn[counter].tau = SYNTAU
syn[counter].e = SYNE
nc[counter] = new NetCon(ns, syn[i])
nc[counter].weight = SYNG
counter = counter + 1
}
}

objref vrec, vpeaks, vmeans
n_trials = 10000

vrec = new Vector(tstop/dt+1)
vpeaks = new Vector(n_trials)
vmeans = new Vector(10)
vrec.record(&soma.v(0.5))

access soma

for a=10, 10 {
 P = a/10
 for s=0, counter-1 {
  syn[s].p = P
}
 for i=0, n_trials-1 {
run()
vpeaks.x[i] = vrec.max
}
vmeans.x[a-1] = vpeaks.mean
}

///save vector///

objref save_file
save_file = new File()
save_file.wopen("/path/data.dat")
vmeans.printf(save_file)
save_file.close()
```

Appendix 4 - Acronyms and Abbreviations

μ	Micron
ACh	Acetylcholine
AMPA	α-amino-3-hydroxy-5-methylisoxazole-4-proprionic acid
AP	Action potential
AP5	DL-2-Amino-5-phosphopentanoic acid
CNQX	6-cyano-7-nitroquinoxaline-2,3-dione
CNS	Central nervous system
CV	Coefficient of variation
DIC	Differential interference contrast
DIV	Days *in vitro*
EM	Electron microscopy
EPP	End-plate potential
EPSC	Excitatory postsynaptic current
EPSP	Excitatory postsynaptic potential
G	Giga
GABA	Gamma-aminobutyric acid
GPSC	GABA-mediated postsynaptic current
hr	hour
Hz	Hertz
IPSP	Inhibitory postsynaptic potential
k	Kilo
L	Liter

LTD	Long-term depression
LTP	Long term potentiation
m	meter
M	Molar / Mega
min	Minute
n	nano
NMDA	N-methyl-D-aspartic acid
NMJ	Neuromuscular junction
PPR	Paired-pulse ratio
p_r	Release probability
PSD	Postsynaptic density
RRP	Readily releasable pool
s	second
S	Siemen
s.e.m.	Standard error of the mean
STP	Short-term plasticity
UV	Ultraviolet
V	Volt
VGCC	Voltage-gated calcium channels

Bibliography

Alger BE (2002) Retrograde signaling in the regulation of synaptic transmission: focus on endocannabinoids. Prog Neurobiol 68: 247–286.

Allen C, Stevens CF (1994) An evaluation of causes for unreliability of synaptic transmission. Proc Natl Acad Sci U S A 91: 10380–10383.

Aravanis AM, Pyle JL, Tsien RW (2003) Single synaptic vesicles fusing transiently and successively without loss of identity. Nature 423: 643–647.

Atwood HL, Bittner GD (1971) Matching of excitatory and inhibitory inputs to crustacean muscle fibers. J Neurophysiol 34: 157–170.

Auger C, Kondo S, Marty A (1998) Multivesicular release at single functional synaptic sites in cerebellar stellate and basket cells. J Neurosci 18: 4532–4547.

Auger C, Marty A (2000) Quantal currents at single-site central synapses. J Physiol 526 Pt 1: 3–11.

Augustine GJ, Santamaria F, Tanaka K (2003) Local calcium signaling in neurons. Neuron 40: 331–346.

Bacci A, Coco S, Pravettoni E, Schenk U, Armano S, et al. (2001) Chronic blockade of glutamate receptors enhances presynaptic release and downregulates the interaction between synaptophysin-synaptobrevin-vesicle-associated membrane protein 2. J Neurosci 21: 6588–6596.

Barrett EF, Stevens CF (1972) The kinetics of transmitter release at the frog neuromuscular junction. J Physiol 227: 691–708.

Bekkers JM (1994) Quantal analysis of synaptic transmission in the central nervous system. Curr Opin Neurobiol 4: 360–365.

Bekkers JM (2003) Convolution of mini distributions for fitting evoked synaptic amplitude histograms. J Neurosci Methods 130: 105–114.

Bekkers JM, Clements JD (1999) Quantal amplitude and quantal variance of strontium-induced asynchronous EPSCs in rat dentate granule neurons. J Physiol 516 (Pt 1): 227–248.

Bekkers JM, Richerson GB, Stevens CF (1990) Origin of variability in quantal size in cultured hippocampal neurons and hippocampal slices. Proc Natl Acad Sci U S A 87: 5359–5362.

Bekkers JM, Stevens CF (1995) Quantal analysis of EPSCs recorded from small numbers of synapses in hippocampal cultures. J Neurophysiol 73: 1145–1156.

Bennett MR, Jones P, Lavidis NA (1986) The probability of quantal secretion along visualized terminal branches at amphibian (Bufo marinus) neuromuscular synapses. J Physiol 379: 257–274.

Bennett MR, Kearns JL (2000) Statistics of transmitter release at nerve terminals. Prog Neurobiol 60: 545–606.

Berne RM, Levy MN (1998) Physiology. 4th ed., Missouri: Mosby.

Betz WJ, Mao F, Bewick GS (1992) Activity-dependent fluorescent staining and destaining of living vertebrate motor nerve terminals. J Neurosci 12: 363–375.

Biro AA, Holderith NB, Nusser Z (2006) Release probability-dependent scaling of the postsynaptic responses at single hippocampal GABAergic synapses. J Neurosci 26: 12487–12496.

Bittner GD (1968) Differentiation of nerve terminals in the crayfish opener muscle and its functional significance. J Gen Physiol 51: 731–758.

Borst JG, Sakmann B (1996) Calcium influx and transmitter release in a fast CNS synapse. Nature 383: 431–434.

Borst JG, Sakmann B (1999) Effect of changes in action potential shape on calcium currents and transmitter release in a calyx-type synapse of the rat auditory brainstem. Philos Trans R Soc Lond B Biol Sci 354: 347–355.

Brodin L, Shupliakov O, Pieribone VA, Hellgren J, Hill RH (1994) The reticulospinal glutamate synapse in lamprey: plasticity and presynaptic variability. J Neurophysiol 72: 592–604.

Brown GL, Dale HH, Feldberg W (1936) Reactions of the normal mammalian muscle to acetylcholine and to eserine. J Physiol 87: 394–424.

Bruns D, Jahn R (1995) Real-time measurement of transmitter release from single synaptic vesicles. Nature 377: 62–65.

Bruns D, Riedel D, Klingauf J, Jahn R (2000) Quantal release of serotonin. Neuron 28: 205–220.

Buhl EH, Tamas G, Szilagyi T, Stricker C, Paulsen O, et al. (1997) Effect, number and location of synapses made by single pyramidal cells onto aspiny interneurones of cat visual cortex. J Physiol 500 (Pt 3): 689–713.

Burrone J, Murthy VN (2003) Synaptic gain control and homeostasis. Curr Opin Neurobiol 13: 560–567.

Burrone J, O'Byrne M, Murthy VN (2002) Multiple forms of synaptic plasticity triggered by selective suppression of activity in individual neurons. Nature 420: 414–418.

Cajal SRy (1923) Recuerdos de mi vida. 3rd ed., Madrid: Impr. de J. Pueyo.

Cajal SRy (1995) Histology of the Nervous System of Man and Vertebrates, vol. 2. OUP, Inc.

Ceccarelli B, Hurlbut WP (1980) Ca2+-dependent recycling of synaptic vesicles at the frog neuromuscular junction. J Cell Biol 87: 297–303.

Ceccarelli B, Hurlbut WP, Mauro A (1973) Turnover of transmitter and synaptic vesicles at the frog neuromuscular junction. J Cell Biol 57: 499–524.

Chen G, Harata NC, Tsien RW (2004) Paired-pulse depression of unitary quantal amplitude at single hippocampal synapses. Proc Natl Acad Sci U S A 101: 1063–1068.

Clamann HP, Mathis J, Luscher HR (1989) Variance analysis of excitatory postsynaptic potentials in cat spinal motoneurons during posttetanic potentiation. J Neurophysiol 61: 403–416.

Clements J (1991) Quantal synaptic transmission? Nature 353: 396.

Clements JD (2003) Variance-mean analysis: a simple and reliable approach for investigating synaptic transmission and modulation. J Neurosci Methods 130: 115–125.

Clements JD, Silver RA (2000) Unveiling synaptic plasticity: a new graphical and analytical approach. Trends Neurosci 23: 105–113.

Cochilla AJ, Angleson JK, Betz WJ (1999) Monitoring secretory membrane with FM1-43 fluorescence. Annu Rev Neurosci 22: 1–10.

Cooper RL, Harrington CC, Marin L, Atwood HL (1996) Quantal release at visualized terminals of a crayfish motor axon: intraterminal and regional differences. J Comp Neurol 375: 583–600.

Couteaux R, Pecot-Deschavassine M (1970) Vesicules synaptiques et poches au niveau des "zones actives" de la junction neuromusculaire. Compt Rend 271: 2346–2349.

Cowan WM, Sudhof TC, Stevens" CF (2001) Synapses. Baltimore: The Johns Hopkins University Press.

Curtis DR, Duggan AW, Felix D, Johnston GA (1970) GABA, bicuculline and central inhibition. Nature 226: 1222–1224.

Dale HH, Feldberg W (1934a) The chemical transmission of secretory impulses to the sweat glands of the cat. J Physiol 82: 121–128.

Dale HH, Feldberg W (1934b) The chemical transmitter of vagus effects to the stomach. J Physiol 81: 320–334.

Dale HH, Feldberg W, Vogt M (1936) Release of acetylcholine at voluntary motor nerve endings. J Physiol 86: 353–380.

Darcy KJ (2006) A study of inter-bouton exchange of synaptic vesicles at central synapses. Ph.D. thesis, University College London.

Darcy KJ, Staras K, Collinson LM, Goda Y (2006a) Constitutive sharing of recycling synaptic vesicles between presynaptic boutons. Nat Neurosci 9: 315–321.

Darcy KJ, Staras K, Collinson LM, Goda Y (2006b) An ultrastructural readout of fluorescence recovery after photobleaching using correlative light and electron microscopy. Nat Protoc 1: 988–994.

Davis GW (1995) Long-term regulation of short-term plasticity: a postsynaptic influence on presynaptic transmitter release. J Physiol Paris 89: 33–41.

Davis GW, DiAntonio A, Petersen SA, Goodman CS (1998) Postsynaptic PKA controls quantal size and reveals a retrograde signal that regulates presynaptic transmitter release in Drosophila. Neuron 20: 305–315.

Davis GW, Goodman CS (1998a) Genetic analysis of synaptic development and plasticity: homeostatic regulation of synaptic efficacy. Curr Opin Neurobiol 8: 149–156.

Davis GW, Goodman CS (1998b) Synapse-specific control of synaptic efficacy at the terminals of a single neuron. Nature 392: 82–86.

Davis GW, Murphey RK (1993) A role for postsynaptic neurons in determining presynaptic release properties in the cricket CNS: evidence for retrograde control of facilitation. J Neurosci 13: 3827–3838.

Davis GW, Murphey RK (1994) Long-term regulation of short-term transmitter release properties: retrograde signaling and synaptic development. Trends Neurosci 17: 9–13.

De Robertis ED, Bennett HS (1955) Some features of the submicroscopic morphology of synapses in frog and earthworm. J Biophys Biochem Cytol 1: 47–58.

Del Castillo J, Katz B (1954) Quantal components of the end-plate potential. J Physiol 124: 560–573.

Del Castillo J, Katz B (1955) Local activity at a depolarized nerve-muscle junction. J Physiol 128: 396–411.

Del Castillo J, Katz B (1956) Biophysical aspects of neuro-muscular transmission. Prog Biophys Biophys Chem 6: 121–170.

Del Castillo J, Stark L (1952) The effect of calcium ions on the motor end-plate potentials. J Physiol 116: 507–515.

Dittman JS, Kreitzer AC, Regehr WG (2000) Interplay between facilitation, depression, and residual calcium at three presynaptic terminals. J Neurosci 20: 1374–1385.

Dobrunz LE (2002) Release probability is regulated by the size of the readily releasable vesicle pool at excitatory synapses in hippocampus. Int J Dev Neurosci 20: 225–236.

Dobrunz LE, Huang EP, Stevens CF (1997) Very short-term plasticity in hippocampal synapses. Proc Natl Acad Sci U S A 94: 14843–14847.

Dobrunz LE, Stevens CF (1997) Heterogeneity of release probability, facilitation, and depletion at central synapses. Neuron 18: 995–1008.

Dodge FAJ, Rahamimoff R (1967) Co-operative action a calcium ions in transmitter release at the neuromuscular junction. J Physiol 193: 419–432.

Dresbach T, Qualmann B, Kessels MM, Garner CC, Gundelfinger ED (2001) The presynaptic cytomatrix of brain synapses. Cell Mol Life Sci 58: 94–116.

Eccles JC (1982) The synapse: from electrical to chemical transmission. Annu Rev Neurosci 5: 325–339.

Eccles JC, Katz B, Kuffler SW (1941) Nature of the endplate potential in curarized muscle. J Neurophysiol 4: 362–387.

Edwards FA, Konnerth A, Sakmann B (1990) Quantal analysis of inhibitory synaptic transmission in the dentate gyrus of rat hippocampal slices: a patch-clamp study. J Physiol 430: 213–249.

Edwards FR, Redman SJ, Walmsley B (1976) Statistical fluctuations in charge transfer at Ia synapses on spinal motoneurones. J Physiol 259: 665–688.

Elmqvist D, Quastel DM (1965) A quantitative study of end-plate potentials in isolated human muscle. J Physiol 178: 505–529.

Emptage NJ, Reid CA, Fine A, Bliss TVP (2003) Optical quantal analysis reveals a presynaptic component of LTP at hippocampal Schaffer-associational synapses. Neuron 38: 797–804.

Engelman HS, MacDermott AB (2004) Presynaptic ionotropic receptors and control of transmitter release. Nat Rev Neurosci 5: 135–145.

Fatt P, Katz B (1950a) Membrane potentials at the motor end-plate. J Physiol 111: 46p–7p.

Fatt P, Katz B (1950b) Some observations on biological noise. Nature 166: 597–598.

Fatt P, Katz B (1952) Spontaneous subthreshold activity at motor nerve endings. J Physiol 117: 109–128.

Feldmeyer D, Sakmann B (2000) Synaptic efficacy and reliability of excitatory connections between the principal neurones of the input (layer 4) and output layer (layer 5) of the neocortex. J Physiol 525 Pt 1: 31–39.

Fesce R, Grohovaz F, Valtorta F, Meldolesi J (1994) Neurotransmitter release: fusion or 'kiss-and-run'? Trends Cell Biol 4: 1–4.

Fiala JC (2005) Reconstruct: a free editor for serial section microscopy. J Microsc 218: 52–61.

Forti L, Bossi M, Bergamaschi A, Villa A, Malgaroli A (1997) Loose-patch recordings of single quanta at individual hippocampal synapses. Nature 388: 874–878.

Foster M, Sherrington CS (1897) A textbook of physiology, part three: The central nervous system. 7th ed., London: MacMillan Co. Ltd.

Frank CA, Kennedy MJ, Goold CP, Marek KW, Davis GW (2006) Mechanisms underlying the rapid induction and sustained expression of synaptic homeostasis. Neuron 52: 663–677.

Frank E (1973) Matching of facilitation at the neuromuscular junction of the lobster: a possible case for influence of muscle on nerve. J Physiol 233: 635–658.

Futai K, Kim MJ, Hashikawa T, Scheiffele P, Sheng M, et al. (2007) Retrograde modulation of presynaptic release probability through signaling mediated by PSD-95-neuroligin. Nat Neurosci 10: 186–195.

Gad H, Low P, Zotova E, Brodin L, Shupliakov O (1998) Dissociation between Ca2+-triggered synaptic vesicle exocytosis and clathrin-mediated endocytosis at a central synapse. Neuron 21: 607–616.

Galante M, Avossa D, Rosato-Siri M, Ballerini L (2001) Homeostatic plasticity induced by chronic block of AMPA/kainate receptors modulates the generation of rhythmic bursting in rat spinal cord organotypic cultures. Eur J Neurosci 14: 903–917.

Gandhi SP, Stevens CF (2003) Three modes of synaptic vesicular recycling revealed by single-vesicle imaging. Nature 423: 607–613.

Gasparini S, Migliore M, Magee JC (2004) On the initiation and propagation of dendritic spikes in CA1 pyramidal neurons. J Neurosci 24: 11046–11056.

Granseth B, Odermatt B, Royle SJ, Lagnado L (2006) Clathrin-mediated endocytosis is the dominant mechanism of vesicle retrieval at hippocampal synapses. Neuron 51: 773–786.

Gulyas AI, Miles R, Sik A, Toth K, Tamamaki N, et al. (1993) Hippocampal pyramidal cells excite inhibitory neurons through a single release site. Nature 366: 683–687.

Hamill OP, Marty A, Neher E, Sakmann B, Sigworth FJ (1981) Improved patch-clamp techniques for high-resolution current recording from cells and cell-free membrane patches. Pflugers Arch 391: 85–100.

Hanse E, Gustafsson B (2001) Vesicle release probability and pre-primed pool at glutamatergic synapses in area CA1 of the rat neonatal hippocampus. J Physiol 531: 481–493.

Harata N, Pyle JL, Aravanis AM, Mozhayeva M, Kavalali ET, et al. (2001a) Limited numbers of recycling vesicles in small CNS nerve terminals: implications for neural signaling and vesicular cycling. Trends Neurosci 24: 637–643.

Harata N, Ryan TA, Smith SJ, Buchanan J, Tsien RW (2001b) Visualizing recycling synaptic vesicles in hippocampal neurons by FM 1-43 photoconversion. Proc Natl Acad Sci U S A 98: 12748–12753.

Harata NC, Choi S, Pyle JL, Aravanis AM, Tsien RW (2006) Frequency-dependent kinetics and prevalence of kiss-and-run and reuse at hippocampal synapses studied with novel quenching methods. Neuron 49: 243–256.

Hardingham NR, Hardingham GE, Fox KD, Jack JJB (2007) Presynaptic efficacy directs normalization of synaptic strength in layer 2/3 rat neocortex after paired activity. J Neurophysiol 97: 2965–2975.

Harris KM, Sultan P (1995) Variation in the number, location and size of synaptic vesicles provides an anatomical basis for the nonuniform probability of release at hippocampal CA1 synapses. Neuropharmacology 34: 1387–1395.

Henkel AW, Lubke J, Betz WJ (1996) FM1-43 dye ultrastructural localization in and release from frog motor nerve terminals. Proc Natl Acad Sci U S A 93: 1918–1923.

Hessler NA, Shirke AM, Malinow R (1993) The probability of transmitter release at a mammalian central synapse. Nature 366: 569–572.

Heuser JE, Reese TS (1973) Evidence for recycling of synaptic vesicle membrane during transmitter release at the frog neuromuscular junction. J Cell Biol 57: 315–344.

Heuser JE, Reese TS, Dennis MJ, Jan Y, Jan L, et al. (1979) Synaptic vesicle exocytosis captured by quick freezing and correlated with quantal transmitter release. J Cell Biol 81: 275–300.

Hines ML, Carnevale NT (1997) The NEURON simulation environment. Neural Comput 9: 1179–1209.

Honore T, Davies SN, Drejer J, Fletcher EJ, Jacobsen P, et al. (1988) Quinoxalinediones: potent competitive non-NMDA glutamate receptor antagonists. Science 241: 701–703.

Huang EP, Stevens CF (1997) Estimating the distribution of synaptic reliabilities. J Neurophysiol 78: 2870–2880.

Isaacson JS, Walmsley B (1995) Counting quanta: direct measurements of transmitter release at a central synapse. Neuron 15: 875–884.

Jack JJ, Redman SJ (1971) The propagation of transient potentials in some linear cable structures. J Physiol 215: 283–320.

Jack JJ, Redman SJ, Wong K (1981) The components of synaptic potentials evoked in cat spinal motoneurones by impulses in single group Ia afferents. J Physiol 321: 65–96.

Johnson EW, Wernig A (1971) The binomial nature of transmitter release at the crayfish neuromuscular junction. J Physiol 218: 757–767.

Jonas P, Major G, Sakmann B (1993) Quantal components of unitary EPSCs at the mossy fibre synapse on CA3 pyramidal cells of rat hippocampus. J Physiol 472: 615–663.

Ju W, Morishita W, Tsui J, Gaietta G, Deerinck TJ, et al. (2004) Activity-dependent regulation of dendritic synthesis and trafficking of AMPA receptors. Nat Neurosci 7: 244–253.

Katz B (1969) The release of neural transmitter substances. Liverpool: Liverpool University Press.

Katz B, Miled R (1965) The measurement of synaptic delay, and the time course of acetylcholine release at the neuromuscular junction. Proc R Soc Lond B Biol Sci 161: 483–495.

Katz B, Miledi R (1965a) The effect of calcium on acetylcholine release from motor nerve terminals. Proc R Soc Lond B Biol Sci 161: 496–503.

Katz B, Miledi R (1965b) The effect of temperature on the synaptic delay at the neuromuscular junction. J Physiol 181: 656–670.

Katz B, Miledi R (1968) The role of calcium in neuromuscular facilitation. J Physiol 195: 481–492.

Katz PS, Kirk MD, Govind CK (1993) Facilitation and depression at different branches of the same motor axon: evidence for presynaptic differences in release. J Neurosci 13: 3075–3089.

Klingauf J, Kavalali ET, Tsien RW (1998) Kinetics and regulation of fast endocytosis at hippocampal synapses. Nature 394: 581–585.

Koerber HR, Mendell LM (1991) Modulation of synaptic transmission at Ia-afferent fiber connections on motoneurons during high-frequency stimulation: role of postsynaptic target. J Neurophysiol 65: 590–597.

Koester HJ, Johnston D (2005) Target cell-dependent normalization of transmitter release at neocortical synapses. Science 308: 863–866.

Korn H, Faber DS (1991) Quantal analysis and synaptic efficacy in the CNS. Trends Neurosci 14: 439–445.

Korn H, Mallet A, Triller A, Faber DS (1982) Transmission at a central inhibitory synapse. II. Quantal description of release, with a physical correlate for binomial n. J Neurophysiol 48: 679–707.

Korn H, Triller A, Mallet A, Faber DS (1981) Fluctuating responses at a central synapse: n of binomial fit predicts number of stained presynaptic boutons. Science 213: 898–901.

Krueger S, Fitzsimonds RM (2006) Remodeling the plasticity debate: the presynaptic locus revisited. Physiology (Bethesda) 21: 346–351.

Kullmann DM (1992) Quantal analysis using maximum entropy noise deconvolution. J Neurosci Methods 44: 47–57.

Kullmann DM, Nicoll RA (1992) Long-term potentiation is associated with increases in quantal content and quantal amplitude. Nature 357: 240–244.

Kuno M (1964) Quanta components of excitatory synaptic potentials in spinal motoneurones. J Physiol 175: 81–99.

Landis DM, Hall AK, Weinstein LA, Reese TS (1988) The organization of cytoplasm at the presynaptic active zone of a central nervous system synapse. Neuron 1: 201–209.

Langley J (1906) On nerve endings and on special excitable substances in cells. Proc R Soc London Ser B 78: 170–194.

Larkman A, Stratford K, Jack J (1991) Quantal analysis of excitatory synaptic action and depression in hippocampal slices. Nature 350: 344–347.

Larkman AU, Jack JJ, Stratford KJ (1997a) Assessment of the reliability or amplitude histograms from excitatory synapses in rat hippocampal CA1 in vitro. J Physiol 505 (Pt 2): 443–456.

Larkman AU, Jack JJ, Stratford KJ (1997b) Quantal analysis of excitatory synapses in rat hippocampal CA1 in vitro during low-frequency depression. J Physiol 505 (Pt 2): 457–471.

Laurent G, Sivaramakrishnan A (1992) Single local interneurons in the locust make central synapses with different properties of transmitter release on distinct postsynaptic neurons. J Neurosci 12: 2370–2380.

LeMasson G, Marder E, Abbott LF (1993) Activity-dependent regulation of conductances in model neurons. Science 259: 1915–1917.

Leslie KR, Nelson SB, Turrigiano GG (2001) Postsynaptic depolarization scales quantal amplitude in cortical pyramidal neurons. J Neurosci 21: RC170.

Lisman J, Raghavachari S (2006) A unified model of the presynaptic and postsynaptic changes during LTP at CA1 synapses. Sci STKE 2006: re11.

Liu G (2004) Local structural balance and functional interaction of excitatory and inhibitory synapses in hippocampal dendrites. Nat Neurosci 7: 373–379.

Liu G, Choi S, Tsien RW (1999) Variability of neurotransmitter concentration and nonsaturation of postsynaptic AMPA receptors at synapses in hippocampal cultures and slices. Neuron 22: 395–409.

Liu G, Tsien RW (1995) Properties of synaptic transmission at single hippocampal synaptic boutons. Nature 375: 404–408.

Lohmann C, Finski A, Bonhoeffer T (2005) Local calcium transients regulate the spontaneous motility of dendritic filopodia. Nat Neurosci 8: 305–312.

Magee JC, Cook EP (2000) Somatic EPSP amplitude is independent of synapse location in hippocampal pyramidal neurons. Nat Neurosci 3: 895–903.

Malinow R (1991) Transmission between pairs of hippocampal slice neurons: quantal levels, oscillations, and LTP. Science 252: 722–724.

Marder E, Goaillard JM (2006) Variability, compensation and homeostasis in neuron and network function. Nat Rev Neurosci 7: 563–574.

Markram H, Wang Y, Tsodyks M (1998) Differential signaling via the same axon of neocortical pyramidal neurons. Proc Natl Acad Sci U S A 95: 5323–5328.

McAllister AK, Stevens CF (2000) Nonsaturation of AMPA and NMDA receptors at hippocampal synapses. Proc Natl Acad Sci U S A 97: 6173–6178.

Meinrenken CJ, Borst JGG, Sakmann B (2002) Calcium secretion coupling at calyx of held governed by nonuniform channel-vesicle topography. J Neurosci 22: 1648–1667.

Meinrenken CJ, Borst JGG, Sakmann B (2003) Local routes revisited: the space and time dependence of the Ca2+ signal for phasic transmitter release at the rat calyx of Held. J Physiol 547: 665–689.

Mennerick S, Zorumski CF (1995) Paired-pulse modulation of fast excitatory synaptic currents in microcultures of rat hippocampal neurons. J Physiol 488 (Pt 1): 85–101.

Meyer AC, Neher E, Schneggenburger R (2001) Estimation of quantal size and number of functional active zones at the calyx of held synapse by nonstationary EPSC variance analysis. J Neurosci 21: 7889–7900.

Miesenbock G, De Angelis DA, Rothman JE (1998) Visualizing secretion and synaptic transmission with pH-sensitive green fluorescent proteins. Nature 394: 192–195.

Migliore M, Hoffman DA, Magee JC, Johnston D (1999) Role of an A-type K+ conductance in the back-propagation of action potentials in the dendrites of hippocampal pyramidal neurons. J Comput Neurosci 7: 5–15.

Muller KJ, Nicholls JG (1974) Different properties of synapses between a single sensory neurone and two different motor cells in the leech C.N.S. J Physiol 238: 357–369.

Murthy VN, Schikorski T, Stevens CF, Zhu Y (2001) Inactivity produces increases in neurotransmitter release and synapse size. Neuron 32: 673–682.

Murthy VN, Sejnowski TJ, Stevens CF (1997) Heterogeneous release properties of visualized individual hippocampal synapses. Neuron 18: 599–612.

Murthy VN, Stevens CF (1998) Synaptic vesicles retain their identity through the endocytic cycle. Nature 392: 497–501.

Oertner TG, Sabatini BL, Nimchinsky EA, Svoboda K (2002) Facilitation at single synapses probed with optical quantal analysis. Nat Neurosci 5: 657–664.

Palay SL, Palade GE (1955) The fine structure of neurons. J Biophys Biochem Cytol 1: 69–88.

Panchuk-Voloshina N, Haugland RP, Bishop-Stewart J, Bhalgat MK, Millard PJ, et al. (1999) Alexa dyes, a series of new fluorescent dyes that yield exceptionally bright, photostable conjugates. J Histochem Cytochem 47: 1179–1188.

Paradis S, Sweeney ST, Davis GW (2001) Homeostatic control of presynaptic release is triggered by postsynaptic membrane depolarization. Neuron 30: 737–749.

Parnas I (1972) Differential block at high frequency of branches of a single axon innervating two muscles. J Neurophysiol 35: 903–914.

Peters A, Palay S, de F Webster H (1976) The Fine Structure of the Nervous System: The Neurons and Supporting Cells. 2nd ed., Philadelphia: W. B. Saunders.

Petersen SA, Fetter RD, Noordermeer JN, Goodman CS, DiAntonio A (1997) Genetic analysis of glutamate receptors in Drosophila reveals a retrograde signal regulating presynaptic transmitter release. Neuron 19: 1237–1248.

Pfenninger K, Akert K, Moor H, Sandri C (1972) The fine structure of freeze-fractured presynaptic membranes. J Neurocytol 1: 129–149.

Phillips GR, Huang JK, Wang Y, Tanaka H, Shapiro L, et al. (2001) The presynaptic particle web: ultrastructure, composition, dissolution, and reconstitution. Neuron 32: 63–77.

Pickard L, Noel J, Henley JM, Collingridge GL, Molnar E (2000) Developmental changes in synaptic AMPA and NMDA receptor distribution

and AMPA receptor subunit composition in living hippocampal neurons. J Neurosci 20: 7922–7931.

Polsky A, Mel BW, Schiller J (2004) Computational subunits in thin dendrites of pyramidal cells. Nat Neurosci 7: 621–627.

Prange O, Murphy TH (1999) Analysis of multiquantal transmitter release from single cultured cortical neuron terminals. J Neurophysiol 81: 1810–1817.

Pun RY, Neale EA, Guthrie PB, Nelson PG (1986) Active and inactive central synapses in cell culture. J Neurophysiol 56: 1242–1256.

Pyle JL, Kavalali ET, Piedras-Renteria ES, Tsien RW (2000) Rapid reuse of readily releasable pool vesicles at hippocampal synapses. Neuron 28: 221–231.

Raastad M, Storm J, Andersen P (1992) Putative Single Quantum and Single Fibre Excitatory Postsynaptic Currents Show Similar Amplitude Range and Variability in Rat Hippocampal Slices. Eur J Neurosci 4: 113–117.

Rabinowitch I, Segev I (2006) The interplay between homeostatic synaptic plasticity and functional dendritic compartments. J Neurophysiol 96: 276–283.

Raghavachari S, Lisman JE (2004) Properties of quantal transmission at CA1 synapses. J Neurophysiol 92: 2456–2467.

Rall W (1969a) Distributions of potential in cylindrical coordinates and time constants for a membrane cylinder. Biophys J 9: 1509–1541.

Rall W (1969b) Time constants and electrotonic length of membrane cylinders and neurons. Biophys J 9: 1483–1508.

Rall W, Rinzel J (1973) Branch input resistance and steady attenuation for input to one branch of a dendritic neuron model. Biophys J 13: 648–687.

Ramakers GJ, Corner MA, Habets AM (1990) Development in the absence of spontaneous bioelectric activity results in increased stereotyped burst firing in cultures of dissociated cerebral cortex. Exp Brain Res 79: 157–166.

Redman S (1990) Quantal analysis of synaptic potentials in neurons of the central nervous system. Physiol Rev 70: 165–198.

Redman S, Walmsley B (1983) Amplitude fluctuations in synaptic potentials evoked in cat spinal motoneurones at identified group Ia synapses. J Physiol 343: 135–145.

Reid CA, Clements JD (1999) Postsynaptic expression of long-term potentiation in the rat dentate gyrus demonstrated by variance-mean analysis. J Physiol 518 (Pt 1): 121–130.

Renger JJ, Egles C, Liu G (2001) A developmental switch in neurotransmitter flux enhances synaptic efficacy by affecting AMPA receptor activation. Neuron 29: 469–484.

Reyes A, Lujan R, Rozov A, Burnashev N, Somogyi P, et al. (1998) Target-cell-specific facilitation and depression in neocortical circuits. Nat Neurosci 1: 279–285.

Rhee JS, Ebihara S, Akaike N (1994) Gramicidin perforated patch-clamp technique reveals glycine-gated outward chloride current in dissociated nucleus solitarii neurons of the rat. J Neurophysiol 72: 1103–1108.

Rinzel J, Rall W (1974) Transient response in a dendritic neuron model for current injected at one branch. Biophys J 14: 759–790.

Rivera C, Voipio J, Payne JA, Ruusuvuori E, Lahtinen H, et al. (1999) The K+/Cl- co-transporter KCC2 renders GABA hyperpolarizing during neuronal maturation. Nature 397: 251–255.

Rizzoli SO, Betz WJ (2005) Synaptic vesicle pools. Nat Rev Neurosci 6: 57–69.

Robitaille R, Tremblay JP (1987) Non-uniform release at the frog neuromuscular junction: evidence of morphological and physiological plasticity. Brain Res 434: 95–116.

Robitaille R, Tremblay JP (1991) Non-uniform responses to Ca2+ along the frog neuromuscular junction: effects on the probability of spontaneous and evoked transmitter release. Neuroscience 40: 571–585.

Rosenmund C, Clements JD, Westbrook GL (1993) Nonuniform probability of glutamate release at a hippocampal synapse. Science 262: 754–757.

Rosenmund C, Stevens CF (1996) Definition of the readily releasable pool of vesicles at hippocampal synapses. Neuron 16: 1197–1207.

Royle SJ, Lagnado L (2003) Endocytosis at the synaptic terminal. J Physiol 553: 345–355.

Ryan TA, Reuter H, Smith SJ (1997) Optical detection of a quantal presynaptic membrane turnover. Nature 388: 478–482.

Ryan TA, Reuter H, Wendland B, Schweizer FE, Tsien RW, et al. (1993) The kinetics of synaptic vesicle recycling measured at single presynaptic boutons. Neuron 11: 713–724.

Ryan TA, Smith SJ (1995) Vesicle pool mobilization during action potential firing at hippocampal synapses. Neuron 14: 983–989.

Sandrock AWJ, Dryer SE, Rosen KM, Gozani SN, Kramer R, et al. (1997) Maintenance of acetylcholine receptor number by neuregulins at the neuromuscular junction in vivo. Science 276: 599–603.

Sankaranarayanan S, De Angelis D, Rothman JE, Ryan TA (2000) The use of pHluorins for optical measurements of presynaptic activity. Biophys J 79: 2199–2208.

Savtchenko LP, Rusakov DA (2007) The optimal height of the synaptic cleft. Proc Natl Acad Sci U S A 104: 1823–8.

Sayer RJ, Redman SJ, Andersen P (1989) Amplitude fluctuations in small EPSPs recorded from CA1 pyramidal cells in the guinea pig hippocampal slice. J Neurosci 9: 840–850.

Scheuss V, Neher E (2001) Estimating synaptic parameters from mean, variance, and covariance in trains of synaptic responses. Biophys J 81: 1970–1989.

Schikorski T, Stevens CF (1997) Quantitative ultrastructural analysis of hippocampal excitatory synapses. J Neurosci 17: 5858–5867.

Schikorski T, Stevens CF (2001) Morphological correlates of functionally defined synaptic vesicle populations. Nat Neurosci 4: 391–395.

Schneggenburger R, Neher E (2005) Presynaptic calcium and control of vesicle fusion. Curr Opin Neurobiol 15: 266–274.

Schnell E, Sizemore M, Karimzadegan S, Chen L, Bredt DS, et al. (2002) Direct interactions between PSD-95 and stargazin control synaptic AMPA receptor number. Proc Natl Acad Sci U S A 99: 13902–13907.

Sharpless SK (1964) Reorganization of function in the nervous system – use and disuse. Annu Rev Physiol 26: 357–388.

Sherrington CS (1897) C. S. Sherrington to E. A. Schafer, letter 1st Dec. 1897. in the Sharpey-Schafer papers in the Contemporary Medical Archives Centre, the Wellcome Institute for History of Medicine, reference PP/ESS/B21/9.

Silver RA (2003) Estimation of nonuniform quantal parameters with multiple-probability fluctuation analysis: theory, application and limitations. J Neurosci Methods 130: 127–141.

Silver RA, Lubke J, Sakmann B, Feldmeyer D (2003) High-probability uniquantal transmission at excitatory synapses in barrel cortex. Science 302: 1981–1984.

Silver RA, Momiyama A, Cull-Candy SG (1998) Locus of frequency-dependent depression identified with multiple-probability fluctuation analysis at rat climbing fibre-Purkinje cell synapses. J Physiol 510 (Pt 3): 881–902.

Sjostrom PJ, Turrigiano GG, Nelson SB (2004) Endocannabinoid-dependent neocortical layer-5 LTD in the absence of postsynaptic spiking. J Neurophysiol 92: 3338–3343.

Slutsky I, Sadeghpour S, Li B, Liu G (2004) Enhancement of synaptic plasticity through chronically reduced Ca2+ flux during uncorrelated activity. Neuron 44: 835–849.

Stevens CF (1993) Quantal release of neurotransmitter and long-term potentiation. Cell 72 Suppl: 55–63.

Stevens CF, Tsujimoto T (1995) Estimates for the pool size of releasable quanta at a single central synapse and for the time required to refill the pool. Proc Natl Acad Sci U S A 92: 846–849.

Stevens CF, Wang Y (1995) Facilitation and depression at single central synapses. Neuron 14: 795–802.

Stevens CF, Wesseling JF (1998) Activity-dependent modulation of the rate at which synaptic vesicles become available to undergo exocytosis. Neuron 21: 415–424.

Stewart BA, Schuster CM, Goodman CS, Atwood HL (1996) Homeostasis of synaptic transmission in Drosophila with genetically altered nerve terminal morphology. J Neurosci 16: 3877–3886.

Stratford KJ, Jack JJ, Larkman AU (1997) Calibration of an autocorrelation-based method for determining amplitude histogram reliability and quantal size. J Physiol 505 (Pt 2): 425–442.

Stricker C, Redman SJ (2003) Quantal analysis based on density estimation. J Neurosci Methods 130: 159–171.

Sudhof TC (1995) The synaptic vesicle cycle: a cascade of protein-protein interactions. Nature 375: 645–653.

Sudhof TC (2004) The synaptic vesicle cycle. Annu Rev Neurosci 27: 509–547.

Sun HY, Lyons SA, Dobrunz LE (2005) Mechanisms of target-cell specific short-term plasticity at Schaffer collateral synapses onto interneurones versus pyramidal cells in juvenile rats. J Physiol 568: 815–840.

Sun JY, Wu LG (2001) Fast kinetics of exocytosis revealed by simultaneous measurements of presynaptic capacitance and postsynaptic currents at a central synapse. Neuron 30: 171–182.

Sutton MA, Ito HT, Cressy P, Kempf C, Woo JC, et al. (2006) Miniature neurotransmission stabilizes synaptic function via tonic suppression of local dendritic protein synthesis. Cell 125: 785–799.

Takamori S, Holt M, Stenius K, Lemke EA, Gronborg M, et al. (2006) Molecular anatomy of a trafficking organelle. Cell 127: 831–846.

Takei K, Mundigl O, Daniell L, De Camilli P (1996) The synaptic vesicle cycle: a single vesicle budding step involving clathrin and dynamin. J Cell Biol 133: 1237–1250.

Tang CM, Margulis M, Shi QY, Fielding A (1994) Saturation of postsynaptic glutamate receptors after quantal release of transmitter. Neuron 13: 1385–1393.

Thiagarajan TC, Lindskog M, Tsien RW (2005) Adaptation to synaptic inactivity in hippocampal neurons. Neuron 47: 725–737.

Thiagarajan TC, Piedras-Renteria ES, Tsien RW (2002) alpha- and beta-CaMKII. Inverse regulation by neuronal activity and opposing effects on synaptic strength. Neuron 36: 1103–1114.

Tong G, Jahr CE (1994) Multivesicular release from excitatory synapses of cultured hippocampal neurons. Neuron 12: 51–59.

Trommershauser J, Schneggenburger R, Zippelius A, Neher E (2003) Heterogeneous presynaptic release probabilities: functional relevance for short-term plasticity. Biophys J 84: 1563–1579.

Turrigiano GG, Leslie KR, Desai NS, Rutherford LC, Nelson SB (1998) Activity-dependent scaling of quantal amplitude in neocortical neurons. Nature 391: 892–896.

Turrigiano GG, Nelson SB (2004) Homeostatic plasticity in the developing nervous system. Nat Rev Neurosci 5: 97–107.

Vautrin J, Barker JL (2003) Presynaptic quantal plasticity: Katz's original hypothesis revisited. Synapse 47: 184–199.

Wadiche JI, Jahr CE (2001) Multivesicular release at climbing fiber-Purkinje cell synapses. Neuron 32: 301–313.

Walmsley B (1991) Central synaptic transmission: studies at the connection between primary afferent fibres and dorsal spinocerebellar tract (DSCT) neurones in Clarke's column of the spinal cord. Prog Neurobiol 36: 391–423.

Walmsley B (1995) Interpretation of 'quantal' peaks in distributions of evoked synaptic transmission at central synapses. Proc Biol Sci 261: 245–250.

Walmsley B, Edwards FR, Tracey DJ (1987) The probabilistic nature of synaptic transmission at a mammalian excitatory central synapse. J Neurosci 7: 1037–1046.

Walmsley B, Edwards FR, Tracey DJ (1988) Nonuniform release probabilities underlie quantal synaptic transmission at a mammalian excitatory central synapse. J Neurophysiol 60: 889–908.

Whittaker VP (1968) The storage of transmitters in the central nervous system. Biochem J 109: 20P–21P.

Wierenga CJ, Walsh MF, Turrigiano GG (2006) Temporal regulation of the expression locus of homeostatic plasticity. J Neurophysiol 96: 2127–2133.

Wu LG, Borst JG (1999) The reduced release probability of releasable vesicles during recovery from short-term synaptic depression. Neuron 23: 821–832.

Yuste R, Majewska A, Cash SS, Denk W (1999) Mechanisms of calcium influx into hippocampal spines: heterogeneity among spines, coincidence detection by NMDA receptors, and optical quantal analysis. J Neurosci 19: 1976–1987.

Zakharenko SS, Zablow L, Siegelbaum SA (2001) Visualization of changes in presynaptic function during long-term synaptic plasticity. Nat Neurosci 4: 711–717.

Zenisek D, Steyer JA, Almers W (2000) Transport, capture and exocytosis of single synaptic vesicles at active zones. Nature 406: 849–854.

Zucker RS (1973) Changes in the statistics of transmitter release during facilitation. J Physiol 229: 787–810.

Zucker RS, Regehr WG (2002) Short-term synaptic plasticity. Annu Rev Physiol 64: 355–405.

Produced with LaTeX